CRANFIELD UNIVERSITY

Michael Croft-White

Measurement and Analysis of Rally Car Dynamics at High Attitude Angles

School of Engineering

PhD. Thesis

CRANFIELD UNIVERSITY

School of Engineering
Department of Automotive, Mechanical and Structural Engineering

PhD. Thesis

2006

Michael Croft-White

Measurement and Analysis of Rally Car Dynamics at High Attitude Angles

Supervisors: M.F. Harrison and D. Greenhalgh

May 2006

This thesis is submitted in fulfilment of the requirements for the Degree of Doctor of Philosophy

Abstract

This research aims to investigate the nature of high β-angle cornering as seen in rallying and in particular the World Rally Championship. This is achieved through a combination of sensor development, on-car measurement and vehicle dynamic simulation.

Through the development of novel β-angle measurement technology it has become possible to measure and study vehicle attitude dynamics on loose gravel surfaces. Using this sensor, an understanding of how a rally driver uses the dynamics of the vehicle and surface to maximise performance has been obtained.

By combining the new data stream with accepted vehicle dynamic theory, the tyres have been considered and general trends in gravel tyre performance unveiled. Through feedback, these trends have been implemented as a means of tuning a dynamic model to improve realism and permit an analysis of cornering trends in rally cars.

Active control systems have been considered that could implement more sophisticated algorithms based on this understanding and potentially use the new sensor information as an input signal. A case study which explores such a possibility is included.

Acknowledgements

The author would like to acknowledge the help and support of the following people and companies, without whom this thesis could not have been completed in its current form:

Professor Matthew Harrison
For leaving me alone to do my own thing but still being there when needed.

Andrew Warr and Duncan Apthorp, Pi Research Ltd.
For all your support and generous assistance with equipment and knowledge.

Christian Loriaux, M-Sport Ltd.
For providing unprecedented access to both WRC test vehicles and the data from them.

My Parents
For helping keep me in the lifestyle to which I have become accustomed.

Patrick Harkness
For being there during initial conception of the β-angle sensor and persistently pursuing some form of recognition.

There are many others but they already know who they are.

Contents

List of Figures

List of Tables

Nomenclature

α	Angular acceleration
α	Tyre Slip Angle
β	Vehicle attitude angle
ΔW	Longitudinal weight transfer
δ	Steer Angle
λ	Wavelength
μ	Coefficient of Friction between Tyre and Road Surface
ϕ	Vehicle pitch angle
θ	Vehicle roll angle
a	Acceleration
a	Distance of Front Axle from CofG
A_x	Longitudinal acceleration
A_y	Lateral acceleration
b	Distance of Rear Axle from CofG
B, C, D, E	Pacejka Magic Tyre Model - Coefficients
C_N	Normalised Yaw Moment
F	Force
F_f	Side force on Front Wheels
F_r	Side force on Rear Wheels

F_y	Lateral Tyre Force
h	Height of Centre of Gravity
I_ψ	Yaw Moment of Inertia
I_{pitch}	Pitch Inertia
K	Inertia Approximation Constant
LLT	Lateral Load Transfer
M	Vehicle Mass
m	Mass
M_ψ	Stabilising Yaw Moment
N	Yawing moment
T_{SAx}	Self Aligning Torque
TW	Track Width
V_x	Longitudinal velocity
V_y	Lateral velocity
W	Vehicle weight
WB	Wheelbase
X	Raw magnetometer measurement - X axis
X	Raw magnetometer measurement - Y axis
X_h	Corrected magnetometer measurement - X axis
X_{max}	Maximum measured value of X
X_{min}	Minumum measured value of X
X_{off}	Magnetometer Calibration Output Offset - X axis
X_{sf}	Magnetometer Calibration Output Scale Factor - X axis
X_{value}	Corrected Magnetometer Reading - X axis
Y_h	Corrected magnetometer measurement - Y axis

Y_{max} Maximum measured value of Y

Y_{min} Minimum measured value of Y

Y_{off} Magnetometer Calibration Output Offset - Y axis

Y_{sf} Magnetometer Calibration Output Scale Factor - Y axis

Y_{value} Corrected Magnetometer Reading - Y axis

MMD Milliken Moment Diagram

MMM The Milliken Moment Method

Chapter 1

Introduction

1.1 Context

In almost all forms of driving a high β-angle[1](or driving sideways) is undesirable and usually associated with being a direct precursor to a driver losing control of the vehicle. The main exception to this rule is rally driving, in particular the World Rally Championship (WRC), where the cars are often seen balanced on the limits of control in an attempt to maximise performance on loose surfaces. This research investigates the nature of high β-angle cornering through a combination of sensor development, on-car measurement and vehicle dynamic simulation in an attempt to understand more about how such a style of driving can increase performance and how the active systems of a car can better react to that style.

Initially it was clear that a greater understanding of the dynamics of vehicles driven in such a manner would be required. Most research up to this point has not covered the extreme performance regions of rallying and as such this work looks to fulfil a need to progress in this direction.

It became clear that as an enabling step, a means for measurement of vehicle development and progression was required that was better than currently available sensor technology and telemetry. Through the development of a β-angle sensor that provided robust and reliable data, even in the loose

[1]Also known as vehicle attitude angle or vehicle sideslip angle.

gravel conditions of rallying, it became possible to investigate the high attitude nature seen in the driving styles of many rally drivers. With this information and real rally telemetry data obtained during WRC testing, many new avenues of investigation became possible, including direct gravel tyre comparison and optimal attitude angle cornering.

With this increased understanding of the influence and effects of β-angle and, if permitted by the rules of the sport, the active control systems could implement more sophisticated algorithms based on this understanding and potentially using the new sensor information as an input signal. A case study which explores such a possibility is included.

1.2 Vehicle Dynamic Simulation in Rallying

At present, simulation has a limited role in rallying particularly when compared to its prolific use in other motorsports such as Formula One. The primary reason for this discrepancy between the sports relates to the differing number of unknown variables in rallying and circuit racing.

Where a Formula One car races repeatedly around a track of approximately 3 miles with the same corners being driven as many as 100 times, rally stages run over longer stretches of road in which each corner differs from all that preceded it or will follow it. Further complications arise from road surface variation, the tendency for the wheels to leave the ground, altitude and weather conditions, particularly on mountainous rallies such as the Monte Carlo rally whose course traverses the Alps.

These factors mean that any attempt at simulation in rallying is better suited to developing more generic concepts in dynamic performance which can handle the problems of uncertainty, rather than the extreme precision and accuracy desired from a single lap simulation of a Formula One car.

Part of this research looks to assist in the development of rally car simulation by the application of new understanding achieved through the use of the β-angle sensor and corresponding telemetry data. In particular, the β-angle sensor was employed as a means of determining tyre performance and characteristics on loose gravel and on tarmac surfaces. As large attitude angles

lead to large tyre slip angles, this method gave insight into the lateral tyre force profile in the super-saturated region (above about 15 degrees) which has previously been considered to be of limited value. Ultimately, with the advantage of access to real world WRC telemetry data using the new sensor, this has resulted in a more realistic tyre force curve that could be directly implemented in a dynamic model, enhancing accuracy and precision.

1.3 Thesis Structure

Chapter One: Introduction
Chapter One outlines the framework of the research detailed in this thesis.

Chapter Two: Literature Survey
Chapter Two sets out the history and previous research relating to the topics covered by this thesis. Reasons and evidence for taking certain decisions as to which direction this research should take are presented along with material that backs up some of the statements and assumptions made.

Chapter Three: The β-angle Sensor
As WRC is a field in which attitude angle appears to play a significant part in performance it was firstly necessary to gauge the extremes and general behaviour of β-angle in such vehicles and circumstances. Unfortunately WRC is an extreme form of racing on rough and loose surfaces that cause problems for many current sensing technologies. Therefore an enabling step was required that allowed accurate and reliable β-angle data to be measured and compared with the existing telemetry data and information.

Chapter Three details the design, development, prototyping and testing of a novel β-angle sensor that provides a means for giving robust and accurate measurements in the harsh environments experienced in the world of WRC. All stages are detailed and descriptions on how design problems were overcome along with refinements necessary to produce the desired level of accuracy. The testing of the sensor, which both verified and validated the sensor, is also described with example telemetry data from real world testing

on both gravel and tarmac surfaces presented.

Chapter Four: Supplementing The Modelling Dataset
Once it became possible to determine β-angle for all road conditions using the new sensor, it enabled the development of a model to investigate the behaviour of such a vehicle at large β-angles. To this end, a seven degree of freedom transient dynamic model was built with accepted tyre, aerodynamic and powertrain models for use in simulating a WRC car. Before its use, however, the model was run through validation and verification process in which the model was compared with both expectations derived from accepted vehicle dynamic theory and also comparison with real telemetry data gathered using the vehicle it was intended to simulate. Both the model and the validation process are detailed in Chapter Four.

Using this model and the sensor of Chapter Three, the process of extracting lateral tyre curves is presented with examples of both tarmac and gravel surfaces.

Such curves are of great benefit in demonstrating the behaviour of the tyre in the super-saturated region as this is often where laboratory tyre curve measurement becomes less accurate or impossible to obtain. A method of producing such curves is presented for both tarmac and gravel, the tarmac curve is generated using both existing optical slip angle sensors[12] and the new sensor whereas the gravel curve is only possible now that the new sensor can provide β-angle robustly in the gravel environment.

Chapter Five: A Case Study
With the set of tools now available, both in telemetry and simulation, the benefits of β-angle can be investigated thoroughly. In addition it became possible to gauge a better understanding of the dynamics of the vehicle. β-angle has long been considered an important factor in vehicle stability and control but research into the topic has been somewhat confined to lower values on the understanding that at higher values, the average driver simply can not control the vehicle.

From a performance point of view, it will be shown that high values of

β-angle can result in higher lateral cornering forces and ultimately quicker manoeuvre times. It will also be shown that the transmission configuration of a 4-wheel drive (4WD) vehicle can play a significant part in altering the benefits of certain angles as well as directly affecting the β-angle of the vehicle.

Chapter Six: Conclusions and Further Work

Chapter Six sums up the progress made with this research and the potential applications of both the new sensor and understanding of high β-angle vehicle dynamics that the simulations have permitted.

Chapter 2

Literature Survey

2.1 β-angle

$$\beta = \arctan\left(\frac{V_y}{V_x}\right) \tag{2.1}$$

β-angle, or as it is sometimes known, vehicle attitude or body slip angle, has become an increasingly important aspect of vehicle dynamics as progress in design has continued to push the envelope of vehicle performance. Despite this, its measurement and application in control systems still holds many difficulties for engineers. In this chapter the importance of β-angle in modern vehicles is demonstrated as well as how it is currently measured or estimated. Then a history of research that has led up to the development of a new β-angle sensor is presented and a background to the research stream that this new sensor has enabled.

This research is heavily biased towards the domain of the rally style car and driver, in particular WRC where extremes of control and β-angle are common as well as some of the most sophisticated 4WD transmissions.

2.1.1 β-angle in Vehicle Dynamics

The importance of β-angle began to be highlighted with the development of the Milliken Moment Method (MMM)[13]. The main aspect of the method is, for a given β-angle and steering angle range, to plot normalised yaw moment

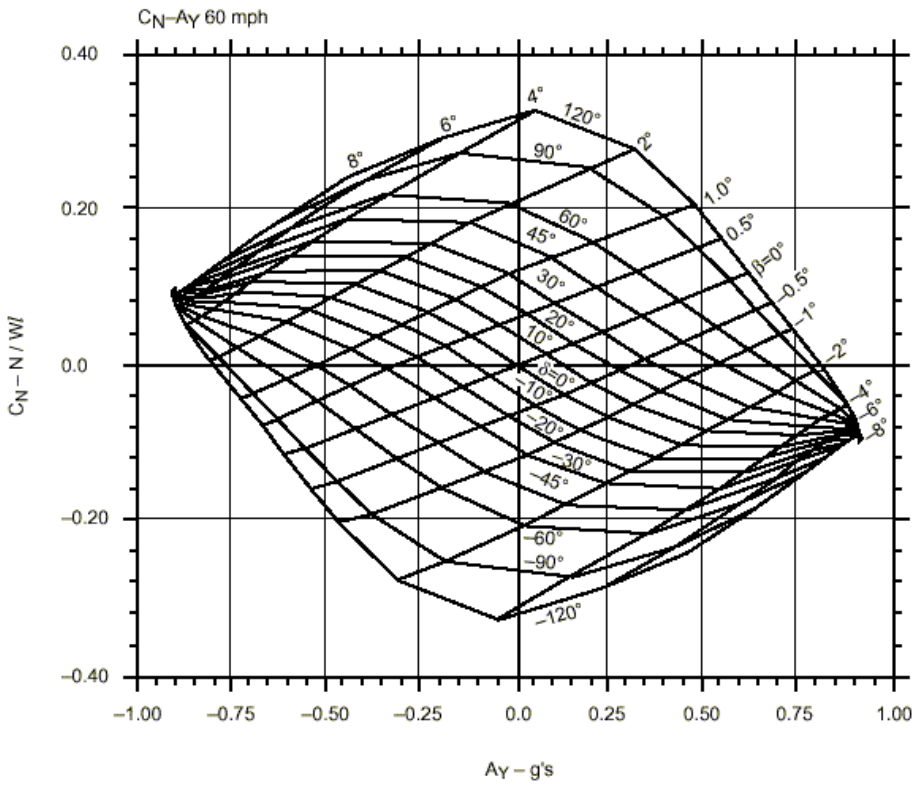

Figure 2.1: A Milliken Moment Diagram[1]

(C_N) against lateral acceleration(A_y)[1], the plot typically being known as a Milliken Moment Diagram (MMD). Using the MMD it is possible to quantify the constraints that are imposed on vehicle stability and controllability by the capabilities of the tyres. Figure 2.1 shows an example of a Moment Diagram.

The Moment Diagram plots the lines of equal vehicle β-angle (running upper right to lower left) and of equal steer angle, δ (running upper left to lower right). This particular example represents a vehicle travelling at 60 mph.

Shibahata *et al.*[14] used similar reasoning to develop the β-angle method.

The β method explains the effect that β-angle has on the yaw moment gain generated by the lateral tyre forces following a steer angle input. It shows that as β increases, this yaw moment gain decreases until at large values of

β the yaw moment can hardly be influenced by a driver's steer input. At these extremes of β, usually above 12 degrees on tarmac, the vehicle becomes extremely difficult to control for all but the most experienced drivers. This can be seen in Figure 2.2 where at low β-angles, any steer input results in a large yaw moment. As β-angle increases, the magnitude of this moment generated by steer input is significantly reduced resulting in a reduction in the drivers ability to control the yaw dynamics of the vehicle.

These reasons have resulted in the majority of research being confined to low values of β-angle, typically under 14 degrees. Such a range covers most aspects of driving, however in the world of rallying and WRC, high attitude angle cornering is common place, particularly on loose surfaces. Nozaki[15] makes the point that large body slip angles do actually allow the tyre to attain a high cornering force but as Shibahata[14] shows the reduction in control makes it a technique that only skilled drivers can use effectively.

2.1.2 ESP and Yaw Moment Control

As the β method demonstrates, β-angle is a crucial factor in the manoeuvrability of the vehicle. Therefore the average or inexperienced driver may struggle to avoid an accident if the vehicle is permitted maintain a state of high β[16].

More recent advances have seen electronic control begin to take over the vehicle in times of extreme situations. Electronic Stability Program (ESP)[16] and Active Yaw Control[17] systems have been developed that protect the driver in the event that the dynamics of a vehicle become unstable. Both are influenced by the β-angle and act to either brake individual wheels or adjust drive-line torque distribution to control the yaw moment dynamics[14]. Both braking and torque distribution methods seem to produce a similar dynamic performance although torque distribution control appears to possess some distinct advantages[18]. Below the typical mechanisms used for yaw moment control are listed with some of their characteristics and advantages[19][20].

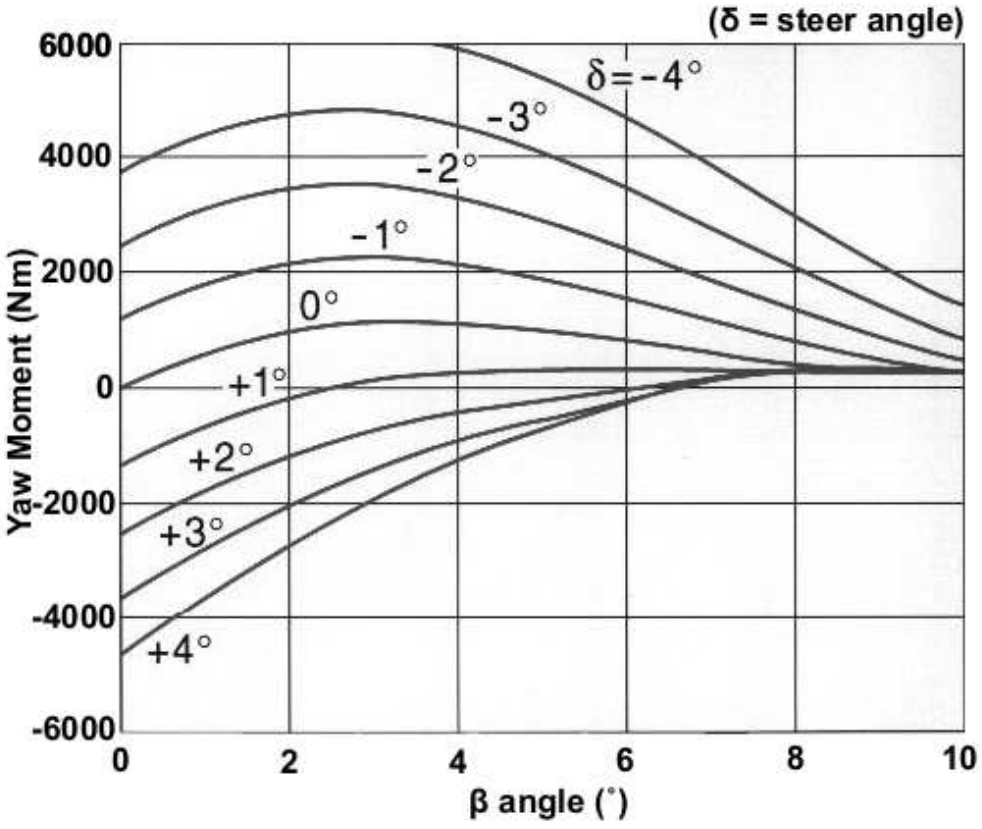

Figure 2.2: Yaw Moment against β-angle

- Braking force Distribution Control
  - Distributes braking torque on left and right wheels by varying the braking force applied to each wheel.
  - Only suitable for controlling yaw moment under deceleration cornering and cornering at critical speed.
- Controlled LSD
  - Capable only of transferring torque from the faster running wheel to the slower one.
- Driving Force Distribution Control
  - Differential imparts differing torques to left and right wheels according to the value of the input torque.

Differential Braking

It has been demonstrated in the literature that by individually braking the left or right wheels it is possible to generate a controlling yaw moment[21]. This method though, suffers in that it is only suitable during deceleration cornering or cornering at critical speed so as not to effect vehicle stability[21].

Despite these limitations, this method has been employed in most forms of traction control or stability control systems[16][22] mainly due to the ease with which it can be implemented, particularly when combined with ABS, when compared to the more complicated differential systems required to control torque distribution.

Torque Distribution

Torque distribution in a differential initially came about through the development of Limited Slip differentials (LSD)[23]. These passive devices allowed variation in the output shafts speeds that is required for cornering, but as

the differences became larger, the use of internal clutch packs act to transfer torque from the faster to the slower shaft. It is also possible to perform the same action using high-helix angle INVEX gears as in the Torsen differentials[24].

The rate at which the differential would transfer torque and the degree of variation in speed that it would allow were dictated by the internal component configuration and as such had to strike a balance between all possible uses of that differential[1].

In order to remove this element of compromise, the Active LSD was developed whereby the internal friction plates could be thrust closer together, hence adjusting their interaction and distribution of torque[1]. Various methods exist for performing this task, such as the Electro-Magnetic Coupling differential, which uses electromagnets to control plate position, or the electro-hydraulic differential which uses a hydraulic piston[25][26]. The latter is implemented in the simulation model used in this research (see Figure 4.3 and Section 4.1.1 for a more detailed description).

Despite the addition of the control element to the LSD, it is still only possible to transfer torque from the faster to the slower output shaft or wheel. In the majority of situations this is acceptable but it can only generate a corrective yaw moment on a vehicle rather than acting to enhance a cornering moment. For that, the differential needs to also be capable of transferring additional torque to the faster spinning shaft.

Mitsubishi introduced the first commercial active torque distributing differential that could perform this task in the 1990's with their Active Yaw Control system[19]. These differentials would work by having two internal shafts, driven from the input shaft, with one sped up 12.5% and the other slowed down by 12.5%. Both the output drive shafts could then be attached to either shaft through a series of clutch plates allowing either a positive or negative transference of torque to that shaft. By attaching the outer, faster shaft to the faster internal shaft (as well as the inner shaft to the slower) additional torque could be transferred to the outer wheel effectively generating additional cornering yaw moment.

As technology progresses, the torque distributing (or torque vectoring)

differentials are becoming more common place opening up the possibility for enhanced and more capable traction control and stability management systems that do not suffer the limitations of active brake distribution. The potential in this area for performance related driving is investigated in Chapter 5.

2.1.3 Estimation and Measurement Techniques

β-angle is notoriously difficult to measure, van Zanten[27] in describing the Bosch ESP system stated that no sensor is available to measure the β-angle of the car. Despite this slip angle can be inferred by a combination of sensors. Sasaki[28] goes further to explain that there are currently two predominant methods of detecting slip angle. The first by non-contact longitudinal and lateral velocity detection and subsequent vector calculation, the second employing a dynamic vehicle model to infer slip angle from various inertial measurement. More recently a third alternative using Dual antennae GPS technology has has begun to be employed[3].

Velocity Detection

Its definition, equation 2.1, shows that β-angle is the inverse tangient of the ratio of lateral velocity to longitudinal velocity. Therefore it is necessary to measure both velocity vectors, which is only possible using non-contact methods.

One commercial product that is available is known as a Correvit[12]. By projecting a optical diffraction grating onto the road surface, the distortion in the reflected pattern can be shown to be directly related to the relative velocity vector of the sensor to the road surface[29]. This product suffers though in that a relatively smooth surface is required for the projection and also any dirt or gravel that may be thrown up could damage or cover the sensor lens.

Alternative non-contact velocity measurement techniques are also available, ultrasonic[30] and microwave[31] Doppler detection can provide a velocity reading. Two orthogonally mounted sensors would then provide the

Figure 2.3: GPS Satellite Orbits (courtesy of www.garmin.com)

necessary vectors. Again both could suffer from being covered by dirt, disrupting the sensors operation.

GPS

The GPS, or Global Positioning System, began life in the 1970's as a U.S. Department of Defense project with the intention to provide military units with accurate information on their position and velocity anywhere on the Earth's surface[32]. It works by having 24 satellites orbiting the earth at approximately 20,200 kilometres in six 12-hour orbital planes. This pattern ensures at any point in time, a receiver will have direct line-of-sight with four satellites[33]. The orbital configuration can be seen in Figure 2.3.

The other side of the system, the GPS receivers, measure time delays and decode messages from the in-view satellites to determine the information necessary to complete the necessary calculations to gauge position and velocity.

Despite its initial purpose as a navigational and positioning aid, recent developments and applications of GPS have seen its usage in more sophisticated analysis and measurement of dynamic behaviour.

By measuring the Doppler shift change in frequency of the signals coming from the satellites as the receiver is moved around, highly accurate relative velocity measurement can be taken[34]. Knowing the velocity and orbit of each satellite allows calculation of the velocity and heading of the receiver relative to the Earth. Xu[34] shows that these measurements can be accurate to a few centimetres a second, with both the VBox GPS unit and the Astech DG-14 unit, which use Doppler-based velocity calculation and are used in this research, reporting an accuracy of 0.1km/h or 2.6 centimetres a second[35][36]. Racelogic[37] have compared this unit to other optical velocity sensors[38] and demonstrated that such a unit could be used to replace and, in some cases, better other optical sensors which have been the industry standard in the past[12]. The accuracy of this velocity vector also results in a highly accurate measurement of heading, of the order of 0.1 degrees[35].

By combining two or more GPS antennae, it becomes possible to measure even more vehicle dynamic properties. These developments were initially driven forward in the fields of marine and aerospace engineering.

In aerospace engineering, it is useful to measure attitude angles in all three planes; yaw, pitch and roll. If multiple antennae are placed at strategic points on the aircraft, Figure 2.4, it is possible to calculate the three-dimensional orientation of the vehicle[2]. The multiple antenna solutions works by comparing the phase of the GPS carrier signals at each antenna. By assuming a planar incoming wavefront from a satellite, Figure 2.5, the orientation of the baselines between antennae can be calculated. This is also known as RTK, or Real Time Kinematics, GPS.

These methods require expensive multiple antenna configurations. It is also possible to determine attitude in aircraft using a simpler single antenna system. To resolve some of the unknown quantities, a simple point mass aircraft model has to be employed. Using this model it is possible to infer the state of the aircraft from dynamic information determined from the GPS, such as the rate of change of the velocity vector[39].

This is effectively the same concept that is applied with the new β-angle sensor although the process for road vehicles is harder due to tyre non-linearity and weight transfer effects.

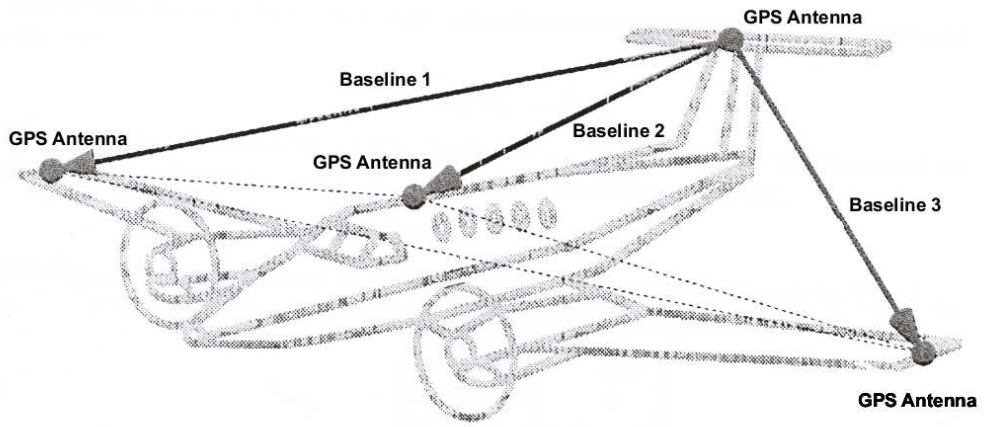

Figure 2.4: Multiple antenna mounting positions on aircraft and their associated baselines[2]

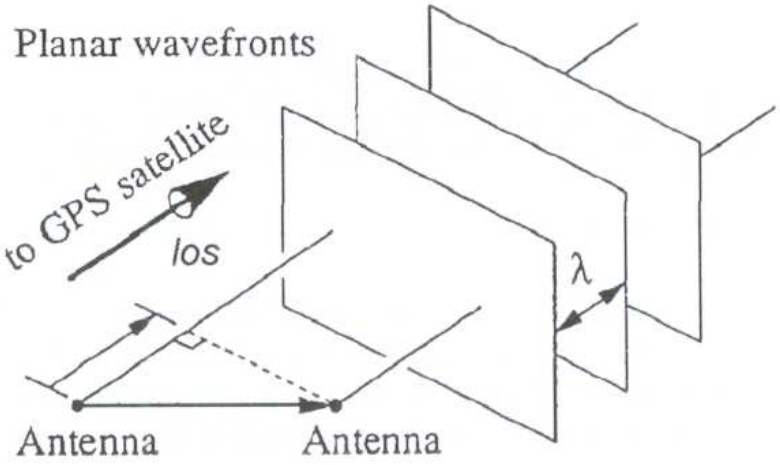

Figure 2.5: Planar incoming wavefronts - multiple antennae[3]

Figure 2.6: Multiple GPS antennae mounting on racecars[3]

Inevitably some of these techniques have crossed over to applications in the automotive field. Again multiple antennae systems can be used to now determine precise velocity, β-angle and racetrack position[3] of a race car. How[3] used a two antenna configuration, Figure 2.6, to compute these values. When compared with the three and four antennae solution employed in aircraft, using only two antenna makes it impossible to determine orientation around the inter-antennae axis. This is not significant however as a racecar is more constrained by running on a track with much less freedom to rotate than an aircraft, which results in significantly less pitch and roll.

Roll angles can also be determined in the same fashion[40] provided that the baseline axis between antennae does not run parallel to the roll axis of the vehicle.

Estimation Methods

In many situations it is not possible to directly measure certain vehicle states. However, with a basic understanding of vehicle dynamics, it is possible to estimate the value of vehicle state by combining available measurements with a simple vehicle model[41]. This builds on the aircraft example discussed in Section 2.1.3.

Bevly *et al.*[42] detailed how using a bicycle, or half-car, model it is possible to infer wheel slip ratio and side slip angle. Using a single antenna GPS for velocity vector calculation, wheel speed sensors for individual tyre rotation rates and fibre optic gyroscopes for yaw rate these values can be accurately estimated. Similarly Hahn[43] demonstrated that a similar model

could be used to estimate the tyre-road friction coefficient which is an essential in traction control systems, while Bae[44] demonstrated methods for estimating road grade.

The Bosch Electronic Stability Program (ESP) version 5[16] typifies the difficulties in reliably estimating β-angle when using it as a primary input to a safety critical control system. A dynamic vehicle model is used to estimate the slip angle for the car and each tyre from vehicle velocity, acceleration and longitudinal tyre forces. Solving the required equations is less simple and dependent on factors such as roll and pitch angle, road gradient and control input. Thus, depending on the driving situation, the accuracy of vehicle slip angle estimation is changeable.

Combined Sensor Estimation

GPS data has been combined with magnetometer data before to determine attitude angles. Crassidis[45] attempted to use three axis magnetometer data in order to quickly resolve some of the integer ambiguities in GPS calculations. Furthermore the magnetometers were used to infill between GPS data drop outs which occur when insufficient information is being recieved from enough satillites to calculate the required angles. Such disruptions in signal may occur due to interference or obstruction from vegetation or terrain.

This method used the magnetometers to assist other sensors but did not combine the output from the two in the same manner as presented in this study.

Another field relates to pedestrian navigation. Ladetto[46] demonstrated that combining magnetometers, configured as a compassing solution, with a gyroscope could increase accuracy and reliability in pedestrian navigation, particularly in areas prone to strong magnetic disturbance. In further work, Ladetto[46] continued this work by including GPS as an input to the navigation system. The notion being that the combination of sensors can produce a more reliable system over most conditions without the problems associated with inertial systems.

Gabaglio[47] followed a similar line by combining GPS measurements with

inertial sensors. Here the aim was to use each sensor as a method for dealing with errors in the other, the two were not combined to produce any additional information.

Current Methods of Estimation

As previously mentioned, the Bosch ESP system[16] is a common commercially available implementation of a stability control system that attempts to determine both β-angle and β-rate in order to use these values as inputs to its stability control system. Although a full explanation of how the system actually goes about estimating these values is commercially sensitive and not available, a overview, which does include a description of some of the problems associated with this form of estimation, is.

Again, as previously mentioned, this system attempts to estimate values of β-angle using a vehicle dynamic model and various inertial sensors. These include four wheelspeed sensors, a lateral accelerometer and a yaw rate sensor (also known as a gyro). These estimation techniques, however, are not as robust as might be expected. In reviewing the ESP system, van Zanten[16] points out that it is not always possible to obtain a reliable value of the β-angle and, at these points, the system has to rely on a seperate stability control method that is not dependent on β. In addition he points out that depending on the driving situation the accuracy of the vehicle β-angle estimation is different and changeable.

With the inertial measurements and individual wheelspeeds, ESP uses a set of equations of motion from a bicycle model to estimate β-angle from the sensor readings. In reality the system actually has a selection of different equations, each of which is tailored to a specific driving condition, such as heaving braking or free rolling, from which the system can choose in order to try and ensure the most accurate estimation of β-angle. These calculations are then heavily filtered to provide a suitable value.

Further complications with these types of estimation system result from the fact that the equations of motions used include factors such as coefficient of friction between the road surface and the tyre as well as the cornering

stiffness of the tyres on the vehicle. These combined with the problems associated with inertial measurement on WRC cars in full stage rally conditions, see sections 3.1 and 3.3.2, makes the implementation of a similar estimation technique unlikely to provide a reliable and accurate measure of β-angle in WRC conditions. In addition, given that the actual algorithms used by such systems are closely guarded secrets, the development of a similar system would be beyond the remit of this study.

As most other estimation methods for β-angle and sideslip angle[41][22] work on similar principles and are heavily dependent on inertial measurement, they are considered equally unsuitable.

2.2 The New β-angle Sensor

The concept of the novel β-angle sensor developed during the course of this research draws inspiration from various sources including Geomatics, Space Science, Aerospace and Marine Navigation. This section explores the background to the sensor and advances that preceded it.

Bevly *et al.*[42] demonstrated that it is possible to measure vehicle β-angle by obtaining the direction of the vehicles velocity vector from a GPS and comparing it to the orientation of the vehicle obtained from the integration of a yaw rate sensing gyroscope. This method has certain drawbacks, primarily due to its inertial sensing and the need to integrate the sensor signal. In a rough environment, such as WRC, the vibration and shock the gyroscope would encounter, results in a signal too noisy to provide accurate vehicle orientation information. An example of gyroscope data from such conditions is examined in Chapter 3.

The new β-angle sensor replaces the gyroscope for orientation determination with a solid state magnetometer to allow calculation of vehicle heading in relation to the Earth's magnetic field.

2.2.1 Space Science

In space science, maintaining a satellite orbital trajectory is a complicated process. Factors such as attitude angle, coning angle, spin rate and coning rate are involved. Magnetometers are commonly employed as a low-cost means of measuring such values with reference to the Earth's magnetic field[48].

In most cases the intended orbital trajectory of a satellite is relatively fixed and well known in addition to the expected magnetic field vector at each point around the orbit. Using a three axis magnetometer to sense this vector in relation to the fixed frame of the satellite, the attitude angle can be determined[49].

As multi-antenna GPS systems started to become available, these became the preferred method used to calculate the orientation of a space vehicle. In the event of a problem with the GPS signal, the magnetometer solution is still used as a fallback as the magnetic field is always available throughout the orbit[45].

2.2.2 Compassing and Magnetometers

Magnetometers are the modern replacement for the traditional compass setups of the past. As the intention is to measure the Earth's own magnetic field, anisotropic magneto-resistive (AMR) sensors were considered the best option[4].

These sensors are made of a nickel-iron (Permalloy) thin film deposited on a silicon wafer and are patterned as a resistive strip. The properties of the AMR thin film cause it to change resistance by 2-3% in the presence of a magnetic field.

Typically, four of these resistors are connected in a Wheatstone bridge configuration so that both magnitude and direction of a field along a single axis can be measured.

For typical AMR sensors, the bandwidth is in the 1-5 MHz range. The reaction of the magneto-resistive effect is very fast and not limited by coils or oscillating frequencies.

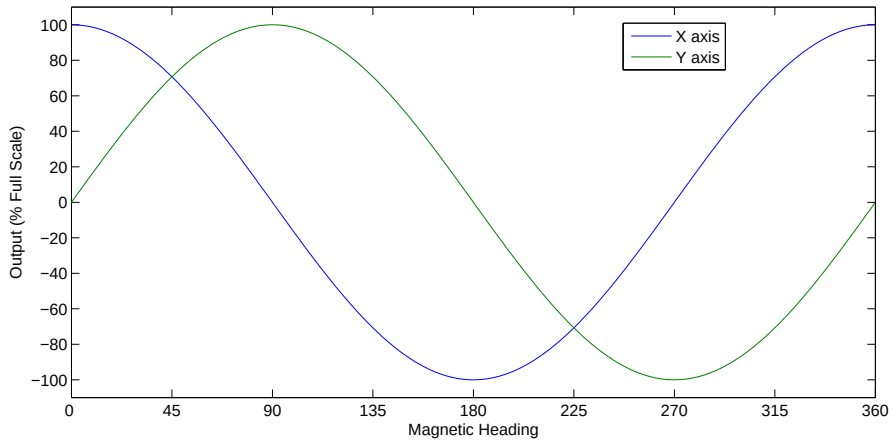

Figure 2.7: Output of two orthogonal magnetic sensors rotated horizontally in the earths magnetic field[4]

As AMR sensors are only sensitive along a single axis, two are required to measure the horizontal component of the Earth's magnetic field and determine magnetic heading. When such a sensor is spun around a horizontal plane starting from magnetic north, the output is a cosine function of the heading angle. This sensor is said to measure the Northings, or X-axis. Mounting a second sensor perpendicularly to the first, the Eastings or Y-axis, should output a sine function as shown in Figure 2.7.

Given the parametric equations for a circle of unit radius, Equation 2.2 and 2.3, it can be seen that, in idealised conditions, plotting the Northings and Eastings against each other will result in a circle.

$$x = cos(t) \tag{2.2}$$

$$y = sin(t) \tag{2.3}$$

2.2.3 Magnetometer Calibration

Unfortunately, determining heading is not quite as simple as it seems as the Earth's magnetic field is deformed and distorted by any ferrous or magnetic

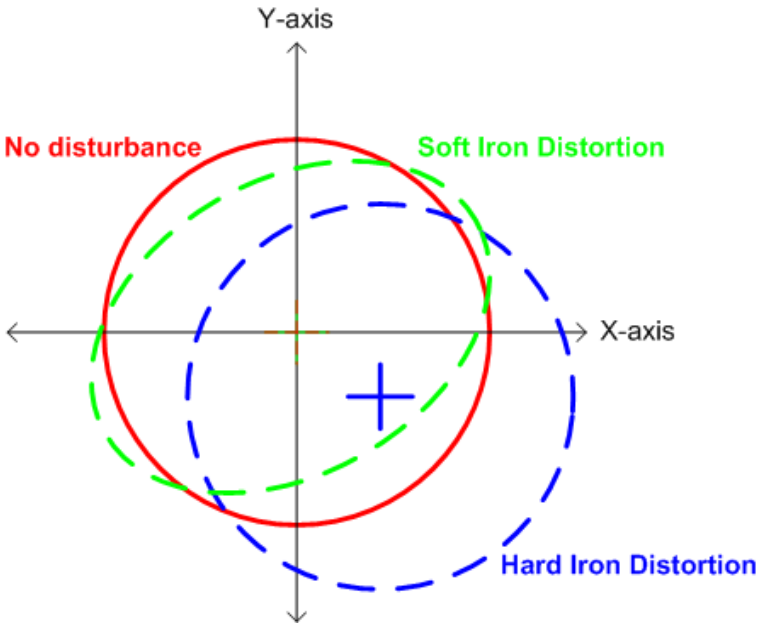

Figure 2.8: Soft and Hard Iron Distortions on Magnetometer readings

object within it. This can occur due to local geology or due to the vehicle which the sensors are mounted to. This interference can be classed as either soft or hard iron distortions[8].

Hard iron distortions arise from permanent magnets and magnetised iron or steel on the compass platform. These distortions will remain constant and in a fixed location relative to the compass for all heading orientations. This distortion causes an additional component field magnitude along each of the axis and appears to shift the origin of the output circle if X and Y are plotted relative to each other, see Figure 2.8.

Soft iron distortions are due to the interaction of the Earth's magnetic field and any magnetically soft materials surrounding the compass. The difference from the hard iron distortion being that the magnitude of the distortion is dependent on the orientation of the compass. Such a distortion will cause the output circle to become skewed as shown in Figure 2.8.

To correct for these distortions and return the X-Y magnetometer outputs to the desired circle, a simple calibration procedure can be applied[50]. Two

scale factors, X_{sf} and Y_{sf} can be determined to change the ellipsoid response to a circle. Offset values X_{off} and Y_{off} can then be calculated to centre the circle around the origin. Applying equations 2.4 and 2.5 to the magnetometer output values, X and Y will eliminate the effects of the distortions.

$$X_{value} = X_{sf} \times X + X_{off} \tag{2.4}$$

$$Y_{value} = Y_{sf} \times Y + Y_{off} \tag{2.5}$$

Caruso[50] describes a simple calibration method can be used to determine these offset and scale factor values for a vehicle mounted compassing module:

- Mount the compass in the vehicle and drive the vehicle in a circle on a horizontal surface
- Find the maximum and minimum values of the X and Y magnetic readings
- Using these four values determine the X and Y scale factors (X_{sf}, Y_{sf}) and the zero offset values (X_{off}, Y_{off}). (Equations 2.6, 2.7, 2.8, 2.9)

$$X_{sf} = \frac{(Y_{max} - Y_{min})}{(X_{max} - X_{min})} \tag{2.6}$$

$$Y_{sf} = \frac{(X_{max} - X_{min})}{(Y_{max} - Y_{min})} \tag{2.7}$$

$$X_{off} = [(X_{max} - X_{min})/2 - X_{max}] \times X_{sf}] \tag{2.8}$$

$$Y_{off} = [(Y_{max} - Y_{min})/2 - Y_{max}] \times Y_{sf}] \tag{2.9}$$

2.2.4 Combining Magnetometers with Other Sensors

Using magnetometers for compassing, orientation and dynamic property sensing has already been presented for space vehicles. Different research has seen magnetometers being combined with data from other sensors to further the potential applications for this technology.

Pedestrian (or dismounted soldier) navigation research has seen magnetometers combined with gyroscopes and GPS systems to improve accuracy and reliability when attempting to navigate using dead reckoning.

Dead reckoning is a method of navigation in which the azimuth, or heading, and distance travelled is used to determine the current position in relation to a known starting point (a fix). In most cases speed and time taken are used to determine the distance travelled and compasses give the azimuth.

Ladetto *et al.*[46] looked to overcome sensor constraints in dead reckoning systems by integrating a range of sensors including a magnetic compass, gyroscopes, accelerometers and GPS systems. The compass and gyroscope were compared as a means of determining azimuth with the conclusions being drawn that an optimal and more reliable system would consist of coupling the two. The gyroscope derived azimuth can be used to identify magnetic disturbances, while the magnetic compass can determine the bias and the gyro and initial orientation. In addition the compass does not suffer the drift that is inherent in most gyroscopic sensors.

In extending this field to look at navigation for the dismounted soldier, Gabaglio *et al.*[47] took those conclusions and implemented a combined gyroscopic and magnetic compass integrated sensor. One of the primary reasons for this being the ability to compensate for magnetic disturbances. It should be noted however that the disturbance to magnetic field is more significant as the error in azimuth increases the error in positioning as the soldier progresses. Furthermore, this research was also considering navigation within build up areas and within buildings that harbour strong magnetic fields, further reducing the accuracy of the magnetic compass.

2.2.5 The DriftBox

At the beginning of 2006, Racelogic Ltd.[37] who are responsible for the VBox[35] range of GPS systems, launched a new product - the DriftBox[51]. This unit uses a similar concept to the β-angle sensor in that the slip angle of a vehicle is measured using the velocity vector as determined by GPS and vehicle orientation. Unlike the β-angle sensor, this orientation is derived from the integration of a yaw rate gyroscope signal. This method of determining β-angle is detailed in Bevly *et al.*[42] and an investigation into this technique can be found in Section 3.3.2.

As gyroscopes are prone to drift, as well as error induced by the unit not being level, the Driftbox makes use of a zeroing algorithm to reset the gyroscope derived heading to the GPS data. Although the precise details are a closely guarded, commercially sensitive secret, the algorithm must make use of the lateral acceleration data and yaw rate to try and establish when the vehicle is at a state of zero attitude. Unfortunately this is not so simple as there are cases in which lateral acceleration and yaw rate can both be zero, yet the vehicle is still travelling with a large β-angle. To this end, it is technically possible to confuse the DriftBox and severely affect its accuracy.

Despite this, the DriftBox was intended to give an idea of β-angle to drivers whose primary intention was to 'drift' their vehicles and is not really suited to vehicle dynamic research.

2.3 Vehicle Dynamic Simulation

Having a new β-angle sensor to provide new information and understanding regarding the dynamic behaviour of a WRC car on gravel surfaces, this knowledge can be put to use improving the quality and usefulness of vehicle dynamic simulation in this field. In particular the application of experimentally derived tyre curves to simulation help to demonstrate how the optimum attitude angle in cornering is extremely tyre and surface dependent. This is the topic of the case study in Chapter 5.

2.3.1 Lap Time Estimation

Vehicle dynamic simulation has been used for as a means of lap time estimation in circuit racing for a long time. Brayshaw[9] states that there are three primary purposes to this form of simulation, to accurately model the dynamic behaviour of the vehicle, to accurately predict lap times and to produce lap simulation results rapidly in order to allow many different vehicle set up and configuration changes to be examined for a particular circuit.

Various techniques for lap simulation exist but Siegler *et al.*[52] showed that they can generally be considered to fall into three categories: steady state, quasi steady state and transient.

Steady State

The steady state modelling strategy is the simplest of the three and the vehicles lateral and longitudinal acceleration components are modelled separately. As such, no lateral dynamics are considered during straight sections of the track and no longitudinal dynamics considered during cornering.

It is clear that this is an overly simplified solution as the notion of a vehicle negotiating a corner with fixed velocity, steer angle, path radius and maximum lateral acceleration does not reflect the true behaviour of competitive racing vehicles.

Quasi-Steady State

As an extension of the steady state strategy, the quasi-steady state solution adopts a similar philosophy but instead of considering a corner to be a single curve, the path is split into a series of discrete smaller constant radius turns with decreasing path radius which simulate the increase of steer angle towards the corner apex.

At each path segment the vehicle is considered to be in a steady state. The lateral tyre force required to generate the necessary lateral acceleration is calculated and using a combined tyre model, for example the Pacejka Magic Tyre Model[53], the remaining longitudinal capabilities of the tyre are found.

This method provides a significantly more realistic approach to lap time simulation and has been used as the underlying method in discovering optimal lap times for open wheel race cars given various adjustable parameters by Brayshaw[9].

Transient

The third strategy is the fully transient solution in which the vehicle is considered to be undergoing non-steady linear or rotational acceleration[54]. This is similar to what occurs in reality as a vehicle is never in a steady state situation as it is always accelerating in a combination of the linear lateral, longitudinal or normal directions and/or the rotational pitch, roll and yaw directions.

Siegler *et al.*[52] compared the three simulation techniques as a means of performing lap time simulation. In concluding, it was shown that the steady-state model was far too simple to provide realistic results. The quasi-static and transient models overcame these limitations but without the fully transient solution it is not possible to take into account all vehicle factors.

Simulation for Rallying

As the transient solution considers the change in attitude and direction of travel of the vehicle, it is the only one of the three strategies that provide the necessary capabilities to investigate the complex yaw dynamics and high β-angle manoeuvres seen in WRC-style driving techniques.

In the case of rallying, lap time simulation is not directly relevant and a different set of priorities for simulation have to be considered. While it is still important to accurately model the dynamic behaviour of the vehicle, the different nature of the course over which rally cars compete make the notion of lap time simulation redundant. In these circumstances it becomes more important to model the general performance envelope of the vehicle in generic circumstances rather than specific circuit modelling. Rapid simulation time is still important due to the need to perform parameter sweep simulations to investigate the dynamic trends of the vehicle under extreme manouevring

conditions.

On loose gravel surfaces, the driving style adopted results in high attitude angles and makes the yaw dynamics of the vehicle on gravel an important area to investigate. As a transient simulation takes into account the response time of the vehicle in changing its attitude and direction of travel, allowing dynamic yaw effects to be considered[52], this method was chosen to simulate a WRC car in all case studies.

2.3.2 Modelling a WRC car

To develop the vehicle dynamics WRC test car model used in this study, a multibody approach as described by Harty[55] and Sharp[56] was employed. This method describes the vehicle model as a collection of individual bodies that are in someway connected and have a series of specified constraints on their freedom to move in relation to each other and the surrounding world.

Despite starting with simple components, such an approach has been shown to be highly effective at modelling extremely complex systems and, by coupling this concept with simulation techniques from different fields, such as aerodynamics or structural mechanics, this technique is often first choice for multidisciplinary vehicle dynamic simulation[57].

The AutoSim[58] software package is one example of a multibody simulation system (others include MSC Adams[59] and SIMPACK[60]) and was used to define the bodies and constraints of the model. AutoSim takes this information about the bodies and derives the equations of motion for the system as a whole, which can then be supplemented with additional models for powertrain[1], weight transfer[61], aerodynamics[61] and tyres[53] to build a realistic vehicle model.

Previous research by Brayshaw[9] and Casanova[62] used the multibody approach in the development of various transient and quasi-steady state simulations of open wheeled race cars. Both models were validated and shown to closely mirror that of their real world counterparts as well as providing the capabilities to perform various dynamic investigations and studies. The WRC model is derived from the 7 degree of freedom model initially imple-

mented by Casanova[62] and later refined by Brayshaw[9]. The model is described in greater detail in Chapter 4.

2.3.3 Driver Modelling

In addition to modelling the vehicle accurately, it is also essential to recreate the actions of a human driver to provide realistic control inputs to the vehicle model. This study required two forms of driver control for simulations, the first producing the desired time-history control input from a simple look up table, the second requiring a more complicated path-following algorithm.

Research into mathematical driver algorithms began in the early seventies[63] and generally concerned themselves with the concept of preview information.

Different driver models have been reviewed by Guo and Guan[64], in particular highlighting those utilising single point preview and showed that preview information is needed for satisfactory modelling of the vehicle/driver system.

Later, Brayshaw[65] in considering potential driver models for simulation, concluded that it was clear that non-linear feedback control with preview information and knowledge of the on-limit vehicle dynamics was necessary for the racing driver to be successful in high speed manoeuvring.

This lead to Brayshaw, and subsequently this study, implementing the empirical driver model of Sharp *et al.*[56] to model the on-limit behaviour of the driver for path following simulations. This method does not require a linear vehicle model and was originally implemented on an open wheel race car but only required minimal adjustment to ensure robust non-linear preview path following control for the WRC model. Further information on the implementation of driver models in this study can be found in Chapter 4.

2.3.4 Tyre Force Curve Inference

Tyre data is essential in motorsport to maximise vehicle performance and large proportions of motorsport teams budgets can be spent trying to improve the tyre and the vehicles use of it. Such information can either be

Figure 2.9: Bridgestone's MTS Flat-Trac Tyre Testing System[5]

obtained from laboratory rig testing or through experimental testing on fully instrumented sports cars[5]. This study is primarily concerned with inferring lateral tyre force against slip angle curves.

Laboratory Rig Testing

In order to generate a lateral tyre force against slip angle curve, various manufactuers have large sophisticated rigs that all work in essentially the same way. By mounting the tyre to be tested on a rolling road and applying a specified vertical load, the lateral force being generated (trying to push the tyre off the rolling road) can be measured. By rotating the tyre carcass with respect to the rolling road surface, different slip angles can be induced.

One example of such a machine is the MTS Flat-Trac tire testing system used by Bridgestone in their motorsport activities. Figure 2.9 is a picture of the Flat-Trac rig with the tyre to be tested at the centre just above the

rolling road. In addition to applying varying vertical loads of up to 3000kg, the rig can also be configured to produce data for varying camber angles and measure self-aligning torque at speeds of up to 200mph.

Unfortunately, these rigs suffer a few drawbacks. The rolling road can simulate a tarmac surface but can not simulate the rough loose gravel surfaces that are of more interest to rally engineers. Also only slip angles in the range of ± 30 degrees can be tested using such rigs[5]. Although 30 degrees of slip is extreme for circuit racing, it is often exceeded in rallying.

Once the rig has determined the lateral forces generated within its range of slip angles, the curve can be fitted to the Pacejka Magic Tyre[53] model and relevant coefficients determined to give an accurate simulation model for that tyre.

The Silsoe Off-Road Dynamics Facility

At the beginning of 2006 the Silsoe Off-Road Dynamics[66] facility was opened with the intention of developing tyre testing rigs for the off road environment. During the course of this study, details were not readily available but the facility has been designed to include off-road tyre performance measurement and characterisation, vehicle drag, thrust and slip quantification and traction surface creation and evaluation. This includes the production of similar tyre data to that demonstrated from the new β-angle sensor and may, in the future, provide a more controllable laboratory-based alternative to the procedures developed in this work.

The key elements of the apparatus in this facility are:

- A whole vehicle controlled moisture soil lane
- A mobile single wheel test apparatus capable of the precise control of wheel torque, vertical load and wheel speed in a wide range of offroad and on-road test environments.
- A variable plane four wheel articulation rig for the measurement of wheel load and static thrust across a wide range of axle articulations.

- A Smart Winch capable of applying precisely controlled loads up to 100kN and 50m on a vehicle

However, use of this facility would be a more expensive option with specific testing for this purpose, whereas, the method defined in this study can be quickly and easily included to a current test program. Furthermore this facility may not be able to replicated conditions seen in full WRC testing.

Despite this, it is a development that may prove a complimentary tyre testing methodology for loose gravel WRC-style environments.

Track Testing

Despite the complexity and continuing development of tyre testing rigs, the importance of dynamic factors in tyre performance, of which there is limited knowledge means that track testing has a valuable place in motorsport engineering. It is said that "the best tire testing machine is a fully instrumented F1 car"[5] but even this has its limitations.

Rowley[6] goes into great depth describing the complexity of development of tyre maps in the racing world, showing how these maps are developed from a combination of manufacturer data and track testing. Rowley breaks track testing down into three components, skid pad, inline and circuit/race track testing.

In all tyre testing, the primary factor is the force produced by the tyre for a given normal vertical loading. This information provides a simple description of what can be expected from the tyre in any given dynamic condition although it does not take into account many secondary factors such as:

- Tyre temperature
- Speed
- Camber angle
- Tyre inflation pressure
- Tyre wear

- Transitional effects on vertical load

Rowley[6] states there may be sixty or more of these secondary factors that may influence the tyre map although, in reality, it is not necessary to consider them all unless a very complete and accurate tyre map is required.

Skid Pan

Although Rowley[6] describes a rather complicated algorithm (Figure 2.10) for the mapping of tyre data from skid pan tests, the principle behind it is quite simple. The concept involves driving the test vehicle around the skid pan in a constant steer angle manoeuvre. Having reached an equilibrium state which can be considered to be the maximum lateral acceleration for that vehicle in that manoeuvre, the steer angle and corner loads are recorded.

Through calculation it is then possible to develop what Rowley[6] calls 'corner tyre factors', or in other words the lateral force contribution of each tyre. By repeating the process for various steer angles, each time determining the maximum speed at which the manoeuvre can be achieved, and repeating the calculations to build a complete map.

Inline

Inline testing is used to determine longitudinal capabilities of a tyre through straight line acceleration and deceleration. Again despite the complexity of Rowley's[6] algorithms, the basic premise is to determine the slip ratio of the tyres through measurement of axle torque and loaded tyre radius velocities as well as determining longitudinal force components from the acceleration. Repetition is then employed to build up a complete map of the tyre characteristics longitudinal characteristics.

Circuit/race track

Circuit/race track testing involves refining the tyre maps developed during skid pan and inline testing by comparing the expectations with what is seen

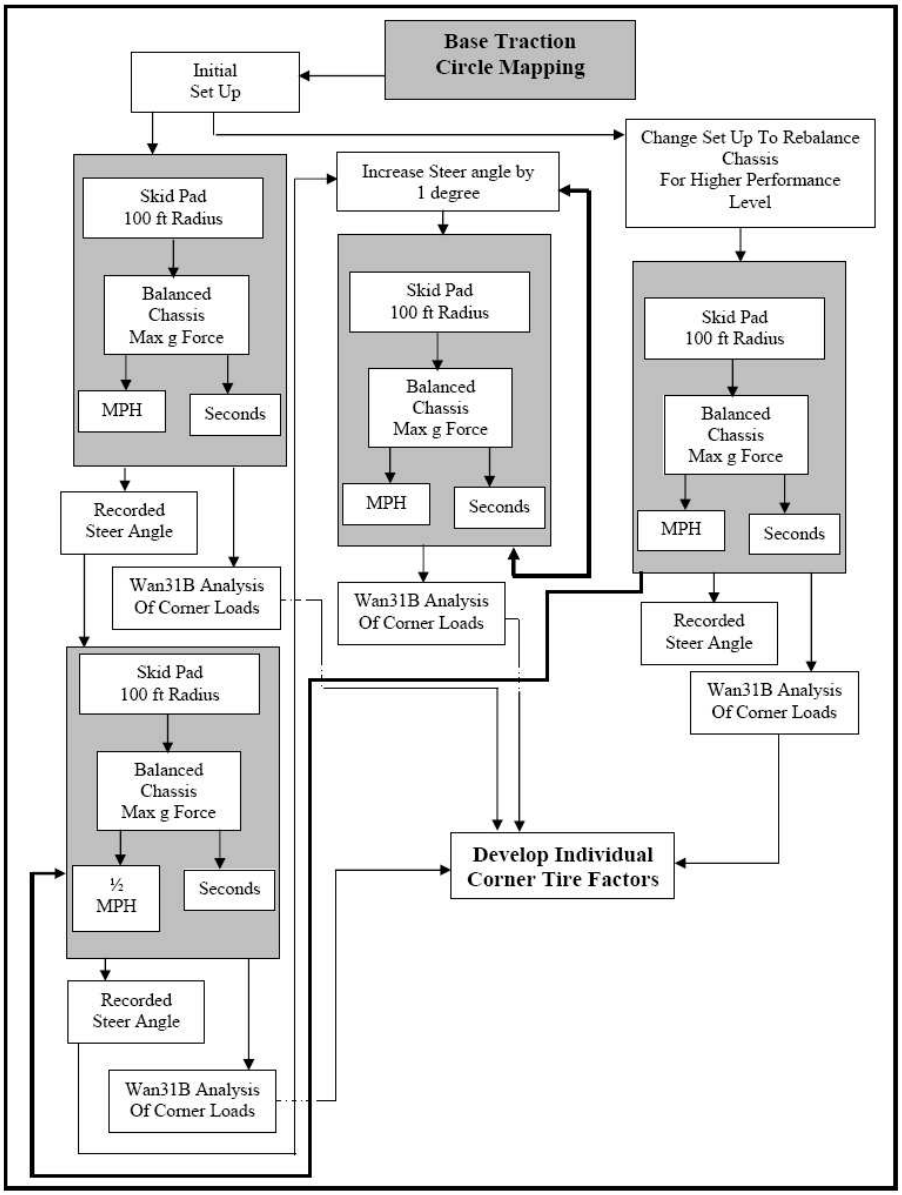

Figure 2.10: Rowley's Base Lateral Acceleration Procedural Algorithm[6]

from telemetry during circuit testing. A notion of best fit is employed to the data to ensure that all maps are, to some extent, realistic of what can be expected.

Although the tyre curve inference found in Chapter 4 is not based on Rowley's[6] processes, it does share some common ground. The elements of testing are similar although, whereas Rowley[6] is determined to develop a highly accurate map for the limited case of circuit racing, the curve inference techniques in this work are more interested in increasing understanding of tyre behaviour in more extreme conditions that are much less understood. The end result being that although the exact tyre forces may not be accurately found, the ability to quantitatively compare different tyre configurations is now possible where it was not before.

Chapter 3

The β-angle sensor

This chapter describes the development of a novel form of sensor for vehicle β-angle that is particularly suited to WRC environments and gravel surfaces. The construction, calibration, testing and validation of a prototype are detailed.

3.1 Introduction

It has already been shown that β-angle is important in the theory behind traction control and vehicle stability systems and that measuring the angle is also quite a difficult procedure. The primary means being the use of a vehicle dynamic model combined with some form of inertial sensing[16], or for more sophisticated applications, optical instrumentation is available[12].

Experience in WRC however has shown that inertial sensors suffer from severe noise on the rough surfaces that are common place. Even with sophisticated filtering, it is still not possible to obtain useful results after integrating the signal in an attempt to determine an accurate value of lateral speed and hence the β-angle. Figure 3.1 demonstrates this level of noise and is taken from a section of gravel data where the vehicle is travelling in a straight line. As it can be seen, the lateral acceleration measured fluctuates wildly between -0.2 and 0.2G, or about one sixth of the total lateral range of the vehicle.

In addition, optical sensors are prone to the loose surfaces effectively sand-

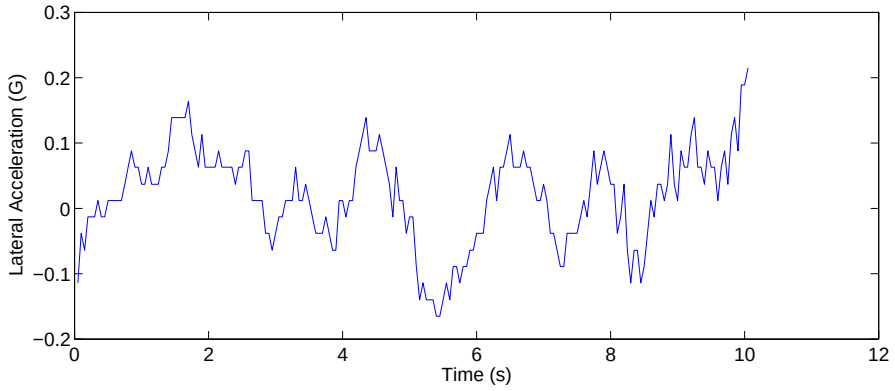

Figure 3.1: Lateral Acceleration noise for straight line motion (gravel)

blasting the lens and rendering the sensor blind. Ultrasonic and Microwave sensors are also very quickly covered in a layer of dirt that restricts their accuracy.

To overcome these shortcomings, a novel form of sensing technology was developed.

In difference to the current methods for measuring β-angle presented in Chapter 2, the new sensor does not use optical or inertial technologies nor does it require expensive multiple antennae or differential GPS with a simpler single antenna solution proving sufficient. Although various concepts in marine navigation and satellite technology consider similar ideas, there has not to date been any published suggestion that the β-angle can be measured in the same manner as the new sensor.

3.2 Principle Behind the Sensor

As equation 2.1 states, the β-angle is the inverse tangent of the lateral velocity divided by the longitudinal velocity of the vehicle. This, however, can also be considered equivalent to the angular difference between the direction in which the vehicle is pointing and the direction in which it is travelling. Therefore if the two vectors can be measured independently of each other, a value for β can be obtained.

The inspiration for the sensor came from a discussion with a colleague regarding space science where knowing the attitude angles of satellites is essential to maintain the desired orbital trajectory. Using magnetometers the orientation of a satellite can be determined relative to the Earth and comparing this with the a priori knowledge of the orbital path, attitude angles are obtained[49]. It was thought that a similar approach could be applied to a ground based vehicle, such as a rally car.

Part of the telemetry sensor configuration already in use on WRC cars includes a GPS system which provides accurate measurement of the vehicle velocity vector through Doppler-shift analysis of satellite signals. This vector is considered extremely accurate[38] and is independent of the orientation of the vehicle to which it is mounted. The GPS system uses this vector to provide a geographic heading value of the velocity vector.

To gauge the alternative heading, that is the direction in which the vehicle is pointing but not necessarily travelling, a compassing system has been employed. In contrast to the floating magnetised needle used in most navigational compasses, a more accurate and sophisticated approach was adopted.

Magnetometers form the basis of modern compassing systems and measure the direction of the local magnetic field vector. In the case of the rally car, that is a combination of the Earth's magnetic field and the distortion and interference due to the car's own magnetic properties. The determination of actual compass heading requires that these car induced effects are filtered out.

In addition, the three-dimensional nature of the field and the freedom of the car to pitch and roll adds further complications to the equations that govern the calculation of the heading angle.

This sensor will measure β-angle at the point where the GPS antenna is attached to the vehicle. This is an important consideration as the velocity vector and hence the β-angle can vary between the front and the rear of the vehicle. The mounting position of the magnetometer is less significant as the orientation of the vehicle body does not change depending on where it is measured.

3.3 Design of the Sensor

3.3.1 GPS

Although initial studies were performed using the VBox[35] GPS unit, in particular the results shown in Figures 3.21 and 3.22, the system used in later experiments was based on an AshTech DG-14 GPS Board[36]. One of the main reasons for changing from VBox to Ashtech was due to the 20Hz data sampling rate each box could produce. In the case of the VBox, the module actually had a 5Hz GPS engine[35] and then uses an interpolation process to add additional sample points to the datastream, resulting in an apparent 20Hz sampling rate. This caused particular problems when the heading signal changed from 0 to 359 degrees as the interpolation would insert an additional 180 degree data point between the two when attempting to log at a rate of 10Hz.

The Ashtech board provided the same functionality but can provide true 20Hz data rates, with the latency between receiving a satellite signal and processed heading information being approximately 6ms. The change to the AshTech unit was also due to its more modern design and it being already integrated into the WRC test car telemetry system.

As these GPS units were already part of the standard telemetry setup on the WRC test car, there was no initial requirement to modify or alter their configuration. In later experiments it became clear that replacing the antenna's magnetic mounting with a non-magnetic alternative would be beneficial in removing the presence of a strong magnetic field in close proximity to the magnetometers.

3.3.2 Gyroscopic Heading Measurement

The integration of yaw rate, measured using a gyroscope, gives an alternative means of determining vehicle orientation. This particular method is employed in Racelogic's DriftBox[51].

Despite this, using gyroscope data was not considered for this study as integrated gyroscope data is prone to drifting due to error in the yaw rate

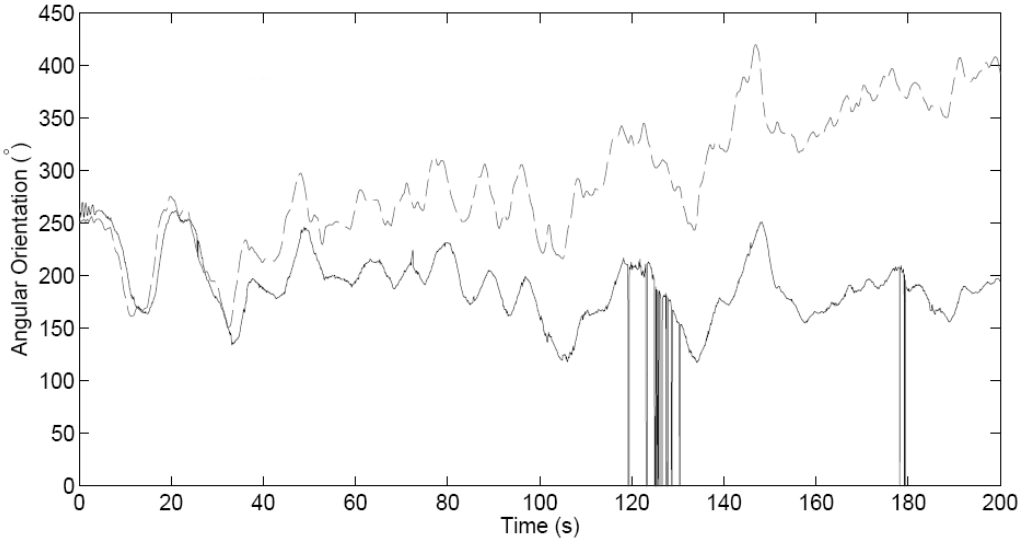

Figure 3.2: Comparison of GPS and Gyroscope-derived Heading Telemetry (—— GPS, – – – Gyroscope)

measurement. That is, over time, the integrated value for vehicle orientation will slowly move further and further away from the actual value. This is shown in Figure 3.2 which is taken from a WRC car and shows both integrated gyroscope data along with GPS heading. It can be seen that the signal drifts at a rate of about one degree per second from the GPS signal. The gyroscope angle has been set to start at the same value as the GPS heading.

This GPS data also demonstrates the problem of satellite signal drop-out. Just after 120 seconds and before 180 seconds in Figure 3.2 the GPS heading value drops to zero degrees. This is the default heading for times when the GPS unit is not receiving the required signal information from enough satellites to allow the true value to be calculated. Some signals may be being blocked by dense vegetation or mountainous terrain but, as soon as the signal is reacquired, the heading returns to the correct value. As can be seen from the data, the signal drop-out only lasts for a few samples and is quickly restored.

It would be possible to apply a linear correction factor for this drifting

after the drift rate has been established but the error in measurement can also be affected by pitch and roll which is not linear in the short term. Acceleration should not cause a problem but, if the gyroscope is tilted, it is possible for it to measure more or less rotation that the vehicle has actually performed. Unlike magnetometers, where the signal does not require integration, returning the gyroscope to the level plane will not undo the error that had been induced.

For a complete and accurate heading solution using gyroscopes, it would be necessary to measure rotation in all three axes to determine 3D orientation rather than just heading. Furthermore, the accuracy required is currently only possible using Fibre-Optic or Ring Laser Gyroscope[67] technology, both of which are considered far too expensive, bulky and heavy for this purpose. For these reasons it was not considered further for this study.

3.3.3 Magnetometers

As the magnetometer modules measure ambient magnetic field, it is necessary to ensure that the unit remains horizontal with respect to the Earth to ensure an accurate heading value.

Gimballing is the process by which pitch and roll error is removed from magnetic compass designs and can take the form of either mechanical or electrical solutions. The mechanical option involves placing the sensor in a complicated frame that maintains the sensor's orientation as the vehicle to which it is fixed moves. This method is highly effective in shipping where accelerations are low and vibration is not a problem. Producing a mechanical gimbal for a WRC environment would be a significant engineering problem and would result in a bulky and heavy unit and is therefore not practical.

As a mechanically gimballed compassing solution was not possible, a strap-down electronically gimballed magnetometer unit was required. This unit needed to measure all three axes of the ambient magnetic field in order to provide the level of accuracy in vehicle heading that was required.

The Honeywell HMC2003 Three-axis magnetic sensor[7] module was chosen for the implementation of a prototype sensor.

The HMC2003 combines three permalloy magneto-resistive sensors mounted orthogonally to each other and provides the required accuracy and resolution for this purpose. The unit provides three analogue voltage outputs, which are automatically filtered by a 1KHz low pass filter.

A drawback of the technology used in the HMC2003 is that the readings of the unit will slowly drift with time and proximity to any large magnetic fields. It is possible to reset the sensors using a brief high current pulse applied to the unit whenever this becomes significant. As part of the validation process, the rate of drift was investigated and shown to be within acceptable bands if the unit was reset on a daily basis.

Also considered was the Crossbow CXM113 module[68] which used flux-gate magnetometers. This module was dismissed however for various reasons including its reduced accuracy, smaller dynamic range and greater susceptibility to extreme temperatures that may be experienced in WRC. Despite this the CXM113 does not suffer from drifting like the HMC2003.

Other magnetometer modules are available that are designed to function as strap-down (non-gimballed) compasses, such as the Honeywell HMR3000[69]. These were quickly dismissed though as the need to correct the heading output for any pitch or roll of the unit is performed by including two inclinometers onboard. In static conditions these provide a reasonably accurate measure of orientation, however, in WRC conditions, the inertial nature of the inclinometer makes them susceptible to vibration and significant reduces their accuracy in the same manner as seen with accelerometers. Furthermore any lateral or longitudinal acceleration applied to these modules will manifest itself as a false inclination reading.

Pitch and roll correction calculations are described in section 3.5.4.

3.3.4 The Prototype

Figure 3.3 shows the prototype unit containing the HMC2003 module, Figure 3.4, as used in all experimental test runs. The unit has two connecting cables. The first providing the three analogue output voltages (X, Y and Z) as well as +12V supply and reference ground connection, marked as Xout,

Figure 3.3: Prototype Magnetometer Sensor

Yout, Zout, V+ and Gnd respectively in Figure 3.4. The second cable provides a connection to the sensor resetting circuitry in the module and can be pulsed using a separate pulse generator, again SR- and SR+ in Figure 3.4.

Although the HMC2003 also has Offset straps to apply an incident magnetic field to each axis measurement and pre-amplified trim outputs, only the five connections mentioned above were used for this study with any signal adjustment being performed within the data logger and with post-processing.

The HMC2003 module was mounted within an IP65-rated[70] polycarbonate weatherproof enclosure which was intended to protect the unit against any ingress of water or dust. Also the polycarbonate nature of the box meant that it itself did not interfere with the magnetic field or the measurement of it by the contained module. Each module was securely mounted within the enclosure to reduce the risk of damage due to vibration. Despite the wet, dusty and rigorous testing conditions, the unit remained in perfect working order throughout all tests.

As the sensors of the HMC2003 are fabricated using Permalloy (NiFe) thin films, that create changes in resistivity with respect to external magnetic fields, strong magnetic fields can disrupt the magnetic domains of the film particles from a smooth factory orientation[71]. Accuracy and resolution of these sensors will suffer until the film magnetic domains are reset to recreate

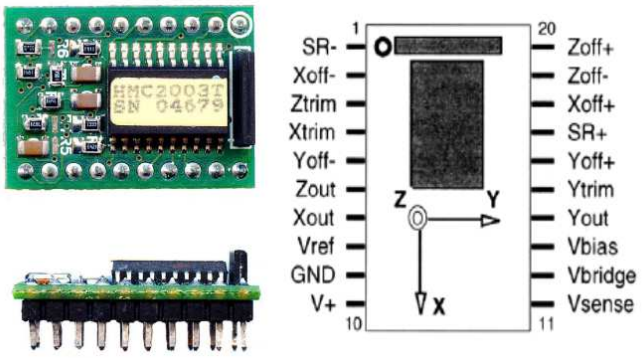

Figure 3.4: The HMC2003 module and Pinout Diagram[7]

a uniform direction.

Resetting the sensors involves applying two high current pulses (approximately 4amps) between the SR+ and SR- pins of the module. This current flows through a coil wrapped around each sensor, exposing it to a magnetic field in excess of 40 Gauss which realign the magnetic domains of the sensor. The induced field of these pulses are significantly higher than the ± 2 Gauss operating range. The specifications for this process are set out in the AN-213 Honeywell datasheet[71].

Each pulse lasts only 40 nano-seconds and frequently application is recommended by the sensor manufacturers to ensure maximum sensitivity. To accompany the sensor used in each test, a set/reset module was designed and developed that could be connected to the SR+ and SR- pins to generate the required pulses from a 12V supply. Part of the purpose of each test was to determine how frequent this process was required to ensure the desired performance of the magnetometer.

The circuit used to generate the required pulses is shown in appendix A.

3.3.5 Logging

Both GPS and the three magnetometer output voltages were logged at a sampling frequency of 10Hz using the Pi LCS Data logger[72] and chassis control system that was already fitted to the WRC car. Although capable

of performing the calibration and calculations necessary to produce a β-angle data channel, the LCS was configured to simply log the data as all calculations were performed in post-processing. This was due to restricted access to the LCS at the time of testing.

The sampling frequency was set at 10Hz as the natural yaw frequency of this class of vehicle is around 1-2Hz[1]. 10Hz, therefore, provided suitable oversampling to allow β-angle behaviour to be analysed whilst trying to reduce the size of the dataset.

It was also noted that at 10Hz, the 6ms of time required by GPS box to calculate heading from the raw satellite signals is not a cause for concern.

3.4 WRC Testing

This study benefits from direct personal participation in the activities of the WRC test team because access to a test vehicle and data (both telemetry and vehicle configuration information) is usually extremely restricted. The development of this sensor was privileged to be fully integrated into the WRC test procedure at all stages and the richness of the data obtained helped towards gaining a more realistic view of the dynamics of this class of vehicle in a competitive environment than has been previously possible.

3.4.1 Construction

Each WRC test vehicle is built specifically for the conditions of the relevant test. At the build stage it was possible to specify various factors such as the β-angle sensor mounting position, surroundings, connection to the vehicles telemetry system and configuration of the data logging and additional sensors that could provide valuable insight.

In addition to input regarding vehicle configuration, feedback also provided the necessary information to tune the vehicle dynamic model used in calculating factors such as pitch and roll, yaw inertia, weight distribution and vertical wheel loading. This was important as the sensor was tested on two occasions with two very differently configured test vehicles, the first for

gravel and the second for tarmac.

Once each test vehicle has been completed, usually the day before being shipped to the test, it is put through a procedure known as shakedown.

3.4.2 Shakedown

For the shakedown, each test vehicle is driven from the factory to an airfield near Kirkbride in Cumbria. The purpose being to run the vehicle at full speed through various manoeuvres to ensure that the vehicle has been put together correctly and nothing has been forgotten or incorrectly installed.

At shakedown all key systems, sensors and components are tested but it was also possible to perform some of the calibration procedures at the same time. This is an advantage as it is not necessarily always possible to perform such procedures when at the test. This is due to time restrictions or limited facilities at the test location.

The airfield provides a flat level surface large enough to drive the test vehicle in large slow circles that generated the magnetometer calibration circles seen later in this chapter.

Following shakedown, assuming everything works as expected, the test vehicle is crated up and shipped to the location of the test. Given the expense of both test vehicle and the logistic cost of running a fully staffed test, shakedown is vital to reduce the risk of the vehicle not working on arrival.

3.4.3 Gravel Test

In February 2005, the β-angle sensor underwent its first WRC test. The test was a standard gravel test run on mountainous roads just outside Malaga in Spain and the conditions were very wet and the drivers described the course as being rather slippery.

The realities of the conditions at a WRC test mean that controlled and consistent manoeuvres are not possible. In order to produce valuable results for the rest of the engineering team, the test team attempts to recreate a special stage as it would be on an event. In this case, the test was run on

a long closed gravel road course at full speed with the driver simply turning round and coming back at the end of the course.

Between each run the telemetry is offloaded and quickly checked to ensure nothing has broken. Then, depending on the test schedule, the vehicle setup is adjusted before being sent out on another run. The advantage of this being the realism of the test data and the confidence that if the sensor can survive these conditions it should survive a full rally. However, the disadvantages include the difficulty in producing consistent conditions and clean data.

This first full test for the sensor was intended to ensure that the magnetometer module could survive the rigours of being shaken about at high speed for a lengthy period as well as to investigate the accuracy of the sensor's output. The issue of sensor drift in the magnetometer was also considered with the unit being reset at the beginning of each day. It was found that the sensor did not suffer from significant drift between each reset pulse, determined by comparison of sensor voltages at the beginning and end of each day. Also the sensor was found to be resilient under the conditions, continuing to work as desired throughout the three days of testing.

3.4.4 Tarmac Test

In February 2006, the β-angle sensor was put through a scheduled tarmac test. The location for this test being just outside Barcelona in Spain.

Following the first test, various issues were identified that could be refined in the second test to provide better results. The magnetometer positioning and surrounding was adjusted to reduce the interference with the magnetic field measurement and steps were taken to improve pitch and roll correction including the logging of GPS vertical velocity.

The test was run on a dry tarmac closed road course over 4 days. Again the sensor did not show any adverse reactions to the conditions and performed as expected throughout the test.

3.4.5 Additional Test Data

In addition to the two scheduled tests that this study was permitted access to, a set of telemetry data from a fully instrumented test vehicle was available. This data also included a β-angle measured using a Correvit optical sensor on the tarmac skidpan at the Millbrook proving ground.

The Correvit did not suffer from the problems previously identified in this test as it was performed on tarmac and the manoeuvres were not performed at full rally stage speed.

This test data was generated in a more controlled environment with clear simple manoeuvres performed with different vehicle configurations and therefore noise levels are significantly reduced.

3.5 Calibration Routines

The GPS unit was supplied pre-calibrated and required no configuration or setup.

The magnetometers in comparison required significant calibration.

3.5.1 Sensor placement and surroundings

As the purpose of the magnetometer is the measurement of the Earth's magnetic field, any local distortion due to the presence of the ferrous chassis and magnetic fields associated with the car have a clear effect on the accuracy of these measurements. The calibration routines will remove these distortions but by careful consideration of the placing and surroundings of the sensor, it is possible to minimise distortion.

Magnetic field distortion diminishes rapidly with distance from the source of interference. As such by mounting the magnetometers as far as possible from the main sources of local magnetic fields and large ferrous objects can help in reducing their influence. Figure 3.5 is for illustration purposes only but demonstrates this effect on the Earth's magnetic field due to the test vehicle.

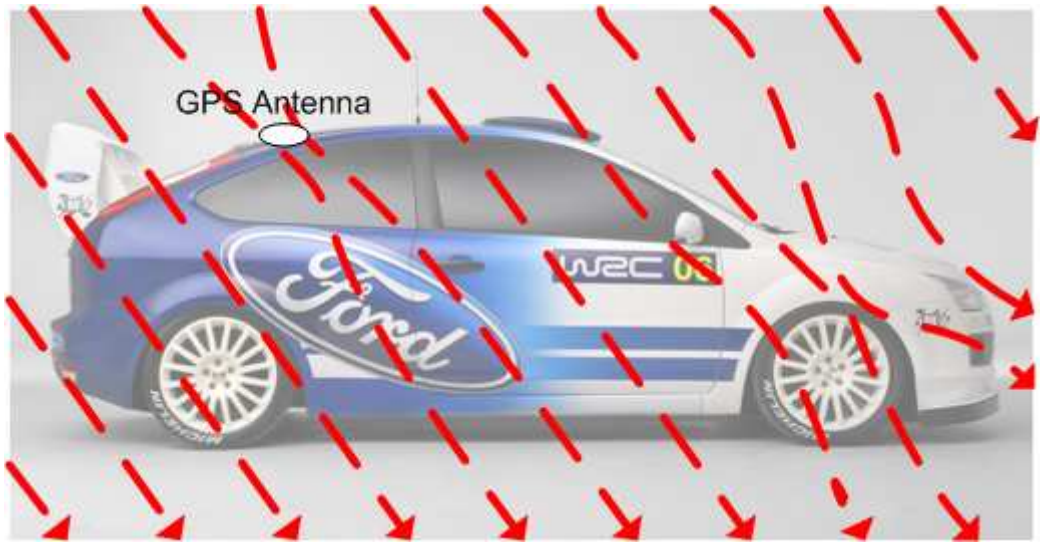

Figure 3.5: Magnetic field distortion due to Engine and GPS Antenna (Original photo courtesy of www.fordteamrs.com)

In initial testing, a compromise was required. The car chassis has an effect, but by far the most significant contributor to distortion of the ambient magnetic field is the engine. Distance from the engine is therefore an important factor, although the GPS antenna used in initial testing was mounted to the top rear of the car roof using a very strong magnetic base.

In later experiments, the magnetic GPS antenna base was removed and the magnetometer unit moved to the extreme rear of the test vehicle. This placement, shown in Figure 3.6 showed significant reduction in the level of interference experienced, which can be seen by the reduction in Z-axis variation with heading. In part, mounting to the wing was also beneficial as it is constructed from carbon fibre, which is a non-magnetic material.

3.5.2 Vehicle Chassis and Engine Interference

As previously mentioned, the chassis and engine will generate some magnetic interference. Routines were developed which, through rotation of the test vehicle, would allow the two components of the Earth's and the car's magnetic fields to be separated and the car's field effects removed.

Figure 3.6: Initial and Optimal magnetometer placement (Original photo courtesy of www.fordteamrs.com)

3.5.3 Calibration by Rotation

Section 2.2.3 detailed a process described originally by Caruso[50] which could be used to perform a 2-axis calibration of the magnetometers to alleviate interference due to the vehicle chassis and engine. This process was carried out on a test vehicle undergoing shakedown at a flat and level Cumbrian airfield. The X and Y axis sensor voltages are shown in Figure 3.7.

Figure 3.7 shows clearly the distorted circle as expected but it also shows two slightly different circles. On further investigation of the telemetry from this test, it was discovered that the first rotation manoeuvre was performed at approximately 3ms^{-1} and the second at 10ms^{-1}. At the slower speed the vehicle is experiencing only a small lateral acceleration and due to the stiffness of the suspension, the roll angle induced can be considered to be very close to zero. At 10ms^{-1} however, the lateral acceleration required to maintain the circular path is significantly larger and hence the vehicle experiences a higher roll angle. The rotation of the sensor in the Earth's magnetic field caused by this roll angle affects the measurement of the circle.

Using the information about the vehicle provided by the test team, which included roll stiffness, approximate roll centre and location of centre of gravity, the roll angle could be calculated[10] for this vehicle at this value of

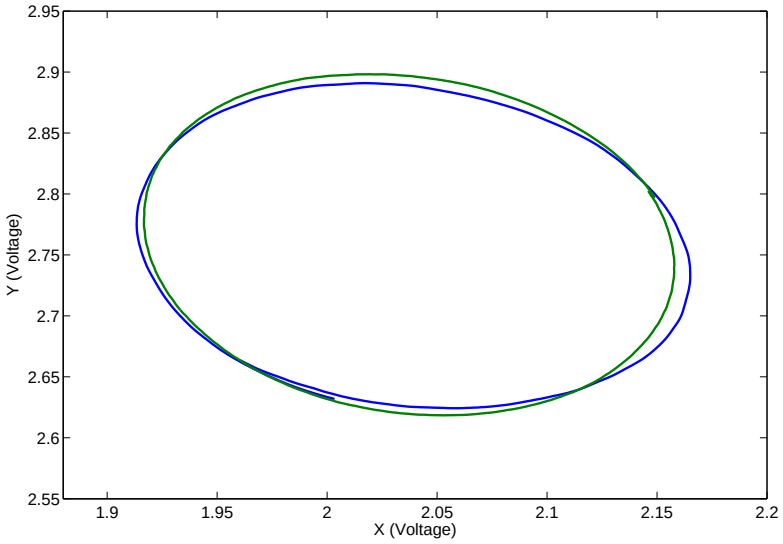

Figure 3.7: Low speed turning calibration tests

lateral acceleration. In this case it meant a roll angle of approximately 2°.

Despite the error induced by the roll angle, the transcribed circles are clear and not affected by excessive noise. What's more, the circles are consistent if the vehicle continues to drive round at the same speed. Distortion due to the magnetic interference of the chassis and engine can be seen as the circle is slightly elliptical and off centre (the sensor's zero output being +2.5 volts in both X and Y) but the application of appropriate X and Y scale factors and offsets remove this distortion as expected.

Therefore, using the calibration process an accurate, reliably consistent, relatively noise free heading calculation can be performed provided the sensor can be levelled either mechanically or electronically to remove pitch and roll induced error.

3.5.4 Pitch and Roll

During initial testing of the prototype a simplified 2-axis magnetometer calibration and heading calculation, as described in Section 2.2.3, was employed.

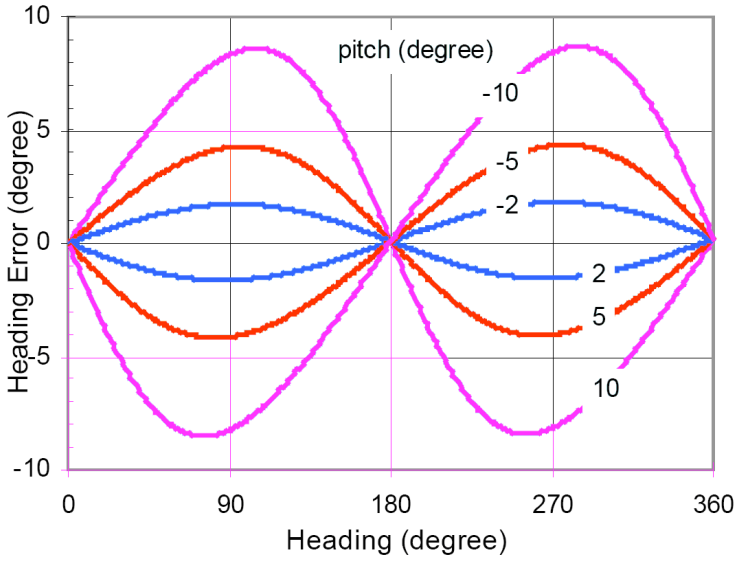

Figure 3.8: Error in heading calculation due to sensor pitching[8]

Although the sensor performed without any technical fault throughout the initial tests, the limitations of the 2-axis magnetic heading calibration system resulted in potentially unacceptable levels of error in the β-angle measurement due to the rotation of the platform (car chassis) about its X and Y axis (pitch and roll). This problem is overcome through a process of electronic gimballing and the adoption of a three-axis magnetometer module.

Pitch and Roll Error

The pitch or roll of the magnetometer unit produced a heading error the magnitude of which depending on the inclination of the magnetic field at that geographical location and the vehicle heading. For example, Figure 3.8 plots the experienced heading error for a unit with various angles of pitch at a geographical location where the Earths magnetic field has a inclination angle of 40° if no tilt correction is applied.

This pitch and roll error is due to the 3D nature of the Earth's magnetic field and therefore corresponds to the orientation of the actual magnetometer unit with reference to the fixed axis system of the Earth. This differs from

the notion of pitch and roll in vehicle dynamics which usually relates to the angular orientation of the vehicle chassis to the road surface. It is therefore necessary to consider both pitch and roll of the chassis of the vehicle (to which the magnetometer unit is mounted) with respect to the road surface but also the inclination of the round surface to the level plane of the Earth's surface to understand this source of error.

This error results in a range of X and Y values for each heading and hence when shown graphically, the data forms a thick circular band where a thin line is expected. Figures 3.9 and 3.10 demonstrate this problem. In Figure 3.9 the test vehicle is being driven in a large circle at a low speed during preliminary shakedown at Kirkbride, this effectively keeps pitch and roll angles near zero. It can be seen that the sensor voltages transcribe a clear and consistent circle. Comparing this to Figure 3.10, which shows the raw voltage telemetry from a run of one of the Spanish tests of the vehicle in which pitch and roll of the vehicle and the mountainous terrain are significant factors, it can be seen that the data now transcribes a thick band of values. The difference in voltages is due to the geographical distance, and hence differing magnetic field declinations, between the two tests.

By including the Z channel data and plotting all three axes, the circle is replaced with a section of a sphere that shows that that the thickness of the band corresponds to varying magnitudes of vertical magnetic field strength and hence the unit must be experiencing some pitch and roll disturbance. Figure 3.11 shows three projections of this sphere using data from one of the Spanish tarmac tests.

Using the Z-axis channel data of the magnetometer, as well as the value of pitch and roll of the sensor module allows the reorientation of the X and Y data to the horizontal plane and hence the reduction of error. It should be noted that this error is transient and if the sensor is returned to its initial level orientation, the error is removed.

As previously mentioned in Section 3.3.3, electrically gimballing a magnetic heading sensor allows the unit to remain fixed to the vehicle, known as being strapped-down, and by knowing or sensing the values of pitch and roll, rotating the three-dimension magnetic vector reading back to that of a level

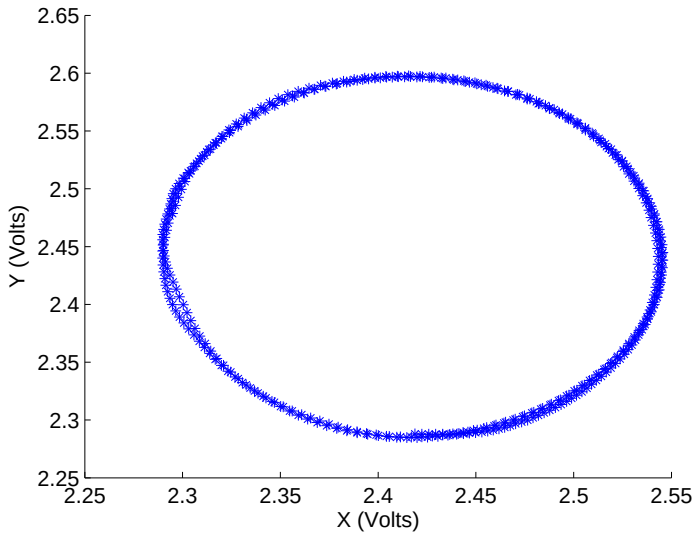

Figure 3.9: Calibration Circle at Low Speed (no pitch or roll) - raw voltages

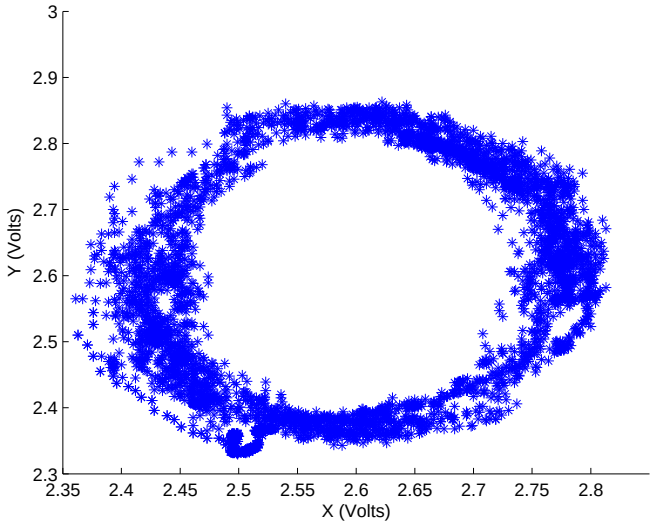

Figure 3.10: Raw X and Y axis voltages for full test run

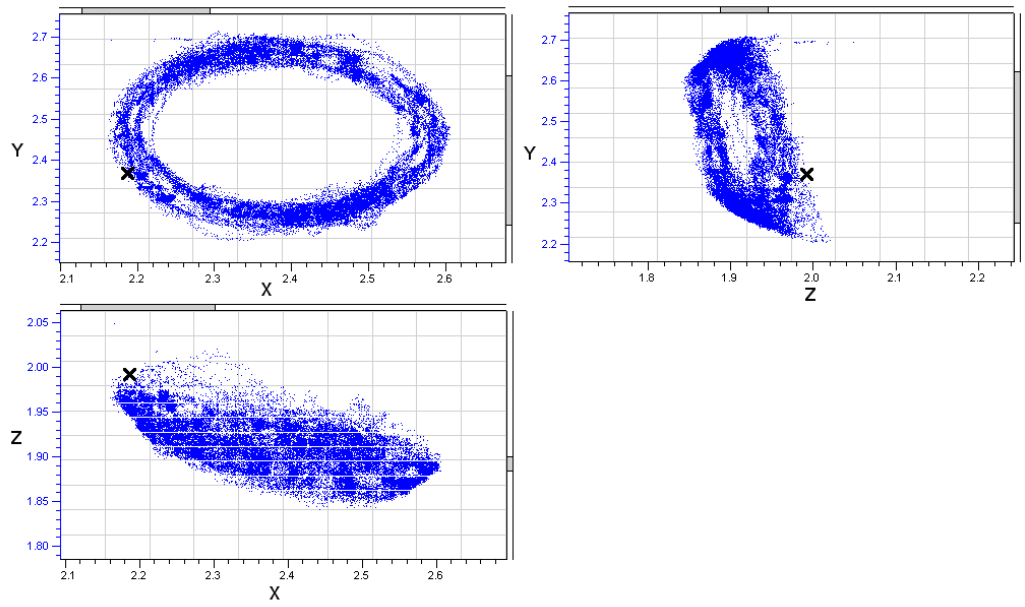

Figure 3.11: Raw X, Y and Z axis voltages for full test run

orientation. The X, Y and Z magnetic readings can be re-orientated to the horizontal plane (Xh and Yh) by applying rotation equations 3.1 and 3.2 for a given pitch (ϕ) and roll (θ) angle[50].

$$X_h = X \times cos(\phi) + Y \times sin(\theta) \times sin(\phi) - Z \times cos(\theta) \times sin(\phi) \tag{3.1}$$

$$Y_h = Y \times cos(\theta) + Z \times sin(\theta) \tag{3.2}$$

Using a similar calibration method, but now also encompassing the Z axis before applying these correction equations and the same heading calculation method now based on Xh and Yh produces a pitch and roll corrected value.

This method requires the pitch and roll angle of the unit to perform the correction. Obtaining pitch and roll angles is described later in this section.

Calibration of the Z-axis

As the pitch and roll correction equations include the Z-axis data, there is now a requirement to perform a calibration routine on this axis to derive the scale factor and offset for that geographic location. As described in Chapter 2, scale factors and offsets are determined for the X and Y axes by rotating the vehicle, with sensor, through a full 360° and attempting to map the plot of the resulting data to a circle centred at the origin. Applying the same logic to the Z-axis would mean rotating the vehicle with sensor around its Y-axis and is therefore extremely unpractical.

As an alternative method, instead of attempting to map a set of data from a complete rotation, it is possible to attempt to map a segment of data from a known angle of rotation. In other words, instead of rotating the car end over end, by jacking up the rear of the vehicle and then the front of the vehicle to a known angle a data segment can be measured. It is then possible to calculate a scale factor and offset that map the data to the segment of a circle expected for that geographic location and angle of magnetic inclination. This is easiest to achieve by initially pointing the vehicle in a Northerly direction and comparing only the X and Z axis data.

Figure 3.12 demonstrates this method by showing the magnetic field vector in the X-Z plane for a level vehicle as well as the effects of jacking the front and rear of the vehicle. The segment created can then be seen to be part of the expected circle (dotted) that would be created if the vehicle could be completely rotated in this plane. The initial vector is inclined to the vertical due to the magnetic field inclination angle for the given geographic location, in this diagram the inclination is 45°.

Given that it is unlikely that the vehicle will experience such rotation to angles in excess of those achieved through jacking this method of calibrating the Z-axis is sufficient. The magnetic distortion due to the presence of a jack is considered to be minimal.

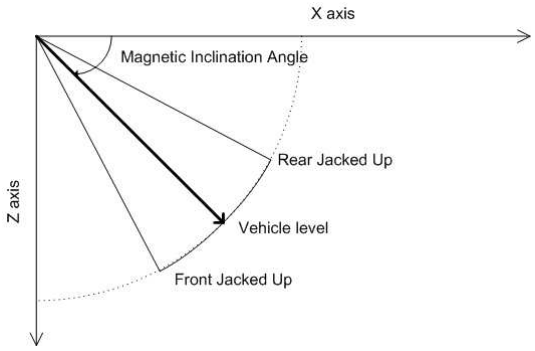

Figure 3.12: Effect of Jacking front/rear of test vehicle on magnetic inclination

Obtaining Pitch and Roll angles

Inertial Sensing

Currently commercially available magnetometer-based compassing solutions either utilise a pair of orthogonal tilt sensors or a tri-axial accelerometer to determine an accurate value for the pitch and roll of the magnetometer module. As the angles involved are quite small (a few degrees) any noise or vibration will significantly affect the accuracy of such units.

Both of these methods attempt to determine orientation with reference to the Earths gravitational field and are only effective if the module is not experiencing any additional acceleration. For example, if the module is experiencing a lateral acceleration of 0.1G, these systems would imply a tilt angle of 5.7°[73]. Given the nature of operation of the WRC car, this method would therefore be completely inappropriate.

Angular Rate Sensors

Angular rate sensors, or gyros, could be used to measure rotation of the unit in its three axes to provide the required angles. These sensors do not suffer the sensitivity to accelerations but have their own drawbacks[73].

The need to integrate the signal from the angular rate sensors increases the likely error in the system and the standard range of sensors cannot provide

the required precision to maintain an acceptable level of accuracy for the required period of time. Section 3.3.2 demonstrates this inaccuracy and again the latest high specification fibre-optic gyroscope[67] sensors could resolve this problem but not in their current form, which would be an excessively expensive, bulky and heavy solution. This technology may, in the future, become more viable a solution.

Vehicle Dynamics Model

Using a basic understanding of the vehicle dynamics of the car to which the module is strapped, it becomes possible to build a model that can infer the vehicles orientation in most situations. By combining data from accelerometers and GPS, with a few assumptions, an acceptably accurate value for pitch and roll can be determined without the problems experienced in the previous methods. This method has been shown to be effective and is further detailed below.

Inferring Pitch and Roll from a Dynamic Model

If the dynamics of a vehicle with suspension are considered, there are four steady-state conditions which can result in a rotation of the chassis about its X or Y axis. Two are concerned with the lateral and longitudinal forces generated on the chassis by driving/braking and cornering, the other two relate to the banking and inclination of the road surface over which the vehicle is travelling.

The suspension system has the added advantage that it works as an effective high pass filter, helping to remove the noise introduced through road surface variations, from the pitch and roll data. Suspension geometry information was provided as a set of Kinematics and Compliance data from test rig measurements of the class of vehicle used. Spring rates were also provided for each of the test vehicles.

Longitudinal Acceleration and Pitch

As the vehicle accelerates or brakes, it will dive or squat on its suspension. The extent of pitching relates to the degree of longitudinal acceleration.

In the simplest situation, a calculation of load transfer of the front and rear of the vehicle can be used to give a good indication of the magnitude of pitch; however this assumes little influence from any anti-dive or anti-squat suspension components.

Milliken[1] defines this change in axle load (ΔW) due to longitudinal acceleration as a function of the acceleration (A_x), the weight of the vehicle (W), the wheelbase (WB) and the height of the centre of gravity of the vehicle (h), thus:

$$\Delta W = \frac{hWA_x}{WB} \tag{3.3}$$

This load transfer approach combined with suspension wheel recession rates gives a very good approximation for the purposes of approximating pitch angle without the need to model the suspension geometry in full. This method has been widely accepted as providing suitably accurate values for the majority of potential simulations and studies and is considered by many to represent a high level of realism.

Figure 3.13 shows a sample of pitch angle data calculated using this method. It can be seen that pitch of the vehicle due to longitudinal acceleration rarely exceeds one degree. This being a consequence of the stiff suspension setup. It is also worth noting that the frequency of changes in pitch angle is generally around 1-2 Hz which is as expected for a vehicle of this class.

Lateral Acceleration and Roll

Under lateral acceleration, a vehicle experiences load transfer. The suspension system of the vehicle then reacts to this load transfer by the compression of the outer springs and expansion of the inner springs. Given the recession

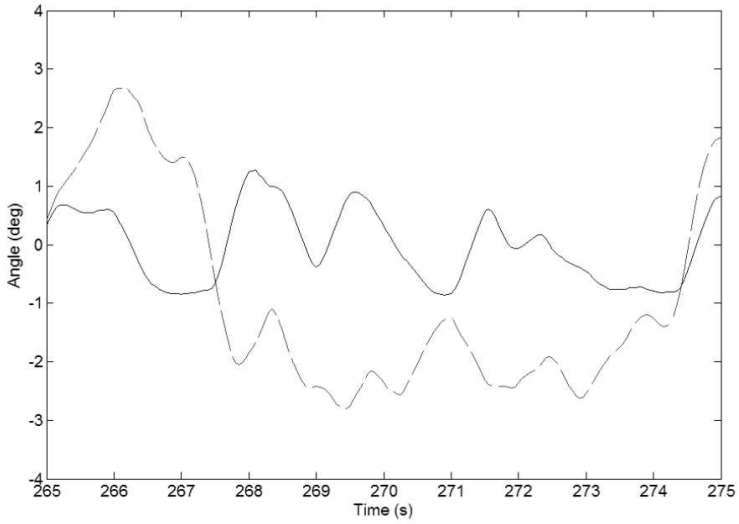

Figure 3.13: Vehicle Orientation Angles derived from Acceleration Telemetry (—— Pitch, – – – Roll)

rates of the wheels and knowing the magnitude of the load transfer, it is possible to calculate the linear expansion and compression of the inner and outer suspension. With this information the roll angle due to lateral acceleration can be inferred.

In the same way as for longitudinal acceleration, Milliken[1] again provides a simplified method of calculating percentage lateral load transfer (LLT) as a function of lateral acceleration (A_y), track width (TW) and height of the centre of gravity (h) of the vehicle, equation 3.4. An accelerometer provides the lateral acceleration information required. Although it has been previously mentioned that the level of noise in this measured acceleration is too severe for integration to determine lateral velocity, this is not required in this case. A moving average filter, as shown in Equation 3.5, is applied to smooth any irregularities.

$$LLT = \frac{A_y h}{TW} \tag{3.4}$$

$$y_f(i) = \frac{1}{2N+1}(y(i+N) + y(i+N-1) + ... + y(i-N)) \tag{3.5}$$

The suspension recession rates differ between the front and rear of the vehicle as well as the effect of the anti-roll bars, so it is necessary to calculate the two independently and average across the two.

As the degree of roll is usually only of the order of a few degrees, the sensitivity of this calculation to error through a simplified modelling approach to the suspension and load transfer from accelerometer measurements is acceptably small.

Figure 3.13 also shows a sample of roll angle data due to lateral acceleration calculated using this method. Roll angle rarely exceeds 3 degrees, again due to the stiff nature of the suspension and also demonstrates frequencies in the 1-2Hz range as expected.

Vertical Velocity, Road Inclination and Pitch

In most situations, the road surface over which the vehicle will be travelling will be subject to some degree of inclination. This will have a clear effect on the pitch of the vehicle, measured relative to the centre of the Earth.

The GPS module can calculate three-dimensional velocity extremely accurately through Doppler shift analysis of the satellite signal. The angle of the road can be considered to be equivalent to the inclination of the velocity vector to the horizontal plane and, with small correction to take into account the slight change in wheel loads due to the angle of the vehicle, the component of vehicle pitch caused by the road inclination can be determined. This technique was initally developed by Bae *et al.*[44].

Unfortunately, despite wanting to log the vertical velocity output of the GPS module for the second Spanish test, it was not possible to reconfigure the LCS data logger to perform this function. This was due to a lack of time in the tight build schedule caused by other issues and technical problems with the electronic components of the test car taking priority. It was, however,

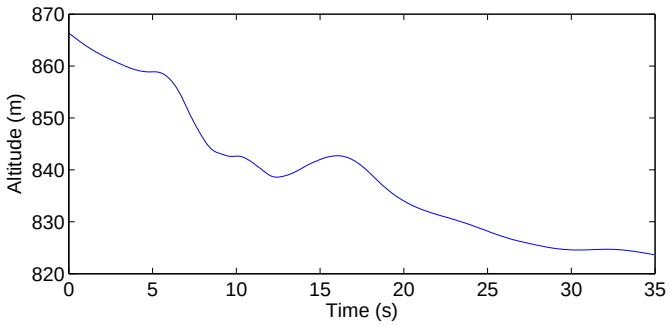

Figure 3.14: GPS Altitude telemetry

possible to log altitude above mean sea level, which provides a similar method of calculating road inclination. Due to the inherent errors in GPS positioning calculations, this is not as accurate as the Doppler-shift vertical velocity calculations but does provide reasonable road inclination calculations.

Figure 3.14 shows a set of GPS altitude data from a test run on a hilly tarmac stage in Spain and the road inclination angle, Figure 3.15, that can be inferred using it and the horizontal velocity measurement.

Both GPS and inclination data have had a moving average filter applied to them. This filter replaces each data point with an unweighted mean of the surrounding data points, the purpose of which being to smooth irregularities and random variations and allow the identification of trends[74]. Equation 3.5 demonstrates this filter. $y_f(i)$ represents the filtered data point replacing the ith element of y, y is the original data set and N represents the size of the moving average window.

In this case a moving average window of one second was applied, by which it is meant that each data sample is averaged with those up to half a second before and up to half a second afterwards.

Super Elevation

The case of super elevation, or banking, of the road surface is an interesting special case as it can not be determined from simple accelerations or GPS

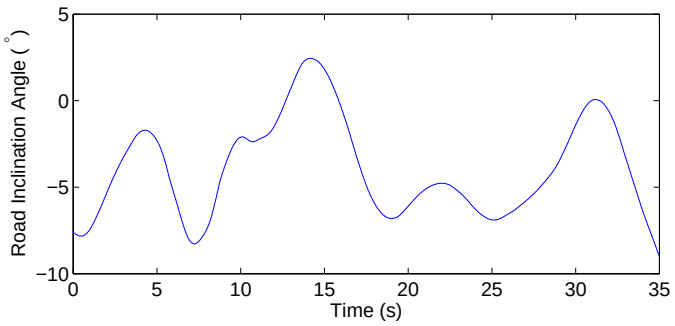

Figure 3.15: Road Inclination Angle

data. It also poses the question as to whether β-angle on a banked surface is the same as a flat surface as the dynamics of driving with zero β along a super elevated surface require some lateral force applied to the system to counter the desire to slide down the bank. Fortunately banked surfaces with an angle of more than a degree or two are relatively rare and due to the difficulty in measurement, it can be overlooked in initial studies. It is technically possible to determine whether road surface banking is present and its magnitude by comparing the 3-axis magnetometer data, corrected with the three other pitch and roll corrections, to the expected value for that geographical location. This, however, was not possible within the scope of this work and would be very susceptible to noise levels.

Combining the Components

These four components should combine to give a reasonably accurate assessment of the current vertical orientation of the vehicle and hence the magnetometer in all situations.

With these values of pitch and roll it becomes possible to correct the magnetometer data to provide significantly more accurate headings under the conditions experienced by the sensor module under testing. Correcting in this manner increases accuracy by removing the pitch and roll error as shown in Figure 3.8. Further degrees of accuracy may be obtained from

further studies into the super elevation issue.

It is also clear from telemetry that road inclination angle is a significantly larger factor in heading error with inclination angles reaching in excess of 10 degrees on typical rally stages, compared with a maximum pitch due to suspension components of less than 3 degrees.

At magnitudes of greater than 10 degrees for pitch and roll, the error in magnetic heading calculation becomes highly significant (see Figure 3.8). This results in an unacceptable level of error in magnetic heading and hence β-angle. As such correction of this error is essential for these road inclination angles. The smaller level of variation in sensor orientation due to vehicle suspension movement, which is the more traditional concept of pitch and roll in vehicle dynamics, is of a suitably low level to not cause excessive error in the range of values seen in WRC.

3.6 Testing and Validation

The prototype sensor was tested for three qualities: the durability of the sensor, the quality of the data obtained from the sensor and to test for any drift in the results obtained from the sensor over a prolonged period of testing.

The prototype unit was mounted to a Ford Focus WRC car. Mounting of the unit was a compromise to alleviate as much of the magnetic field distortions generated by the vehicle as possible. The engine, the strong magnetic bases of the GPS antennae and the metal chassis of the vehicle generate the majority of the distortion. Distance from all three is optimal although this is clearly not an option. A compromise of the centre of the roof, just behind the cockpit air inlet, provided a position with acceptable levels of distortion. For future tests the GPS antenna base was replaced with a non-magnetic alternative allowing for increased distance from the engine as previously described.

The tests were conducted in southern Spain as part of a scheduled test session for the WRC team on a gravel surface. They were undertaken on a hilly track surfaced with wet rough gravel. The track was a single carriageway but varied in width from narrow to relatively wide. Vehicle speeds were in

the range 60 to 140 kph.

Data was available for 14 test runs each of which varied between 15 and 30 minutes long and spanned three days of testing.

The three signal outputs from the magnetometer were logged at a 10Hz sampling frequency by the onboard telemetry system. The GPS heading was also logged accordingly.

The resulting data was filtered with a moving average filter, and then calibrated using calibration functions as described in section 3.5. There was no opportunity to conduct these calibration tests in Spain, although careful analysis of the Spanish data revealed a correction factor to take account of the change in angle of magnetic field declination from Cumbria to Spain. Headings were calculated using the magnetometer data. This was combined with GPS data to yield β-angle time histories.

Raw β-angle Data

Figure 3.16 and 3.17 show two examples of the raw β-angle telemetry obtained in Southern Spain. Both represent the same road stage course but each is driven by a different driver.

These figures represent the raw data and as such the signal can be seen to exhibit a few sources of noise. Firstly, the angle trace is slightly jagged and every so often the angle peaks up to values in excess of 100 degrees. These peaks are caused by GPS dropout problems when then GPS unit is not receiving sufficient information from the satellites to provide a heading value. Fortunately the GPS unit quickly reacquires the satellite signal so the data stream is quickly restored.

In addition, for approximately the last 20 seconds of each run and the first few seconds of run 2, the data stream becomes extremely noisy and erratic. This is due to the vehicle actually having come to rest and could be removed by including a velocity threshold.

Without any filtering or sophisticated analysis, it can be quickly seen from these two graphs that the β-angle sensor can be used for driver comparison with each figure representing the same course but with different drivers. The

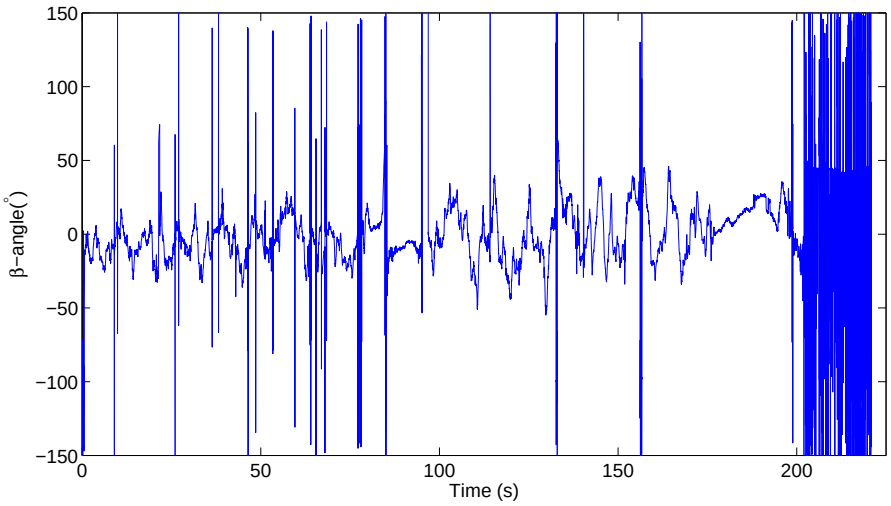

Figure 3.16: Raw β-angle Telemetry (Run 1)

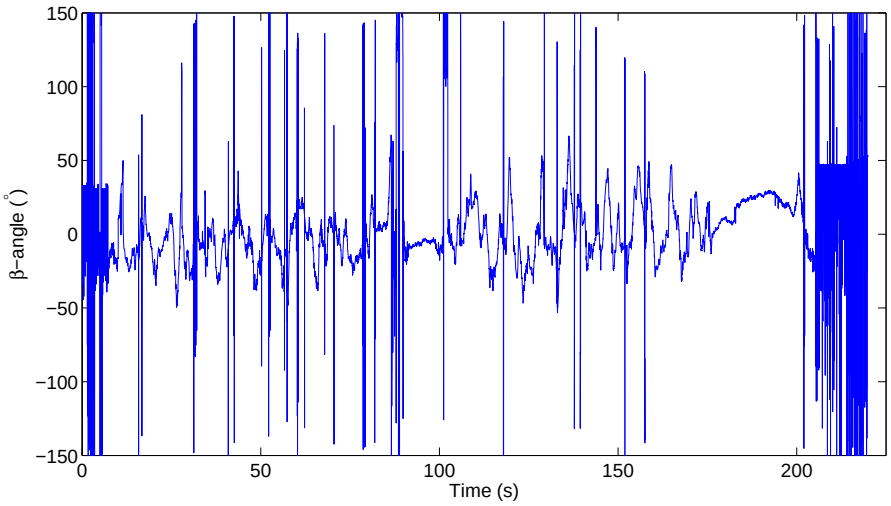

Figure 3.17: Raw β-angle Telemetry (Run 2)

two traces show that the drivers are using a similar techniques with the vehicle being excited to high β-angles at the same points and resulting in a similar shape to the trace. However, the driver in Run 1 seems to be achieving peak angles around 25 degrees where driver 2 is closer to 35 degrees which could correspond to many factors including driver performance.

Other factors could also influence these traces such as a sudden downpour during the driver switch overs resulting in a more slippery road or a change of tyres, but with further development it is clear that the sensor could be used as a quantitative tool for driver comparison.

Example Manoeuvres

In order to validate the β-angle, the data was analysed for manoeuvres where the expected β-angle is widely accepted. Three are presented for consideration.

Straight Line Running

The first, Figure 3.18, demonstrates driving in a straight line at relatively high speeds between 70 and 100 kph as can be seen in the upper right graph. The upper left graph of Figure 3.18 shows both the GPS velocity heading measurement as well as the magnetometer derived vehicle heading, in this case the two appear to be almost equal as the β-angle (shown in the lower left graph) in such conditions is, as expected, close to zero.

It is worth noting that the steering angle input seems quite dramatic given the high vehicle speeds, shown in the lower right graph. This is due to the road conditions of loose wet gravel. For this particular test the driver described the conditions as "extremely slippery" and he struggled to maintain the straight line orientation of the vehicle, ultimately requiring the drop in velocity half way through this data segment to avoid going off the road.

The results of these conditions and the efforts of the driver are shown in the slight fluctuations in the values of β-angle measured. Despite this the β-angle does not increase beyond 2° and is quite stable. This is as expected from such a class of vehicle driven in this manner and nicely demonstrates

the loosely coupled nature of β-angle to high frequency steer inputs at high speeds. By considering similar situations throughout the entire set of test run data, it was seen that the sensor was consistent in producing expected results and therefore boosting confidence that the sensor performs as it should in such conditions.

Vigorous Cornering

The second, Figure 3.19, shows a vigorous cornering manoeuvre where the path of the road turns a little to the left, then to the right and then back to the left in a similar manner to a double lane change or chicane manoeuvre. Again the upper left graph shows both GPS velocity heading and magnetometer derived heading, upper right gives vehicle velocity, lower left shows steer angle and lower right is the vehicle's β-angle.

The approach to the manoeuvre shows significant braking during which the driver slows the vehicle from 80 to around 30kph. As the driver applies some counter steer under braking, the rear tyres of the vehicle becomes saturated and a high β-angle of about 15° is induced.

Next the driver turns into the corner and applies some throttle. This results in an slight increase in vehicle speed and sees the rear of the vehicle swing back in the opposite direction. This is sometimes known as a 'Scandinavian Flick'. As the swing occurs, the β-angle drops suddenly to around -28°.

Coming out of the corner, the driver initially slows down to help bring the vehicle back under control and reduce the β-angle. Once the vehicle attitude drops to a much lower level he accelerates and straightens up but due to the loose gravel surface the vehicle fish-tails and the driver works erratically to again reduce the β-angle back to smaller values.

The behaviour of the value of β-angle in this manoeuvre follows the expectation given the nature of the path taken and the control inputs.

Handbrake Turn

The third manoeuvre, Figure 3.20, is a handbrake turn performed by the driver to turn the vehicle around on a tight section of road. Vehicle velocity has been replaced in Figure 3.20 with the handbrake sensor to better demonstrate the timing of the manoeuvre.

Initially the driver counter steers to move the vehicle to one side of the road, before making a large steering input and inducing a high negative angle. As the handbrake is applied to the rear wheels, resulting in rear tyre saturation, it causes the rear of the vehicle to swing back round as it loses lateral capability. At this point the β-angle climbs quickly to around 25° and is sustained and controlled by the steer action of the driver and application of throttle.

From the heading comparison it can also be seen that during this manoeuvre the vehicle has rotated through a full 180° as expected. Once the vehicle reaches it intended heading orientation, the β-angle is allowed to return to lower figures.

It can be seen that the clear change in β-angle from negative to positive occurs directly after the application of the handbrake and the magnitude extremes of about 25° correspond with what is accepted to occur during such a manoeuvre and, therefore, partially validates the sensors output.

To increase the confidence in the sensor further, three validation methods could also be used. By using a visual reference field the observer could get an idea of the β-angle and compare it with that being read by the sensor. This would be achieved using a video of the run from the drivers perspective that could be indexed to the data. Due to the wet and muddy conditions of the Spanish test this was not possible.

The second method involves rotating the mounting of the sensor to induce an artificial attitude angle. The resulting data from a straight-line test should mirror that of a run with the original sensor mounting, but with the β-angle being increased by the degree of rotation of the sensor. This test was planned on the WRC car but due to the weather conditions time was not available to perform it. However, a similar experiment was performed during initial

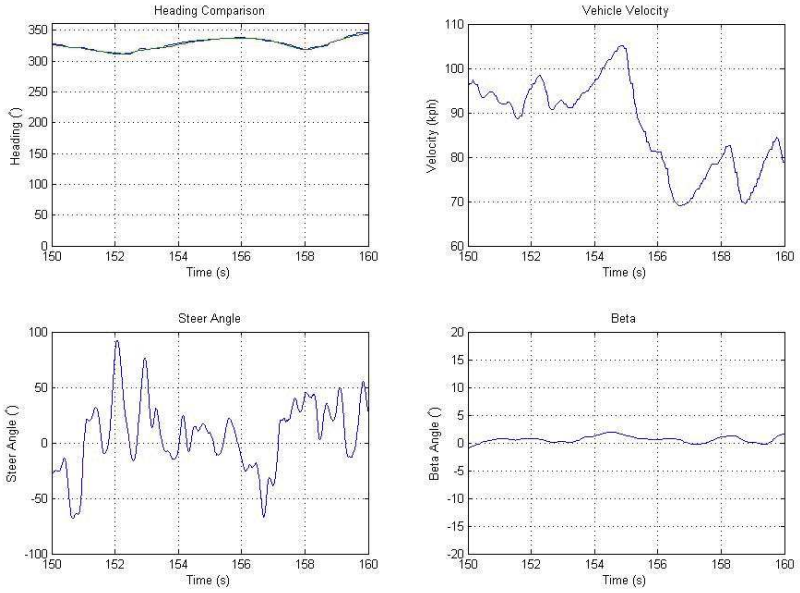

Figure 3.18: Straight line operation, wet conditions on gravel

feasibility studies in which the magnetometer sensor was rotated by 20°. This test used a standard road car and a two axis magnetometer for a brief test run at significantly lower speeds than the WRC test runs. Figure 3.21 show the magnetic heading and GPS heading data, while Figure 3.22 clearly shows the β-angle to be around the 20° mark as expected.

The momentary drop in β-angle at around 130 seconds occurs when the vehicle has an heading of approximately zero degrees or Due North. As previously mentioned in Section 3.3.1, the VBox unit used in this experiment infills between data points to create the appearance of a higher sampling rate that it can actually achieve. The downside of this being intermediate data points when the vehicle moves past Due North from 359° to 0°. This results in an intermediate value around 180° on the GPS data stream and, as the magnetometer does not suffer the same problem, the β-angle calculation is momentarily affected. A more sophisticated filtering method could be employed to remove this problem or the replacement of the GPS with a unit that does not infill between data points - in further experiments the latter

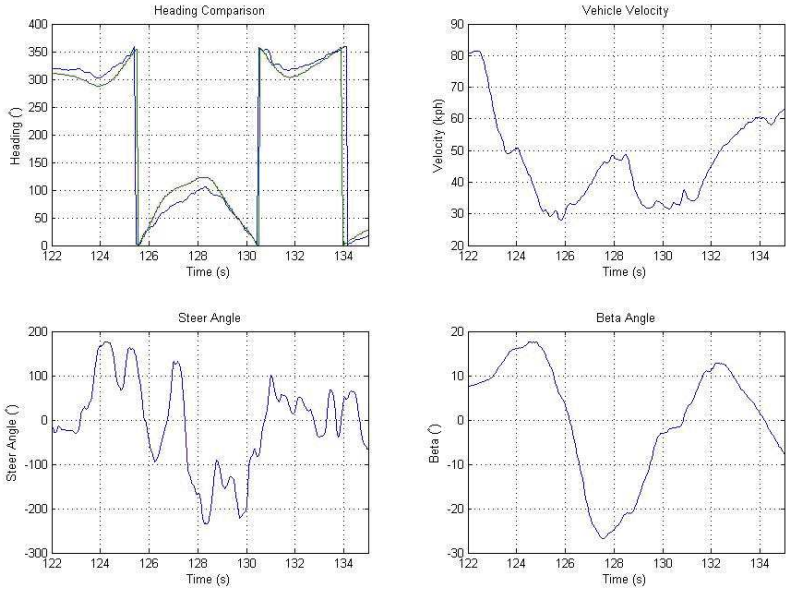

Figure 3.19: Vigorous cornering with initial counter steering on approach, wet conditions on gravel

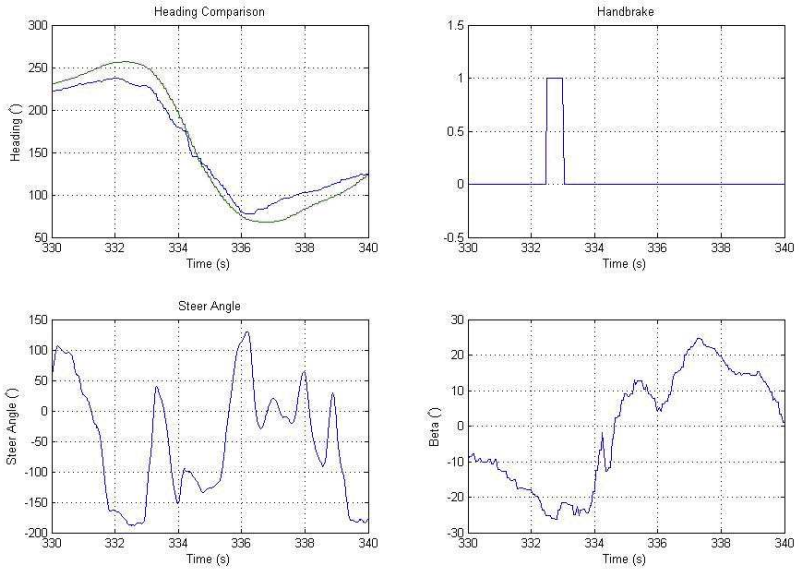

Figure 3.20: Handbrake turn, wet conditions on gravel

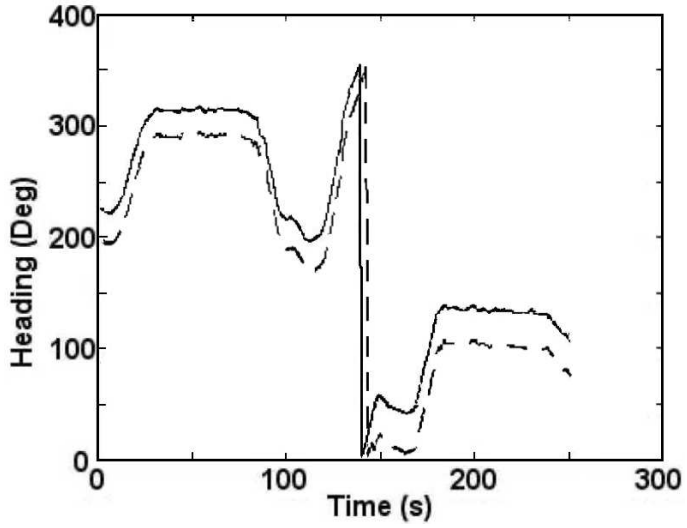

Figure 3.21: GPS and Magnetometer Heading Measurement-20° simulated β (——- GPS, – – – Magnetometer)

approach was taken.

The third method and the preferred option for a comprehensive validation of the sensor measurements would see the β-angle sensor's output being compared with that of existing sensor technologies. For tarmac surfaces this would be achieved through direct comparison with the already accepted accuracy of the Correvit[12] and for gravel comparisons using the dual-antennae GPS systems that are starting to become available.

As already mentioned, the Correvit is limited by its susceptibility to damage on loose surfaces and the dual-antennae being a very costly piece of equipment that has only just become commercially available. Despite this, the comparison of the measurements taken with these sensors with the novel β-angle sensor would give a very precise indication of both accuracy and resolution with an analysis of both magitude and transient response of a vehicle's β-angle.

Despite this being a clear method of validation, it was not possible to perform such a validation using either the Correvit or a dual-antenna GPS system during the course of these studies. It is hoped that further work and investigation might permit this in the future.

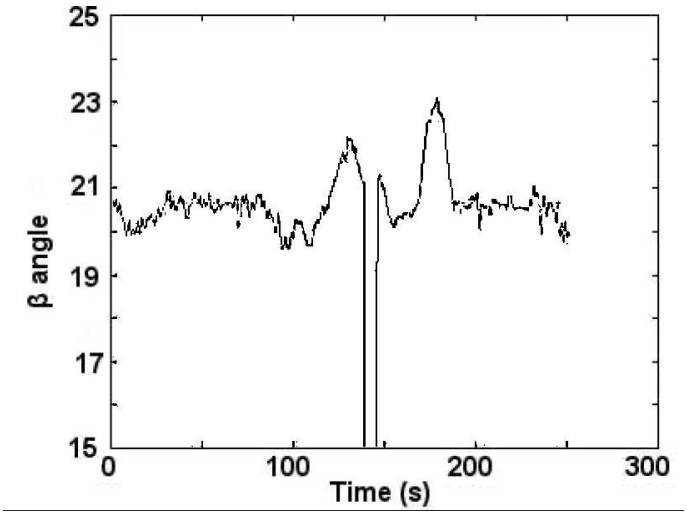

Figure 3.22: β-angle - 20° simulated β

Chapter 4

Supplementing the Modelling Dataset

Having developed the β-angle sensor, it is now interesting to re-evaluate the usefulness of vehicle dynamic simulation for WRC class cars.

One major advantage of the sensor when combined with a vehicle dynamics model is the ability to derive lateral tyre force curves for any surface. Current methods of constructing tyre force curves involve laboratory testing on rolling roads which limits the ability to test tyre dynamics on loose surfaces. These are detailed in Chapter 2.

Although deriving from vehicle test telemetry has been possible with previous sensor technology, the limitations already discussed of β-angle measurement makes it difficult to collect sufficient data for loose surfaces. These problems have been overcome with the new sensor.

This chapter details the development of a suitable vehicle model, its verification and validation and the methodology in determining a lateral tyre force curve.

4.1 Construction of the Model

4.1.1 Vehicle dynamic model

For the purpose of this research a World Rally Championship-style vehicle model[75] was required. The model developed was based on a previously published and validated rear wheel drive vehicle model with extensions to include two additional differential units, implementing a 4-wheel drive system standard on this class of vehicles. The equations of motion were derived using the AutoSim[58] multibody modelling system.
A summary of this model is provided below.

Chassis

The car model has seven degrees of freedom. The vehicle body is free in longitudinal (X) and lateral (Y) displacement and yaw about the vertical (Z) axis, observing the standard SAE axis conventions[1]. This is shown in Figure 4.1

In addition, each of the four wheels has an independent rotational spin degree of freedom relative to the vehicle chassis. The use of a seven degrees of freedom model provides acceptable simulation computation times for large parameter sweeps[76]. The model is both non-linear and transient.

The lateral and longitudinal load transfers are included as steady-state approximations.

Aerodynamics and Vertical Tyre Loads

Aerodynamic lift and drag forces are included using constant coefficients. Drag is applied at the height of the centre of gravity of the vehicle. Down force distribution is defined between the two axles and applied equally to each wheel on the axle. The static wheel load is derived from the centre of gravity of the vehicle, in this instance there is a 60/40 front to rear mass distribution.

An approximation of the lateral and longitudinal load transfer is calculated corresponding to an acceleration of the mass centre and a simple

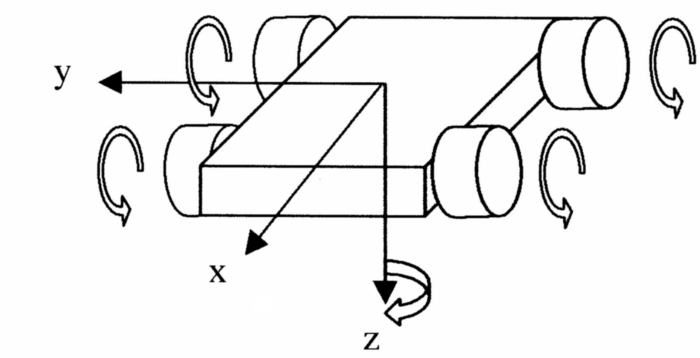

Figure 4.1: Seven Degree of Freedom Model[9]

roll-axis model.

Tyre Forces

The lateral and longitudinal tyre forces are produced using a variant of the 1997 Pacejka Magic Tyre Model[53]. These forces are vectored for the front tyres to simulate a steer angle. The parameters for the model are initially based on data from a high performance road tyre on tarmac. Static wheel camber angle is included.

Although the tyre parameters for the high performance road tyre are used as a starting point, further investigation questions the accuracy of this particular set of parameters, particularly when considering loose surfaces. This will be discussed in more detail in later sections.

Powertrain and Transmission

A two dimensional engine map characterises engine torque by engine speed and throttle position. Gear ratios are automatically selected based on vehicle speed. Braking torque is characterised by a maximum braking torque and is delivered as a function of throttle position. That is a negative value for throttle corresponds to a braking action being applied to the wheels.

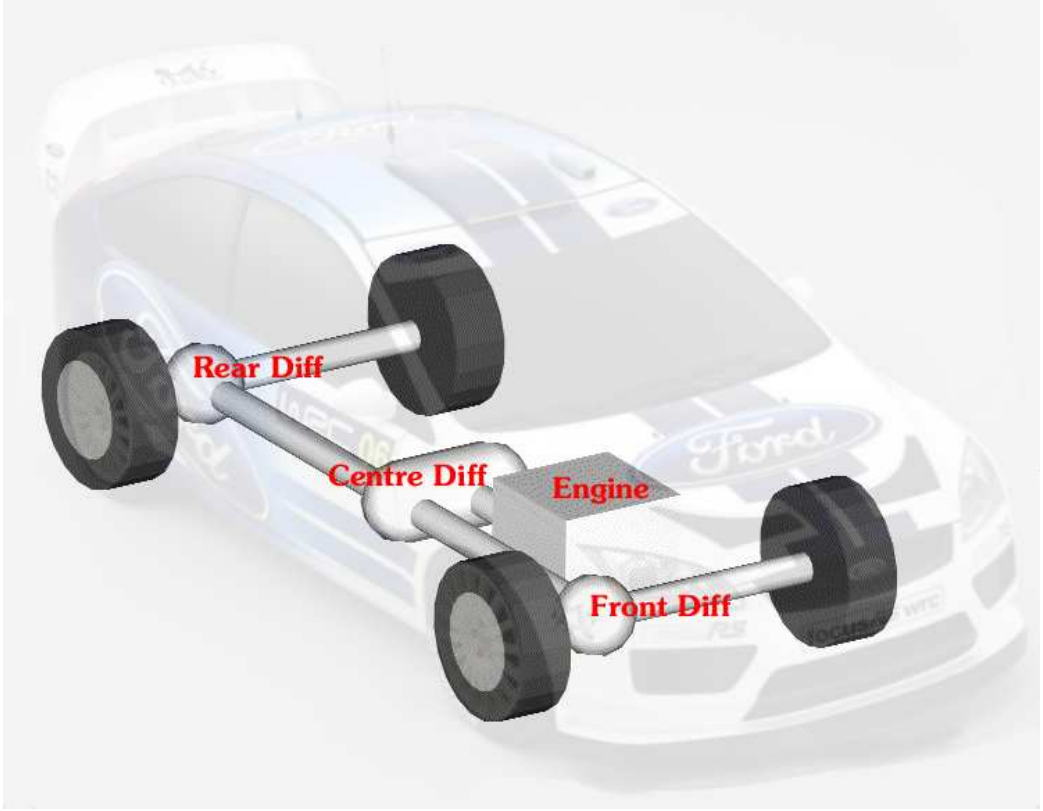

Figure 4.2: Model Transmission Configuration (Original photo courtesy of www.fordteamrs.com)

The braking torque is applied to the front and rear wheels based on a constant front/rear distribution.

Extensions to the Brayshaw[9] model include two additional differentials, converting his model from rear wheel drive (RWD) to four wheel drive (4WD). The three differentials distribute drive torque to the front and rear of the vehicle, and to the left and right at each axle, each with a 50-50 torque output ratio. See Figure 4.2

The differential models implemented in this model are based on the limited slip Salisbury-type [1] differential, see Figure 4.3, with electro-hydraulic actuation[26] employed in most forms of motorsport including the World Rally series[75]. Figure 4.3 shows the inner workings of such a differential. The standard gearing of an open differential are shown with the standard

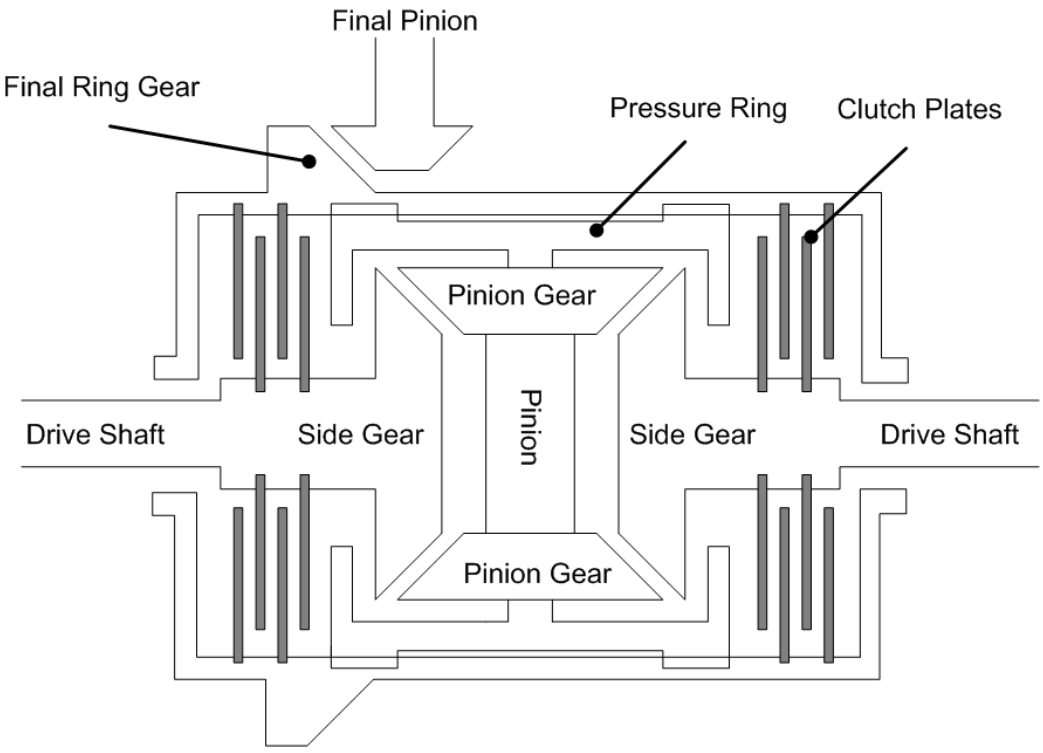

Figure 4.3: Limited Slip Differential[9]

pinion and side gears that permit a difference in rotational speed of the output shafts. In addition there are clutch plates attached to each output shaft and the main casing of the differential. As the difference in output shaft speed increases, these clutch plates interact and generate a torque to reduce the difference.

The pressure ring, seen in Figure 4.3, acts to push the clutch plates together as the input hydraulic pressure in increased. This results in increased friction between the clutch plates and the locking action between the fixed and rotating plates increases.

Figure 4.4 demonstrates this action. With no input pressure, the unit works like an open differential with only a small amount of torque transfer between the clutch plates occurring despite high differences in output shaft speed. As the hydraulic pressure increases, the torque transfer also increases resulting in more locking action.

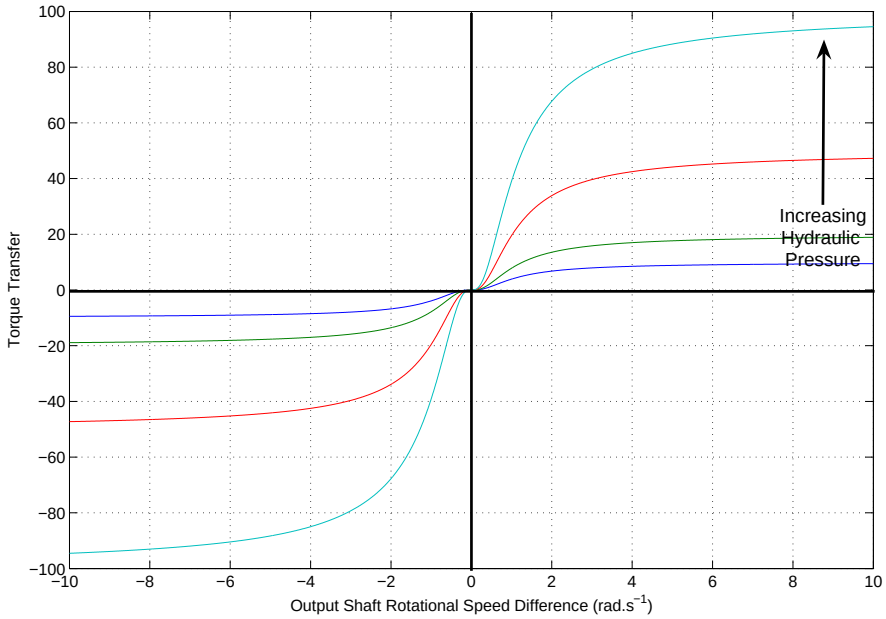

Figure 4.4: Torque Transfer in an Electro-Hydraulic Limited Slip Differential

As the model developed simulates the individual clutch plates and hydraulic pressure, the model can be adjusted to match differentials with differing numbers and sizes of clutch plates. In addition, an open differential can be simulated with the same model by setting zero hydraulic pressure (excluding pre-load). Likewise, a locked differential can be modelled with a very high hydraulic pressure. The origins of the model are described in Casanova[62] and Brayshaw[9].

AutoSim Model Overview

Figure 4.5 depicts the structure of the AutoSim 7-DOF WRC Model. The blue lines represent a physical connection between individual bodies with the wheels and differentials attached to the chassis. Each body is attached to its parent and allowed to rotate about the specified axis.

The red line can be thought of as the powertrain, with the rotational speed of the crankshaft constraining the centre differential, which subsequently

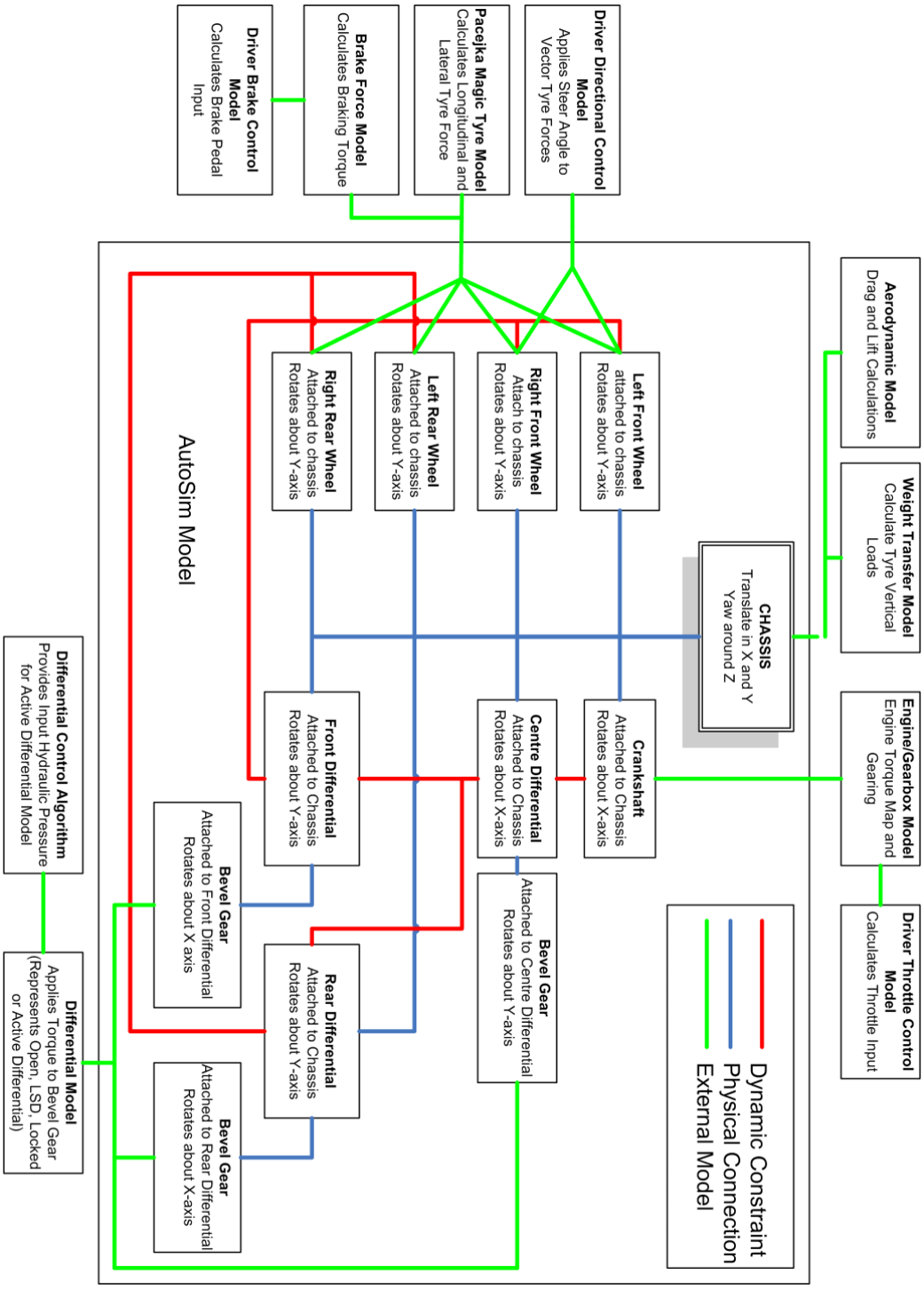

Figure 4.5: 7DOF WRC Model Overview

constrains the rotation of the front and rear differentials. The bevel gears on each differential influence these constraints to model a real differential action. Finally each tyres rotation is constrained by either the front or rear differentials.

Outside the AutoSim marked box, additional models are implemented to represent external factors such as driver controls, engine and gearbox models, aerodynamics and tyre force models. These connect into the model along the green lines and influence the behaviours of those bodies through the application of a relevant force or torque.

4.1.2 Driver models

Directional Control

Two methods of direction control have been implemented to simulate the actions of a driver. The first sets the steer angle using a pre-specified table, the angle being a function of either simulation time or distance travelled by the model. This method provides no means of feedback or consideration of vehicle state but allows a consistent control input to be applied independently of the state of the vehicle.

The second method, a path following driver model, allows the vehicle to be driven through a set path manoeuvre in differing states until the manoeuvre becomes beyond the abilities of the vehicle. The driver model would also react to the current state of the vehicle.

This method models a human driver more closely and attempts to follow a specified path. The control algorithm adjusts to counter any undesirable dynamics, for example, excessive oversteer, and allows the model to be driven through a set path manoeuvre with varying velocity control.

This non-linear, preview method[77] works by projecting a so-called optical lever forward of the vehicle (Figure 4.6) and compares the relative path and yaw errors between the current path and intended path at various preview distances from the vehicle. The error in the expected and actual vehicle state is also considered. The preview distance over which the optical lever is projected is dependent on the velocity of the vehicle as at higher speeds

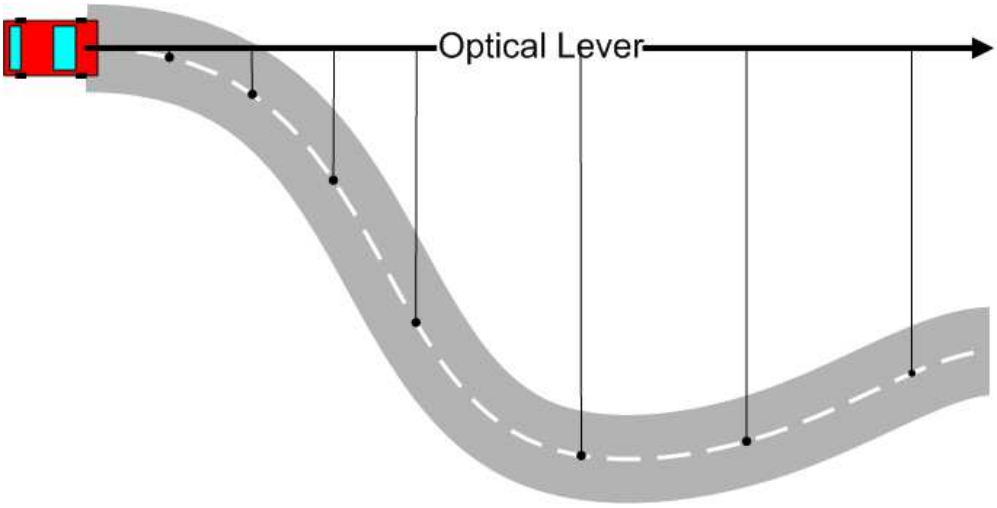

Figure 4.6: Path Following Directional Control - Optical Level

more preview information is required that for slower manoeuvres.

At each distance, a gain is applied to the relative path error as well as a saturation function which limits certain contributions to the equation and prevents the tyres from being forced to work too far beyond their saturation point.

The purpose of this being to rate the relevance of the error between the vehicles projected path and intended path to the required control input. That is, the further away from the vehicle for which preview information is considered, the less significant its effect on what the current steer input should be. As the vehicle progresses toward this initially distant point, its significance increases and hence a larger gain is applied when the point is closer to the vehicle.

A simple arithmetic function then calculates the required steer angle from the set of weighted path errors from preview information and the current vehicles yaw error. This method was originally devised for the model used in Casanova's research[62].

For example, by shortening the preview distance too far the controller may have to make drastic steer input changes to attempt to maintain a relatively simple path, while lengthening the preview distance too far could

result in the vehicle moving off the intended path in pre-emption of a distance corner. Therefore there is a requirement to tune these values to ensure that good path tracking and vehicle stability is preserved.

The tuning of the path following algorithm is accomplished using a trial and error technique. Starting with the parameters used in previous research by Brayshaw[9] for differing types of vehicle model it was possible to obtain an approximation to a suitable set for the 7-DOF model being used. During the validation process of the model, various manoeuvres were attempted. For each manoeuvre the effects of adjusting the parameter set was investigated and it was discovered that the values inherited from Brayshaw[9] provided acceptable path tracking and stability for the requirements of this research.

A suitable preview distance for this model was found to be the distance the vehicle would travel in one second at its current velocity. The points on the lever at which error is calculated and the effective gain applied at these points is shown in Table 4.1, distances are shown in terms of time to travel.

Table 4.1: Optical lever path following - Parameters

Preview Distance (s)	0.0	0.1	0.2	0.3	0.4	0.6	0.8	1.0
Relative Gain (%)	100	100	60	20	8	1.6	0.4	0.1

Velocity Control

Again two methods of velocity control have been implemented for the vehicle model to permit a wide range of vehicle simulations. By specifying the exact throttle/brake position dependent on time or distance travelled, a consistent and repeatable profile can be employed for the required manoeuvre. These values being interpolated from a simple look-up table specified before the simulation.

The alternative method is a PI (*proportional plus integral*)[78] throttle controller which attempts to maintain an acceleration target. The success or failure of the controller to perform this task being determined by the limitations of the dynamics of the vehicle. This method was also originally implemented and tested in Casanova's[62] and Brayshaw's[9] work.

4.2 Validating the Model

Brayshaw[9] makes the case for the use of a 7-DOF model clear by demonstrating that such a model provides acceptable realism and accuracy whilst still maintain the simplicity required to allow for large parametric sweep simulations without significant computation time. The open wheeled racing car model of Casanova[62] and Brayshaw[9] was modified to include additional differential models and standard vehicle parameters changed to match a WRC-style vehicle, the model was re-validated to confirm that the alterations had not affected the realism and accuracy of the initial model.

Brayshaw's[9] validation process compared his model to that of an accepted and published version as well as a comparison of the equations of motions of the model with the set of hand-derived equations. In addition the effects of different transmission configurations were investigated, showing the effects on yaw rate and lateral acceleration. Although Brayshaw's[9] results correlate with accepted thinking on vehicle dynamics for rear wheel drive vehicles, they are further confirmed with reference to telemetry data from a 4WD WRC vehicle.

The validation of the extended model used here consisted of two stages in which the model was driven through a set of simulated manoeuvres. In the first stage, the performance of the model was compared with expectations based on the results of hand calculations using accepted standard vehicle dynamics equations[1].

The hand calculations considered the expected weight transfer, pitch and roll angles, accelerations and yaw rates during the steady state manoeuvres of straight line acceleration, deceleration and steady state cornering. The results show indicate that the model produces a very close match to that calculated. The results of the hand calculations and values from simulation can be found in appendix B.

The second validation stage compares the model to a set of real-world telemetry data.

4.3 Telemetry comparison

Thanks to the availability of a set of telemetry data from a 2001 WRC-class vehicle it was possible to make a direct comparison between the telemetry and a simulation of certain manoeuvres.

The comparisons relate to steady state constant radius and speed cornering. Three transmission configurations are examined as defined in Table 4.2.

Table 4.2: Transmission Configurations for Telemetry Comparison

Configuration	Front Differential	Centre Differential	Rear Differential
1	Open	Open	Open
2	Locked	Locked	Locked
3	Open	Locked	Open

The first of the three transmission configurations examined is one in which all three differentials are left open and differing wheel speeds are unconstrained. As both the vehicle and model are fitted with electro-hydraulic activated units, the open configuration can be simulated by setting the hydraulic pressure to zero.

In the second configuration the three differentials are locked, whereby the two output shafts of the differential are locked together ensuring they rotate at the same speed. This can again be simulated using the active differentials by setting the hydraulic pressure to its maximum value for the duration of the test.

The third configuration is a combination of the two with the centre differential, which distributes torque to the front and rear axles, is locked. The front and rear units are configured to be open as in the first case.

In order to verify that the model is producing an accurate simulation of a real vehicle, it was compared with the telemetry for lateral, longitudinal and vertical acceleration, yaw rates, individual wheel speeds and throttle position.

4.3.1 Constant radius and speed cornering

For each of the transmission configurations, the vehicle was driven in a circular path around the 12 metre radius circle at the Millbrook proving ground. The driver attempted to hold the vehicle on or near to the limits of its dynamic range whilst maintaining the desired path trajectory.

To simulate this manoeuvre, the model was configured with the path-following steer controller setup to follow a 12 metre radius circle. The model was also configured to attempt to maintain the same speed achieved, by the real driver, by setting the acceleration target of the model to $0ms^{-2}$ and the initial vehicle speed from the telemetry.

The telemetry includes a steer angle as measured at the steering wheel whereas the simulation works on wheel angle. Unfortunately the steering column ratio is not known with certainty but by comparing the first simulation with the telemetry, a ratio of 1:7.5 is apparent. The second and third simulation verify this. The tables shows the adjusted wheel angle from telemetry with the original steering wheel angle in bracket.

A torque curve for the engine of the test vehicle was also not available and as such comparison of throttle pedal position is of limited value. It was, however, noted that for the three open and locked centre configurations the same amount of throttle was required to maintain the desired path and speed in the simulations. This corresponded to the telemetry. The three locked configuration required approximately 33% more throttle than the other two configurations in both telemetry and simulation.

Longitudinal and vertical accelerations were checked to ensure that they were both zero for simulation and telemetry as expected from this type of manoeuvre.

An initial glance at an unfiltered wheel speed graph, Figure 4.7, indicates that there is significant noise in the telemetry data compared with the simulation. As this noise is around 10Hz, it can be attributed to vibration within the tyre carcass. The application of a moving average filter removes this noise and smoothes the graph down to something much closer to the simulation output. It is also the case that the driver model benefits in terms of an abil-

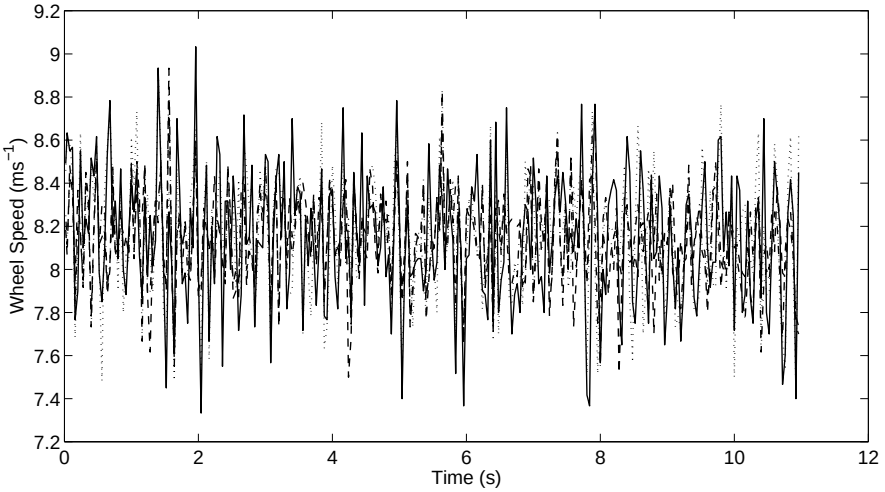

Figure 4.7: Unfiltered Wheel Speed Telemetry - Three Locked Differentials (– – – Front Left, – - – Front Right, - - - Rear Left, —— Rear Right)

ity to react significantly faster and more precisely than the real driver. This results the driver model being able to very quickly obtain the exact throttle and steer requirements to maintain a perfect match to the desired trajectory.

For each transmission configuration, the wheel speeds from both telemetry and simulation are shown, along with tables 4.3, 4.4 and 4.5, comparing averaged values for steer angles, lateral acceleration and four individual wheel speeds. The percentage differences between simulation and telemetry are also calculated. All results demonstrate a close correlation implying that the model accurately represents the real vehicle. Any differences can be attributed to the simulation using a standard set of tyre data for a performance road car as tyre data for the vehicle used to gather the telemetry was not available.

Three Open Differential configuration

With three open differentials, any differing wheel speeds caused by the cornering action are unhindered by the actions of the differential unit. This can clearly be seen in both Figure 4.8 and 4.9 where the four wheel speeds are

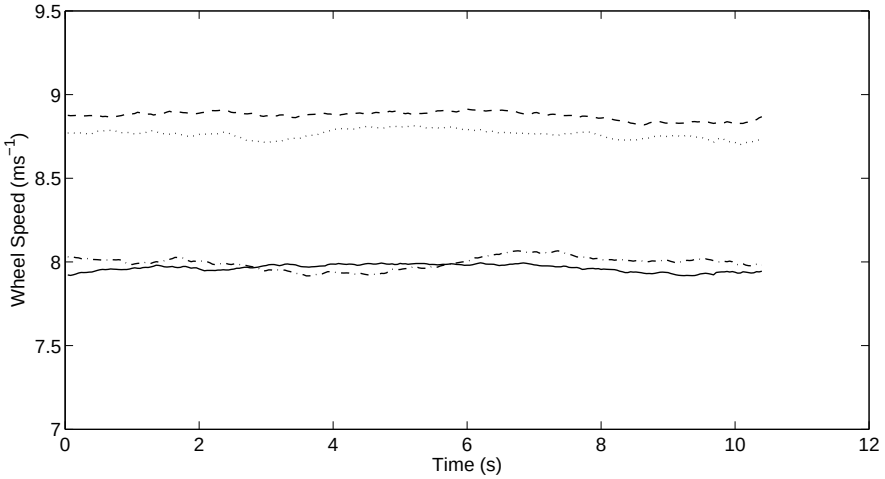

Figure 4.8: Telemetry of Individual Wheel Rates-Three Open Differentials (– – – Front Left, – - – Front Right, - - - Rear Left, —— Rear Right)

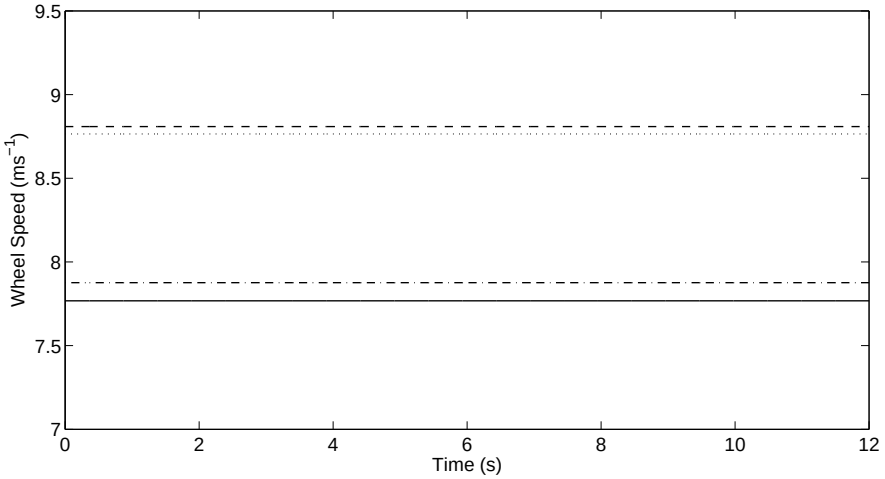

Figure 4.9: Simulated Individual Wheel Rates — Three Open Differentials (– – – Front Left, – - – Front Right, - - - Rear Left, —— Rear Right)

Table 4.3: Three Open Comparison

Metric	Simulation	Telemetry	% Difference
Speed (ms^{-1})	8.09	8.09	0
Steer (Deg)	16	15.6 (117)	2.6
Lat Acc (ms^{-2})	5.40	5.43	0.6
LF (ms^{-1})	8.81	8.87	0.7
RF (ms^{-1})	7.88	7.96	1.0
LR (ms^{-1})	8.77	8.76	0.1
RR (ms^{-1})	7.77	7.99	2.8

clearly different. The average figures are shown in Table 4.3 and along with steer angle and lateral acceleration can be seen to correlate closely with each other.

Three Locked Differential configuration

By locking the three differentials the four wheels should be constrained to rotate at the same velocity. Comparing the results with the three open configuration shows that the wheel speeds have been dramatically brought together. The variation that remains, Figure 4.10 and 4.11, is now a result of the different slip ratios of the tyres as they are deformed from the cornering forces and to a lesser extent, torsional effects on the driveshaft and play in the differentials.

Again, after removing the noise seen in the telemetry data, the average figures are a very close match for the results from the simulation, as shown in Table 4.4.

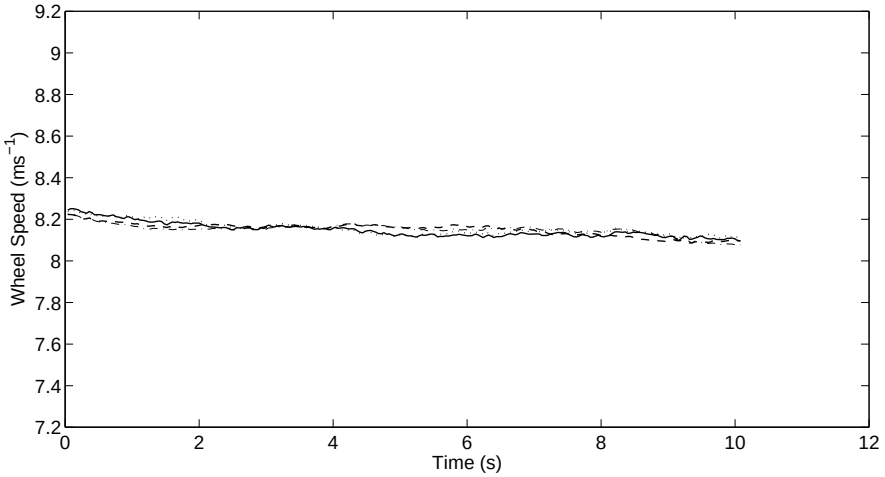

Figure 4.10: Telemetry of Individual Wheel Rates-Three Locked Differentials (– – – Front Left, – - – Front Right, - - - Rear Left, —— Rear Right)

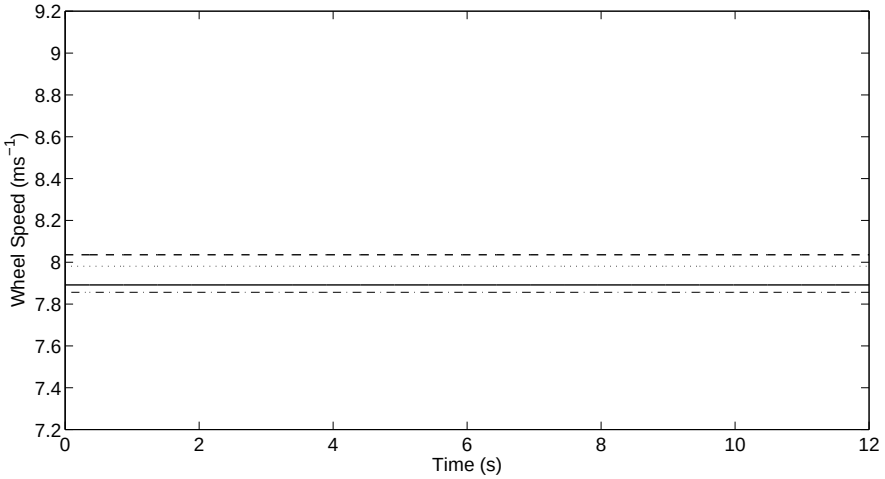

Figure 4.11: Simulated Individual Wheel Rates - Three Locked Differentials (– – – Front Left, – - – Front Right, - - - Rear Left, —— Rear Right)

Table 4.4: Locked Comparison

Metric	Simulation	Telemetry	% Difference
Speed (ms^{-1})	7.66	7.66	0
Steer (Deg)	20	20.1 (151)	0.5
Lat Acc (ms^{-2})	4.80	4.95	3.1
LF (ms^{-1})	8.04	8.14	1.2
RF (ms^{-1})	7.86	8.14	3.5
LR (ms^{-1})	7.98	8.15	2.1
RR (ms^{-1})	7.89	8.16	3.4

Table 4.5: Locked Centre Comparison

Metric	Simulation	Telemetry	% Difference
Speed (ms^{-1})	8.05	8.05	0
Steer (Deg)	16	15.6 (117)	2.6
Lat Acc (ms^{-2})	5.37	5.42	0.9
LF (ms^{-1})	8.74	8.83	0.9
RF (ms^{-1})	7.81	7.89	1.0
LR (ms^{-1})	8.71	8.76	0.6
RR (ms^{-1})	7.72	7.94	2.8

Locked Centre Differential configuration

Locking the centre differential, whilst leaving the front and rear differentials open permits the left and right wheel of each axle to rotate freely although the rotation of the two input shafts to the front and rear differential is locked together. In other words, the sum of the wheel speeds on the front axle is constrained to be the same as the sum of the wheel speeds on the rear axle.

This results in similar wheel speeds to the three open configuration in the steady state circular path manoeuvre presented here.

β-angle comparison

The telemetry data included a vehicle β-angle as measured using a Correvit[12]. As the model was intended to simulate manoeuvres in which β-angle is a key

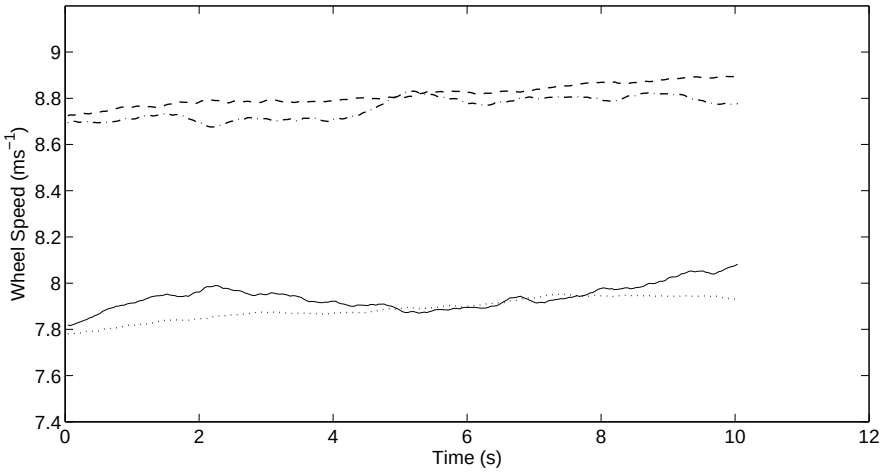

Figure 4.12: Telemetry of Individual Wheel Rates-Locked Centre Differential (– – – Front Left, – - – Front Right, - - - Rear Left, —— Rear Right)

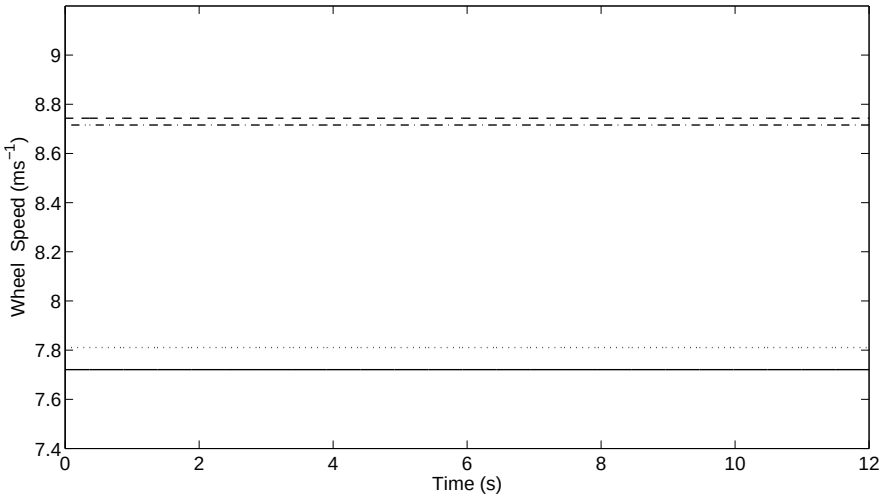

Figure 4.13: Simulated Individual Wheel Rates - Locked Centre Differential (– – – Front Left, – - – Front Right, - - - Rear Left, —— Rear Right)

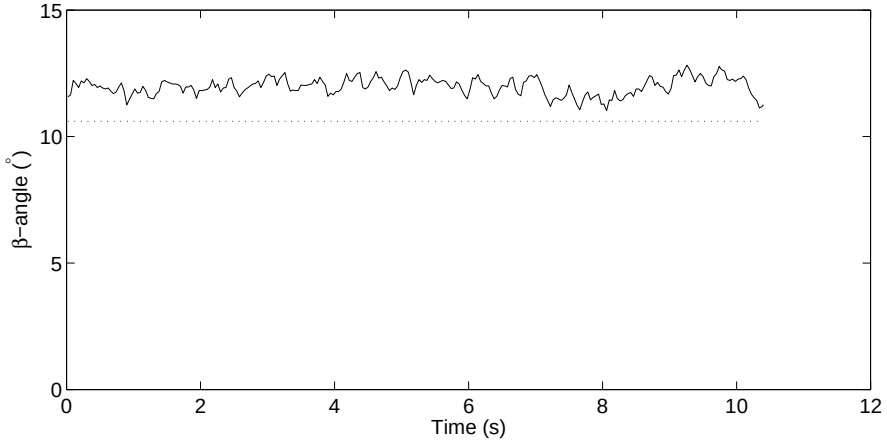

Figure 4.14: Simulated and Measured β-angles - Three Open Differentials (—— Measured, – – – Simulated)

Table 4.6: β-angle Comparison

	Three Open	Three Locked	Locked Centre
Telemetry (Deg)	12.0	13.3	12.0
Simulation (Deg)	10.6	11.6	10.7
% Difference	13 %	14 %	13 %

component, it was important to ensure that the telemetry from the three transmission configurations was accurately recreated in simulation.

Figures 4.14, 4.15 and 4.16 show both the measured and simulated values for the manoeuvres.

Table 4.6 shows the average values of β-angle. In both simulation and telemetry, this angle was relatively stable.

Although the difference is between 13 and 14%, this is directly related to the tyre model parameters being used. The effect on attitude due to the change of transmission, however, is the same in both telemetry and simulation, hence the model is verified.

From the constant radius and speed cornering comparisons of wheel speed, accelerations and control inputs, along with the hand calculation comparison

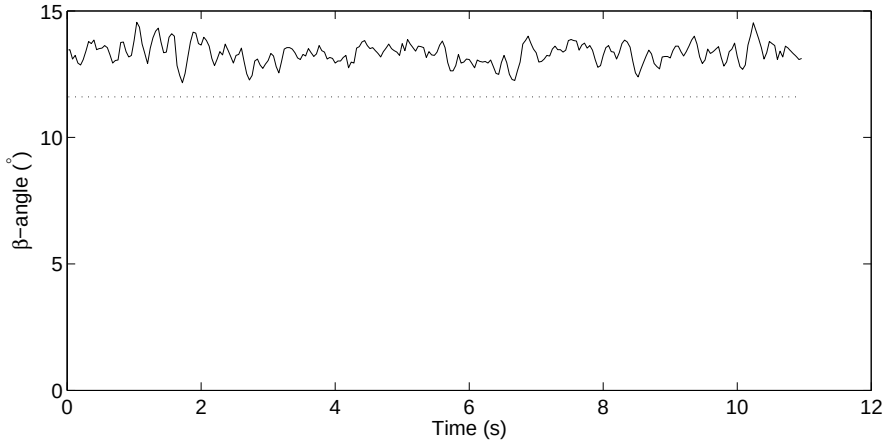

Figure 4.15: Simulated and Measured β-angles - Three Locked Differentials (—— Measured, – – – Simulated)

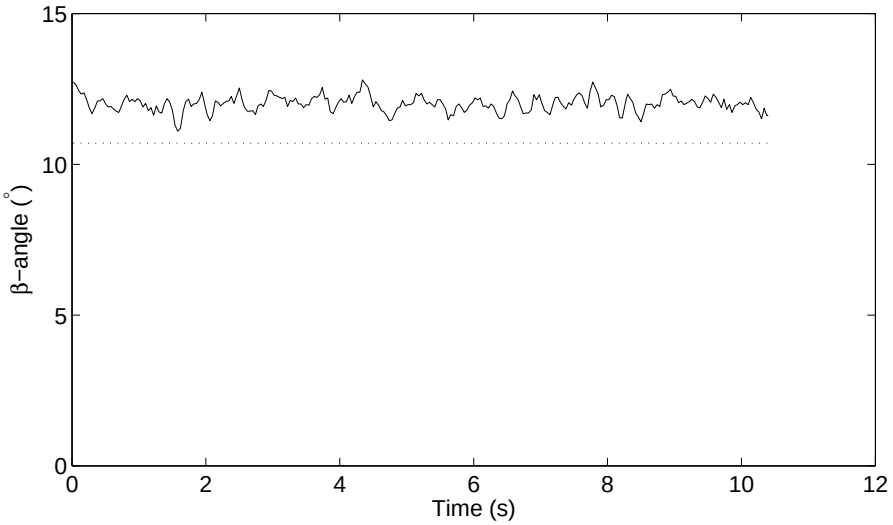

Figure 4.16: Simulated and Measured β-angles - Locked Centre Differential (—— Measured, – – – Simulated)

Table 4.7: Transient Manoeuvre Speeds

	Three Open	Three Locked	Locked Centre
Constant Speed (ms^{-1})	16.0	14.1	14.0

in Appendix B, it can be seen that the general geometry and behaviour closely match to the telemetry of the test vehicle. This includes the effects of differentials and powertrain on the wheelspeeds and chassis.

Through comparing β-angles, this begins to demonstrate that the dynamics of the body and the mechanics of the tyres match those of the test car. The subsequent section continues this through the comparison of a more dynamic transient manoeuvre.

4.3.2 Transient Manoeuvre Comparison

In addition to the constant radius circular path telemetry data, the test vehicle was subjected to a more transient manoeuvre at the Millbrook proving ground. In this case the vehicle was driven at constant speed through a slalom style manoeuvre with the same three transmission configurations as seen previously.

To validate the dynamic behaviour of the WRC model, the steer angle time history from the telemetry was applied directly to the model as it progressed at the same constant speed. For both telemetry and simulation, the vehicles β-angle was compared.

Figures 4.17, 4.19 and 4.21 show the steer inputs applied to each model.

The constant speed at which each manoeuvre was attempted are detailed in Table 4.7.

Figures 4.18, 4.20 and 4.22 show clear agreement between telemetry and simulation β-angle. As with the constant radius cornering, however, there is a difference of around 15% in actual values, again this is contributable to an inexact match in tyre model.

The slight fluctuations that can be seen to occur in the β-angle telemetry data relate to the human driver being less capable at maintaining a constant

speed when compared to the acceleration target PI model used in the simulation. This results in the human driver having to make small adjustments to the throttle input as he progresses and indirectly affecting the β-angle. Other factors such as vibration noise and suspension effects, which are not considering in the simulation model, also contribute to the fluctations.

In the case of the three open and locked centre differentials, the β-angles stay relatively low at around 4 degrees. However, by locking all three differentials and effectively restricting the potential for a difference in wheel speed between the left and right tyres, β-angle increases to around 7 degrees. This increase in the measured values being matched in the simulation results.

Despite this there is a clear match between the simulated results and the measured telemetry that confirms this model is a close dynamic representation of the real test vehicle used to generate the telemetry.

Combined with the constant radius and speed cornering of the previous section and the hand calculation comparison in Appendix B this provides a conclusive validation of the 7-DOF WRC model.

Three Open Differentials Configuration

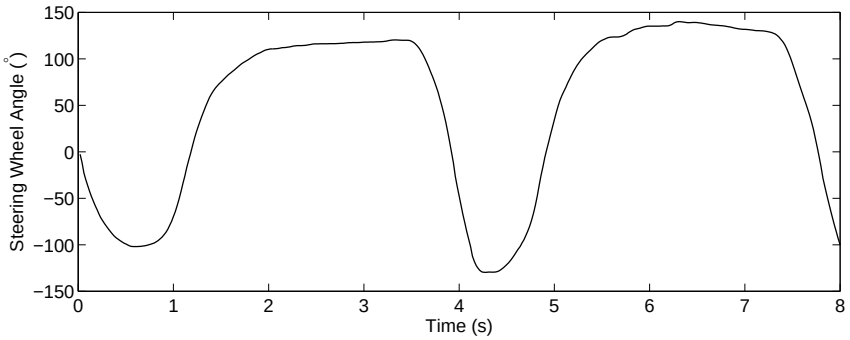

Figure 4.17: Steer Angle Telemetry and Simulation Input for Three Open Comparison

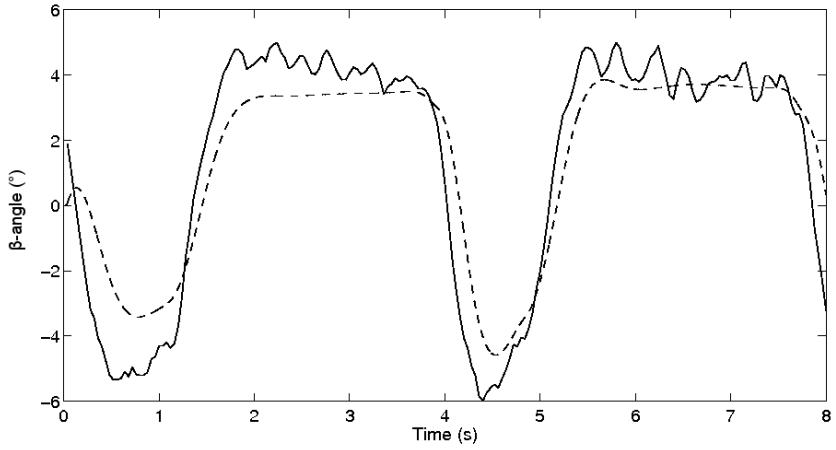

Figure 4.18: Comparison of β—angle for Three Open Differentials Model (—— Telemetry, – – – Simulation)

Three Locked Differentials Configuration

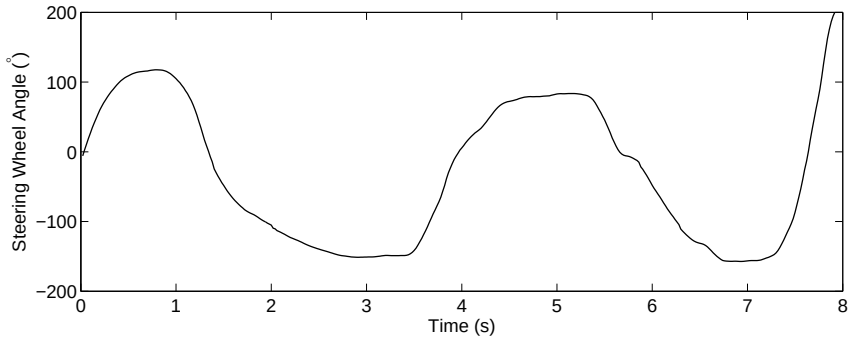

Figure 4.19: Steer Angle Telemetry and Simulation Input for Three Locked Comparison

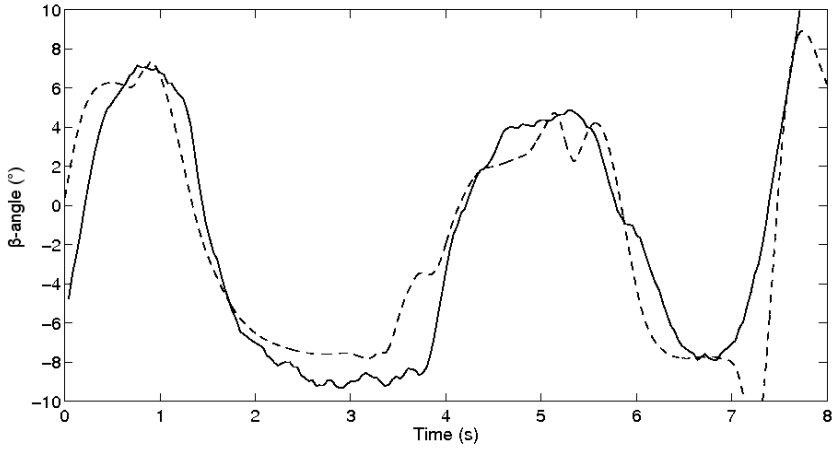

Figure 4.20: Comparison of β-angle for Three Locked Differentials Model (—— Telemetry, – – – Simulation)

Locked Centre Differential Configuration

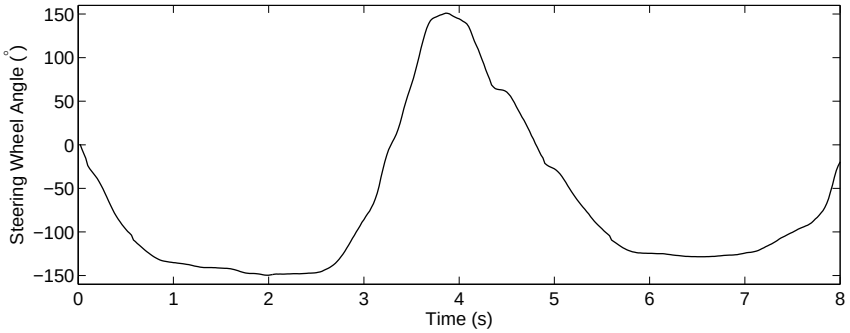

Figure 4.21: Steer Angle Time History for Locked Centre Comparison

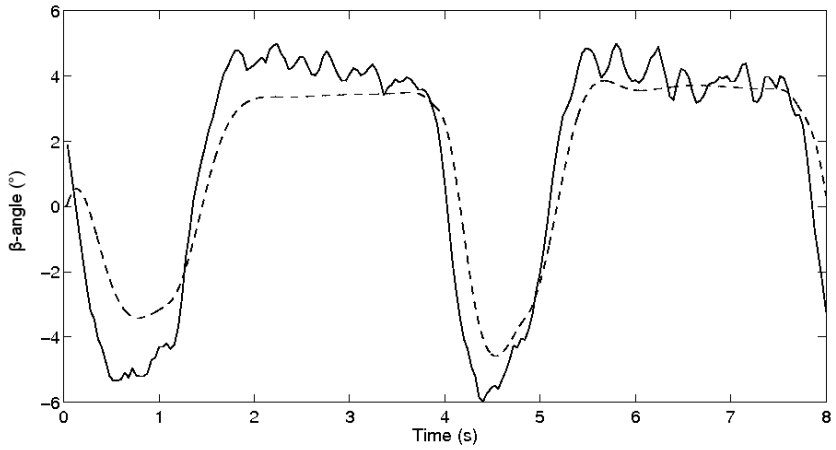

Figure 4.22: Comparison of β-angle for Locked Centre Differential Model (—— Telemetry, – – – Simulation)

4.4 Lateral Tyre Curve Inference

Having developed a robust β-angle sensor along with a validated and verified model of the vehicle to which such a sensor can be fitted, various new opportunities are opened up for investigating vehicle behaviour. One of the most significant is the ability to derive lateral tyre force curves (with tyre slip angle plotted against lateral force) from telemetry data irrespective of the surface conditions.

This section presents a method of applying a set of telemetry data to the equations of motion used for the 7-DOF model to construct a lateral tyre curve. The method can be applied to a more conventional slip angle sensor as well as the new sensor described. Where the conventional sensors are restricted to tarmac surfaces, as previously described, the β-angle sensor is robust enough to produce a realistic measurement on a gravel surface.

The curves generated are for pure side slip and in order to produce the graphs, certain assumptions have to be made. These are:

- The tyres are always working in pure side slip conditions
- Lateral weight transfer effect is considered to average out between inside and outside tyres
- The vehicle is considered to be in discrete steady states at each sample point. Transient effects are ignored.
- Rear axle compliance is considered negligible such that rear slip angle is equivalent to body slip angle
- All other tyre factors, such as temperature and wear, are considered to be constant.
- All other external factors, such as road surface, are considered to be constant.

In practical experimentation under controlled manoeuvres and circumstances, it is shown that these assumptions are not unreasonable and that

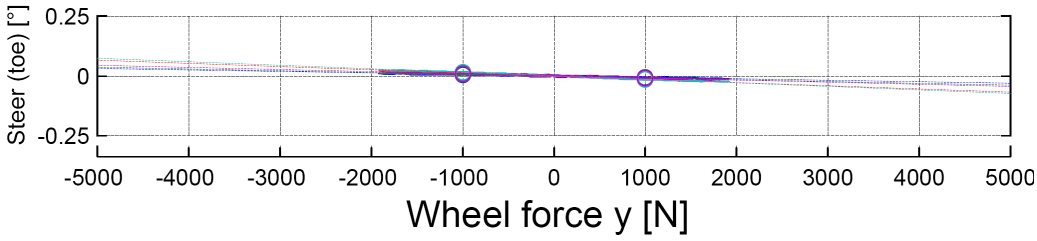

Figure 4.23: Variation in Toe Angle of Rear Wheel under Lateral Force

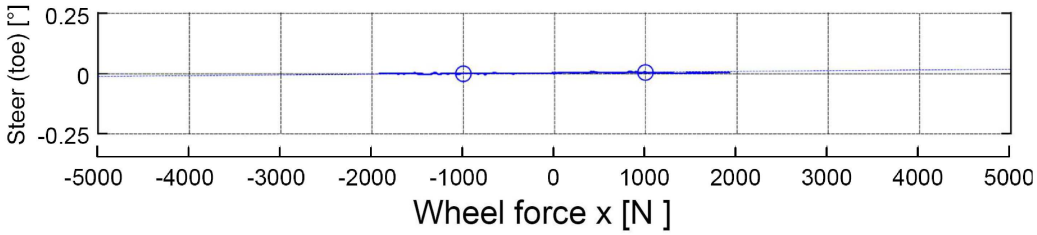

Figure 4.24: Variation in Toe Angle of Rear Wheel under Longitudinal Force

realistic tyre curves can be obtained. In particular the magnitude of rear axle compliance can be shown using two extracts from experimental observations obtained using a kinematics and compliance test rig on this class of vehicle. Figure 4.23 and 4.24, both extracted from a set of data provided by a WRC team, demonstrates the variation in toe angle of the rear wheels under an applied longitudinal and lateral force of a WRC car. From these figures it can be seen that even at high forces, the rear axle compliance only results in an extremely small change in toe angle, at most less than 0.1 degrees. This confirms that such an assumption would be valid.

However, in applying the same theory and methodology to standard stage test run data, it is shown that some of the other assumptions no longer hold and combined with increased high frequency and transient effects, the clarity of the tyre curves become significantly degraded. Despite this it is still possible to see a degree of correlation between expected and actual results

which provide some insight into driver behaviour and tyre performance.

Three sets of results are presented, the first using a Correvit[12] on a tarmac skid pan under controlled test conditions. The data being collected from the set of manoeuvres described below. The second and third sets are collected from stage test runs on gravel and tarmac surfaces using the β-angle sensor.

4.4.1 Determining Tyre Slip Angle

Vehicle β-angle can be measured using a variety of techniques as described in Chapter 2 and 3. Due to the relatively fixed nature of the rear wheels in respect to the chassis, it is possible to equate vehicle β-angle to rear wheel slip angle directly when the GPS antenna of the β-angle sensor is mounted above the line of the rear axle. This removes any necessary consideration of potential effects due to applied steer angle at the front wheels but also assumes that the vehicle is in a steady state. During transition between states, tyre relaxation or changes to the carcass distortion may result in a difference between rear wheel slip and vehicle slip.

As attempted curve generation is concerned with pure side slip conditions, it is assumed that the longitudinal tyre slip ratios are zero. This is on the basis that the vehicle is being driven at a steady speed and that the aerodynamic drag effect is negligible meaning that no longitudinal tyre forces and hence slip ratio is being generated. Camber angle and other suspension geometry effects are also assumed to be static and negligible on the extremely stiff test vehicle.

4.4.2 Determining Lateral Tyre Force

Determining an individual tyres lateral force consists of two steps. The first considers total vehicle lateral force whilst the second resolves the front and rear axle contributions to that total.

Although previously discounted as a means for measuring lateral velocity due to excessive noise and problems with using integrated signals, accelerometers[79] can still provide suitably accurate measurement of lateral

acceleration. Then using Newton's Second Law, equation 4.1, and knowing m, the mass of the vehicle, the total lateral force being applied to the vehicle can be determined.

$$F = ma \tag{4.1}$$

This force is a product of the four tyre forces. As the slip angle is being taken at the rear tyres, this force must be divided into front axle and rear axle components. Any difference in the distribution of force between the front and rear of the vehicle results in a yawing moment and hence a yaw acceleration, as the rotational equivalent of equation 4.1 shows.

$$N = I_\psi \alpha \tag{4.2}$$

Angular acceleration can be measured using a gyroscopic yaw rate sensor and, given the yaw inertia of the vehicle, the rear axle force can be calculated. Assuming that the slip angle and vertical loading of both rear tyres is the same, the individual lateral tyre forces can be considered equal and therefore each is generating half the total axle force.

Unfortunately the assumption of equal vertical loading on both rear tyres is difficult to justify as generating higher slip angles requires higher lateral acceleration and hence more lateral weight transfer.

By using the lateral weight transfer equations of the 7 DOF WRC model it is possible to calculate an approximation of the static vertical loading for each individual data point. Using this data it becomes possible to overcome this problem as the data can be separated out into sets with similar vertical loading on the tyre. This method requires significantly more data to produce a set of complete graphs for each value of vertical tyre load.

The alternative, and the method used in this study, is to produce a curve which represents half the axle lateral force generated, that is the sum of the inside (less loaded) and the outside (more loaded) tyres. This is akin to using a bicycle model where only one front and one rear tyre are considered. Using this method it is assumed that the vertical load on each of the tyres is equal throughout the manoeuvre and equivalent to the static vertical load which

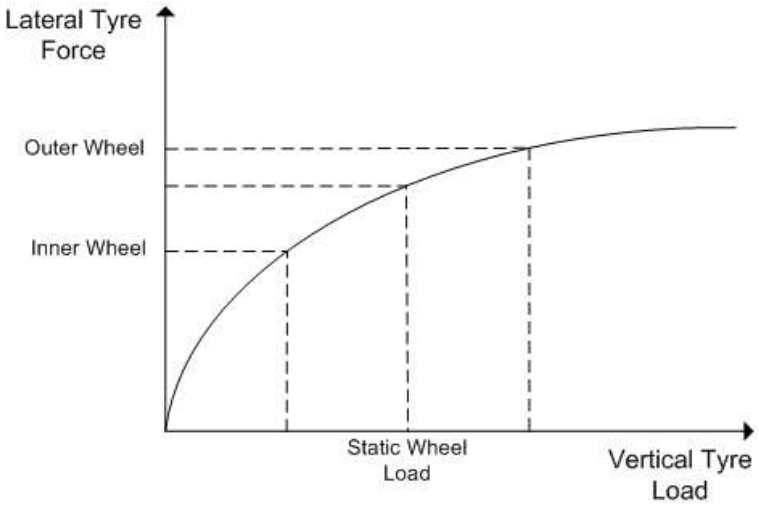

Figure 4.25: Tyre Lateral Force against Vertical Load[10]

can be easily measured.

Although this does not give a direct insight into what each individual tyre is doing as the load of the vehicle is transferred to the outside wheel, it does allow analysis of the general properties of the combined axle and hence the dynamics of the vehicle system.

If it were important to isolate a single tyre for analysis, it would be necessary to rebalance the vehicle with either ballast or using some other method to ensure consistent vertical load throughout all manoeuvres. This seems somewhat unrealistic however as high slip angles invariably produce high lateral accelerations and hence significant changes in vertical loading from the static condition.

Longitudinal weight transfer is considered to be zero as the vehicle is travelling at constant speed in the controlled test manoeuvres.

Estimating Yaw Inertia

Despite the detailed information provided about the test vehicle, the yaw inertia was not provided or available from the test team. In addition, detailed drawings of the vehicle, which would have allowed a calculated value to be

determined, were also not available for this study. Unfortunately this meant an estimation was required. Although not perfect, this was the only option for obtaining the essential value for the yaw inertia.

Fortunately, there exists a rule of thumb, Equation 4.3 and 4.4, and an approximation method, Equation 4.5, which have been used in previous research as suitable replacements. The implications of this first rule is that yaw inertia is equal to pitch inertia and that pitch inertia is approximately the product of the vehicles mass, the distance of the CofG from the front axle and the distance of the CofG from the rear axle.

$$I_{\psi} = I_{pitch} \tag{4.3}$$

$$I_{pitch} = Mab \tag{4.4}$$

To verify this rule of thumb, the National Highway Transport Safety Administration (NHTSA)[80] compared the results of various measured inertias from their Inertia Parameter Measurement Device(IPMD) rig to the inertias derived from Equation 4.4. It was shown that this is an accurate enough approximation of true yaw inertia for this form of vehicle dynamics calculation.

The second estimation method for yaw inertia[81], again derived from a wide range of vehicle measurement is shown in Equation 4.5. Both methods produce a very similar value for yaw inertia which helps to increase confidence in the results.

$$I_{\psi} = \frac{(TW) \times (WB)}{K} \times M \tag{4.5}$$

K represents an approximation value for each class of vehicle. For yaw inertia and a standard passenger car, a value of 2.1942 is recommended[81].

4.4.3 Process Overview

Figure 4.26 shows a simplified flowchart intended to give an overview of the tyre curve calculation process.

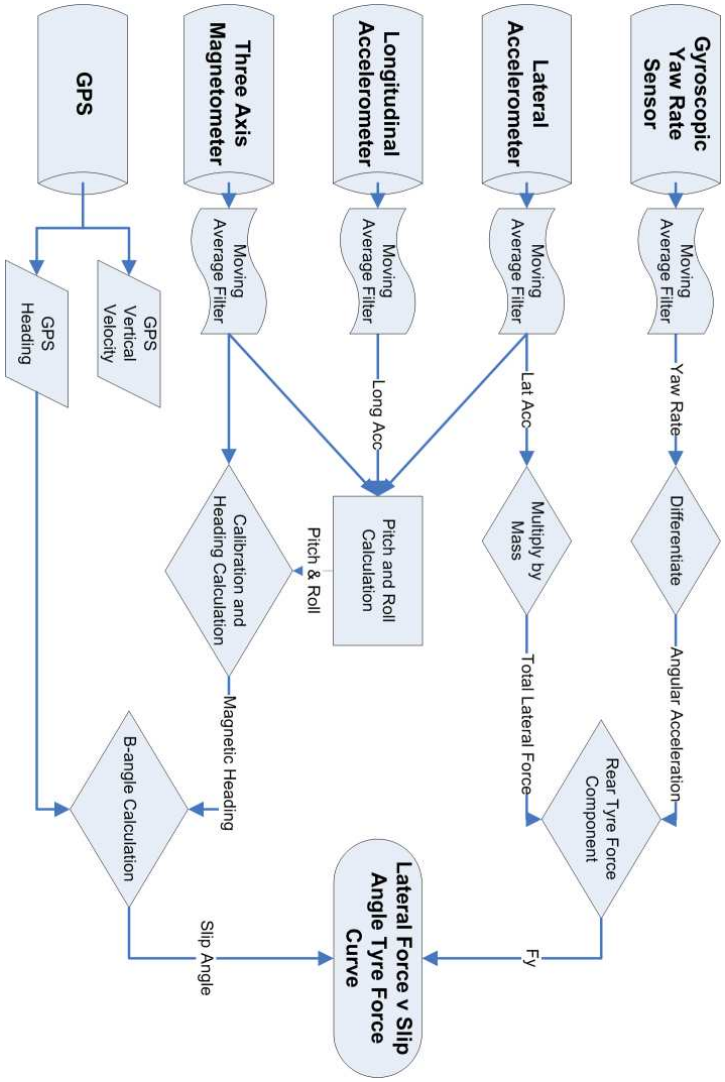

Figure 4.26: Tyre Curve Generation Process Overview

4.4.4 Populating the tyre curve

In order to produce the necessary conditions to fully populate a complete tyre curve, whilst at the same time minimising excessive transient effects, the curve is split into two intersecting regions. For each region a set of manoeuvres are suggested that yield the required range of slip conditions.

The first region is known as the linear region as lateral force increases linearly with respect to slip angle. This is the region in which the majority of standard road driving occurs, tyre performance is highly predictable and the vehicle feels more controllable.

The second region covers the area leading up to saturation, at which the tyre generates its maximum lateral force, and beyond into super-saturation. This is the region more commonly inhabited by high ability drivers looking to maximise vehicle performance. Super-saturation occurs after the force peaks and begins to tail off. This is the area of most interest to rally drivers when they drive with high vehicle attitude angles. These two regions and the expected shape of a lateral tyre curve according to the Pacejka[53] model are shown in Figure 4.27.

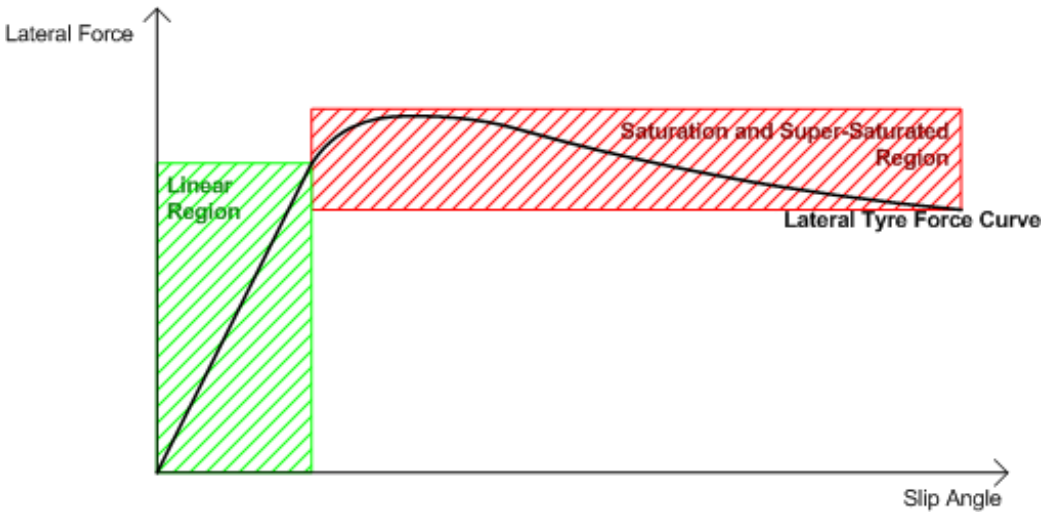

Figure 4.27: Lateral Tyre Curve Regions

The Linear region

The simplest manoeuvre to cover the linear range is a slalom course in which a sinusoidal steer input is applied at a moderate constant speed. As the steer angle is progressively increased, slip angle increases as the vehicle begins to yaw. Once the vehicle approaches the saturation region, the steer angle is eased off and applied in the opposite direction, thus producing both positive and negative slip angles. Furthermore as the manoeuvre is simple, with slip angle and lateral force increasing and decreasing progressively, any erroneous readings or significant noise can be easily spotted and corrected.

For increased confidence in the results this manoeuvre can be repeated at various speeds although it may be difficult to reach the higher end of the linear region at lower speeds.

An alternative to this method involves a circular course where the test vehicle is driven at a constant speed around a constant radius circle. By progressively increasing the speed, the lateral force requirements also increase leading to higher steer angles and higher slip angles.

At each speed it is necessary to obtain a steady state with a constant steer angle and throttle position to maintain forward velocity before completing a few circuits to collect the relevant data.

Unlike the first method, the circular path requires less physical space in which to perform the manoeuvre but suffers as it generates data at various points along the linear region rather that the transition through the region seen with a sinusoidal manoeuvre. Ultimately a combination of the two would provide the most comprehensive dataset.

Saturation and Super-Saturation

To populate the saturation and super-saturation region, the test vehicle needs to be driven in a more vigorous manner that pushes the tyres beyond their saturation point. This can be achieved by a skilled test driver inducing the test vehicle to drift round a circular path to varying extents while trying to maintain constant speed. By changing the radius of curvature a richer dataset can be obtained.

The driver must attempt to maintain the state of saturation without large throttle inputs as these would result in high slip ratios and affect the lateral capabilities of the tyre[82]. This is dependent on the highly developed skill of the test driver, they need to gauge the feel of the vehicle in such a manner to achieve this as it is relatively easy to produce an unstable drift through large fluctuations in throttle input and steer angle.

As shown by Shibahata[14] and discussed in Chapter 2, the tyres of a vehicle generate a stabilising yaw moment as the attitude of the vehicle increases. This moment can be calculated by Equation 4.6.

$$M_{\psi} = -aF_f + bF_r + (T_{SA1} + T_{SA2} + T_{SA3} + T_{SA4}) \tag{4.6}$$

Therefore, if the vehicle is induced to a state of high attitude angle, it will try to return to a more stable state and the attitude angle diminishes. If the initial state is at the far end of the super-saturated range, the tyre will experience a range of conditions during this transition that allow data to be collected across the desired part of the tyre curve.

The driver would be asked to excite the vehicle to a high value of β, a method for this is shown in Chapter 5, and then allow the angle to diminish naturally while using the throttle only to maintain forward velocity. Unfortunately such a manoeuvre is very difficult to duplicate exactly each time but is necessary to see the tyres working at the higher slip angles and in the super saturated region. Some variation will therefore be expected in peak angles and rate of slip angle reduction although this should not affect instantaneous slip angle and lateral force measurements. Again as with previous manoeuvres, different forward velocities are tested although it is not possible to induce higher angles at lower speeds.

During these periods, the lateral tyre forces can be calculated as previously shown and the corresponding region of the tyre curve can be filled in.

As the higher tyre slip angles are generating higher lateral accelerations, lateral weight transfer begins to have a more significant influence on the individual vertical wheel loads. At these points, the assumption that any loss in

tyre force on the inside of the rear axle will be compensated for by an increase on the outer side becomes less tenable. It should be remembered, though, that the process described here is not intended to produce highly accurate tyre maps due to this and the large number of other unknown quantities.

Despite these factors, the procedure will be shown to give a good overview of the tyre performance on loose gravel surfaces where tyre curves have not been seen before as well as a means of comparison with test rig generated tarmac curves.

4.4.5 Testing Process Overview

Figure 4.28 shows a flow diagram depicting the collection of tyre data used in generating the lateral force curve.

Having performed the testing process and produced a lateral tyre force curve, the data is compared with the expectations from the Pacejka Magic Tyre[53] model defined tyre curve, see Equation 4.7.

$$F_y = Dsin(Carctan(B\alpha - E[B\alpha - arctan(\alpha)])) \tag{4.7}$$

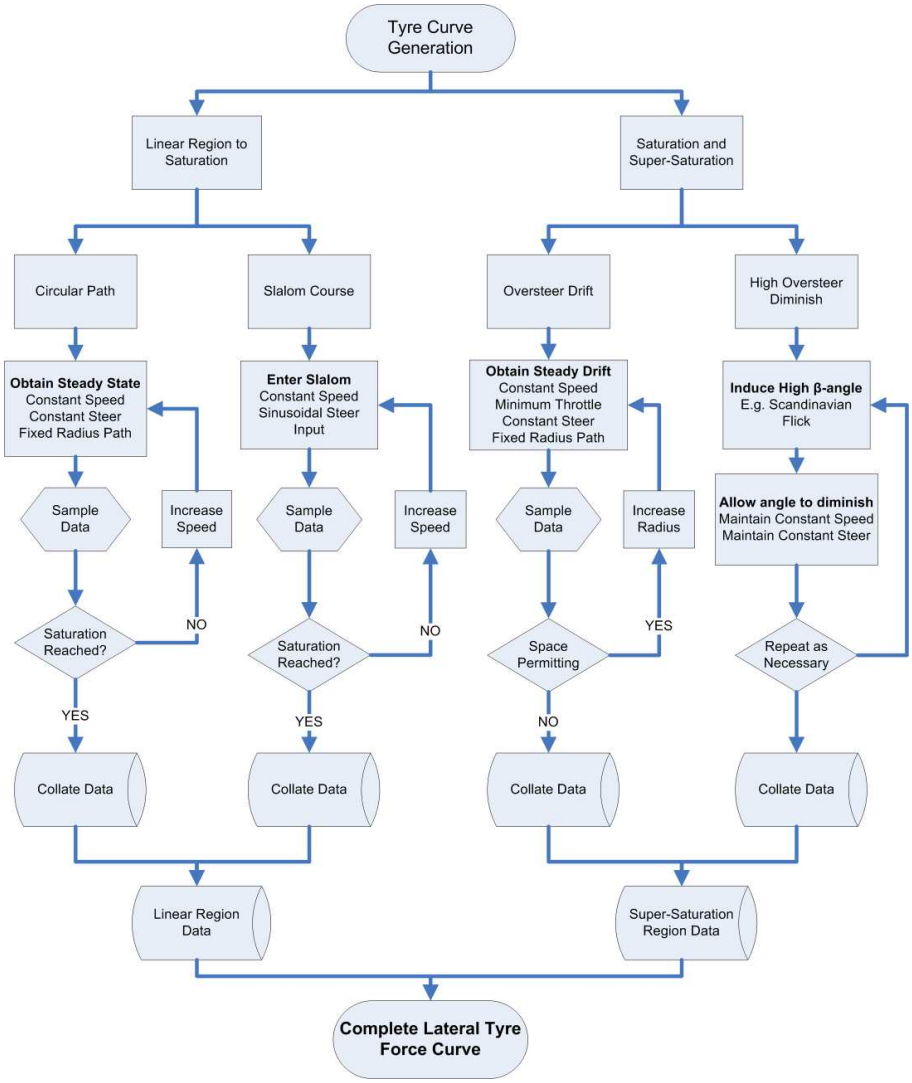

Figure 4.28: Data collection Flow Chart

4.5 Resultant Tyre Curves

Presented below are three tyre curves, the first derived from Correvit-based telemetry data and the second from the β-angle sensor.

4.5.1 Correvit Tyre Curves

Figure 4.30 is derived from the same Millbrook proving ground telemetry data used for validating the 7-DOF model. The vehicle was fitted with a Correvit[12] which measured the slip angle of the vehicle by projecting a diffraction grating onto the tarmac surface.

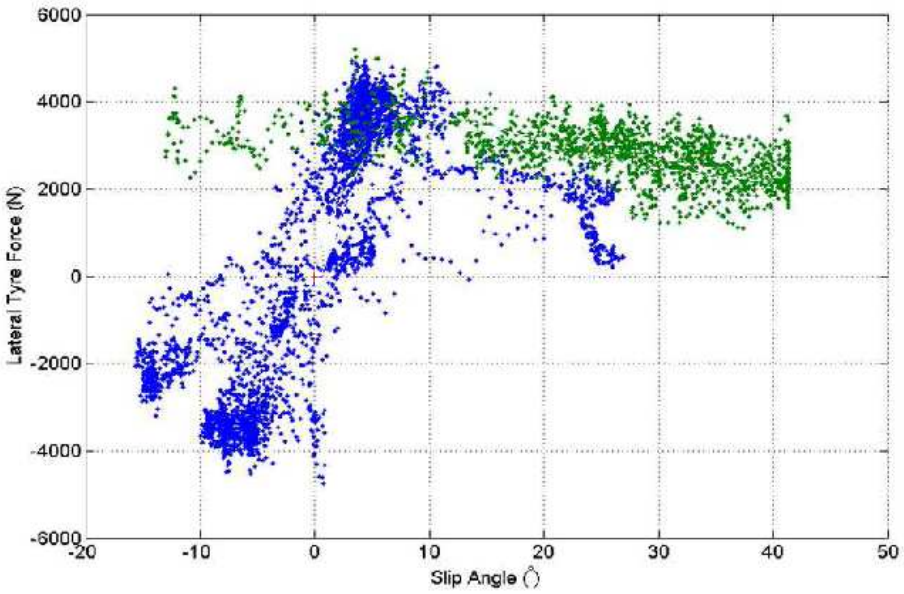

Figure 4.29: Lateral Tyre Curve - Tarmac ($F_z = 3000N$)

In Figure 4.29, two datasets are shown. The first in blue covers the linear region whilst the second green data covers saturation and beyond. The telemetry data used to construct the data set is not perfect and as such is quite noisy. The manoeuvres that were logged are more transient than the steady state manoeuvres suggested for constructing a cleaner curve. This

transient nature affects the curve as each point in the tyre curve should represent a steady state equilibrium. As such, factors such as the time required to distort the tyre carcass and the effects of the damper force on vertical loading conspire to generate a less that perfect fit.

By ignoring this problem, a degree of uncertainty can be seen in the graph as a tyre force band rather than a sharper line.

Despite this, the expected shape for a lateral tyre curve as prescribed by the Pacejka Magic Tyre Formula[53] is clearly seen. It should be noted that this set of tyres appears to be saturating at around eight degrees of slip angle and 4000 Newtons of lateral force. Beyond saturation, the tyre appears to steadily drop off to a lateral force of around 2500 Newtons at 30 degrees of slip.

The linear region can be seen to be symmetric through the origin as both left and right turning manoeuvres are available. Beyond saturation data is only available for a left hand drift.

4.5.2 β-angle Sensor Derived Tyre Curves

Figure 4.30, 4.31, 4.32 and 4.33 are from a vehicle fitted with the β-angle sensor driven on gravel and tarmac surfaces and at full rally special stage speed. Because of this the data shows more noise and variation from the expectations than seen in the Correvit derived curves. Unfortunately it was not possible to obtain data for the controlled test manoeuvres described previously. Despite this there are some points that than be extracted from the data.

Values for static vertical tyre loading were provided for the test vehicle and were 3000 Newtons for the rear tyres.

Tarmac

Figure 4.30 shows the tyre data extracted from the telemetry of a test run through a tarmac stage in Spain. It was run at full rally speed and as such shows significant noise. In addition to this, the GPS module used for this test seemed to suffer problems in acquiring a suitable GPS signal lock. As

such the GPS data demonstrated multiple drop out points which affected the calculation of β-angle. This data set has therefore been truncated to remove these regions.

Despite the noise, this graphs show clear similarities with the Correvit[12] generated curve of Figure 4.29. Again this set of tyres appears to become saturated at between eight and ten degrees of slip angle with a maximum lateral force generated of just below 4000 Newtons. Beyond saturation, although there is only limited data, the tyre appears to drop off to a lateral force of approximately 2500 Newtons at 30 degrees of slip - the same as the Correvit generated curve.

As a simple check on these figures, the telemetry from the vehicle showed peak lateral accelerations of around 1.4G. A quick calculation shows that to obtain such a value, each tyre would need to generate just below 4000 Newtons.

From this data, it is not only possible to gauge the performance of the tyre, it is also possible to analysis the driver's style. For these tarmac stages the vast majority of the data shows the tyre working in the linear region and around the saturation point (between zero and 15 degrees). This matches expectations and demonstrates that the driver is adopting a more track-like racing style. There are still a few points at which the driver induces slip angles of up to 25 or 30 degrees but these are usually attributed to the driver not necessarily being aware of the nature of the corner. That is, each corner is new to the driver until they have actually entered it and hence the driver may require a more aggressive correction if it is tighter than expected. This problem does not exist in circuit racing as the driver will be already aware of each corner and its relevant dimensions.

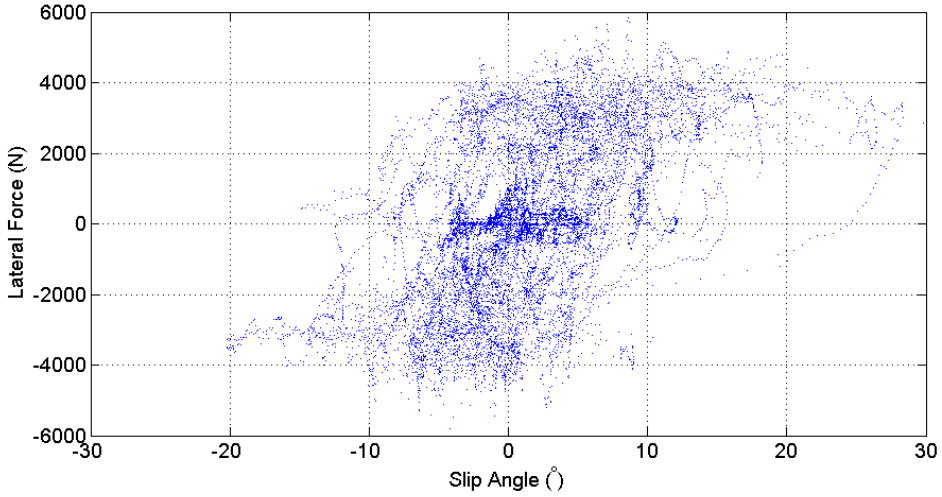

Figure 4.30: Lateral Tyre Curve 1 - Tarmac ($F_z = 3000N$)

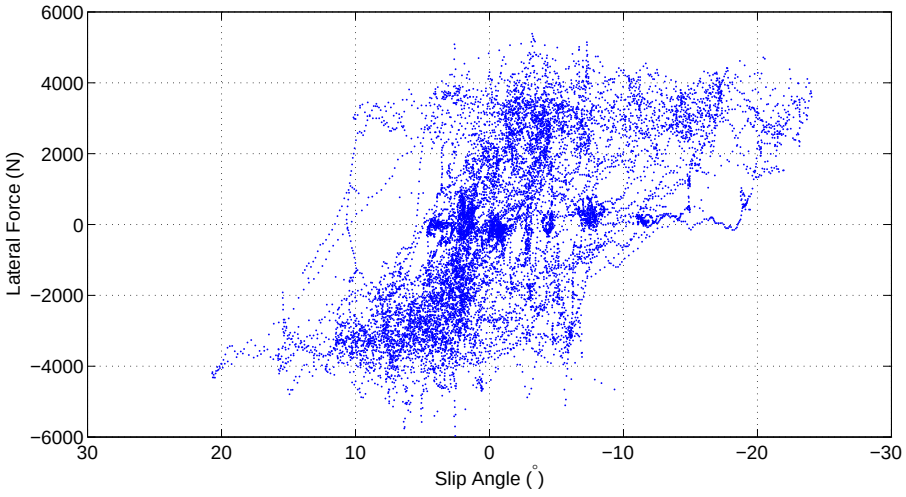

Figure 4.31: Lateral Tyre Curve 2 - Tarmac ($F_z = 3000N$)

Gravel

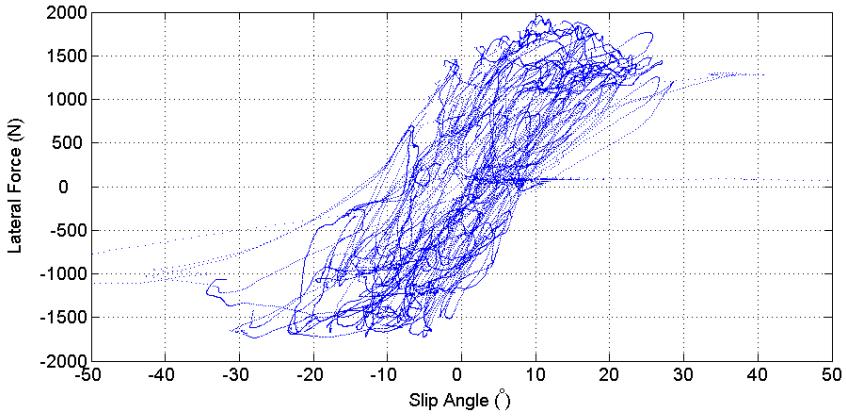

Figure 4.32: Lateral Tyre Curve 1 - Gravel ($F_z = 3000N$)

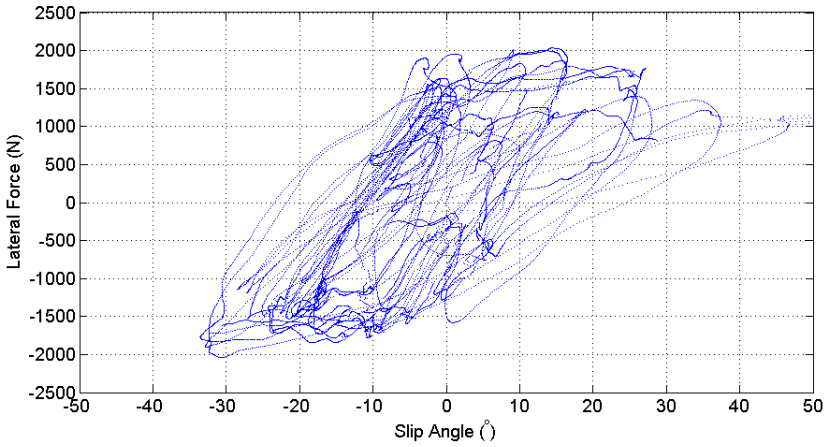

Figure 4.33: Lateral Tyre Curve 2 - Gravel ($F_z = 3000N$)

Figure 4.32 shows the tyre data extracted from a test run on wet loose gravel. Figure 4.33 show the same features but from a slightly shorter run by a different driver.

As the data presented here does not represent the specific manoeuvres detailed previously, the assumptions regarding the variation in vertical tyre loading are less tenable. Whereas the specified manoeuvres represent either a steady state cornering action or a linear increase and decrease in weight distribution, this is not the case with this data. The more erratic nature of the control inputs and hence the action of the suspension and the dampeners combine to significantly affect the changes in vertical tyre load between the inside and outside wheels. This is the primary reason for the broad band of data that is seen in the results and could be improved through repeating the data collection and conforming to the recommended procedure detailed previously.

Both graphs, although noisy as described, show some important characteristics about the tyres and also the driving style used for these vehicles on loose gravel surfaces.

Despite the static vertical loading on the tyre being 3000 Newtons, the graphs show that the peak lateral tyre force does not exceed 2000 Newtons. This demonstrates a significant reduction in lateral ability compared with the data from the tyre on tarmac. In addition the tyre becomes saturated somewhere around 12 degrees of slip angle, slightly higher than seen for tarmac.

Beyond saturation, the tyres drop off in a similar manner to the tarmac tyres with lateral forces down to about 1250 Newtons around 30 degrees of slip.

Performing the same check as for the tarmac curve, again the telemetry shows peak lateral accelerations of approximately 0.6 to 0.7G. This would imply each tyre generating just below 2000 Newtons each.

Although saturation occurs only slightly higher than the 8-10 degrees seen in tarmac tyre data, the driver routinely excites the vehicle to higher slip angles in the 20-30 degree range. This is due to the vehicle's yaw mode becoming under-damped and oscillatory on low friction surfaces, as demon-

strated by Casanova in optimal simulations on a surface with a coefficient of friction as low as 0.6[62]. The driver takes advantage of this by sliding the car in order to enhance the vehicles yaw rate when turning, ultimately achieving greater corner speeds. This driving technique, including the method used to induce high slip angles, is investigated more thoroughly in Chapter 5.

4.5.3 Conclusions from the Tyre Data

Despite the limitations listed below, the generated tyre graphs produce a good match to the expectations from the Pacejka Magic Tyre model[53]. By repeating the tyre measurements in a more rigourous manner using the prescribed manoeuvres which are intended to minimise some of this points, a clearer result would be obtained.

- Pure lateral slip conditions not maintained due to acceleration and braking
- Transient effects from suspension effects and tyre carcass deformation
- Changes in the vertical tyre forces
- Errors and noise in Accelerometer measurements
- Errors in yaw inertia estimation and other model parameters

The tyre curves, though, still provide invaluable results from a real WRC car driven in realistic conditions on both tarmac and loose gravel surfaces. Where as the tarmac data can be compared to similar data from a suitable test rig, the gravel data gives an understanding of the tyre characteristics that have not been previously seen.

In concluding it can now be confirmed that a tyre on gravel will have around 50 to 60% of the lateral force generating capabilities of a tyre on tarmac. In addition, the linear region appears to continue until higher values of slip angle than that of the tyre on tarmac, with saturation occuring at 12 degrees rather than 8-10 degrees. Unfortunately the uncertainty in

the collected data does not allow a closer comparison of the exact point of saturation in either case.

It is worth noting that although the tyres used for the two tests were similar, they were not identical with different hand cut tread patterns for the wet tarmac and gravel surfaces. No further information about the difference in tyres was available.

Beyond saturation the change in road surface does not appear to have a significant effect on the rate of deterioration of the lateral tyre forces. This should not be considered conclusive though as there are many grades gravel which may demonstrate different results.

The implications of these results would suggest that a simple adjustment in the coefficient of friction to model a tyre on gravel, as implied is the case by Wong[83], is not sufficient to truely represent the real tyre behaviour. By determination of a suitable set of Pacejka coefficients to match the data obtained, a more realistic model can be implemented that matchs the change in peak forces and the movement of the saturation point. These coefficients and tyre model then result in the ability to produce a more accurate simulation of a rally car on gravel, particularly when simulating manoeuvres where the tyres are working in the saturation region and beyond.

Chapter 5

Modelling Case Study

This chapter presents three case studies relevant to rallying and, in particular, the application and effect of extreme β-angles, and the ability to sense them, on the vehicle's dynamics. Through the first case study, the importance of β-angle is stressed and it is shown that the notion of using control systems to strictly limit a vehicle, such as a rally car on gravel, to low values during cornering will not necessarily result in optimal performance. The influence of aspects such as tyres, differential and torque distribution is also shown, demonstrating that β-angle characteristics of a vehicle are dependent on many factors. The second case study continues this investigation into the corner exit scenario.

The third case study demonstrates a potential development of the β-angle sensor as a control system input.

One of the most spectacular and dramatic aspects of rallying is the method that skilled drivers use to negotiate tight corners on loose surfaces at high speeds. Their technique involves extreme β-angles and gives the impression that the vehicle is on the verge of losing control and sliding straight off the road. This represents a stark contrast to circuit racing where β-angles are kept near zero.

The first case study examines this behaviour and through simulation demonstrates the performance gains that are available. The influence of different transmission configurations are also studied to gauge what effect

they may have on cornering speeds given that the well understood thinking applied to circuit cars does not necessarily hold at higher β-angles.

Through the simulations presented, it is clear that the primary influence on the results from each simulation is the tyre model employed. To that end, a tyre sensitivity exercise is performed to show how differing tyres could affect the results. This is also examined in the context of the experimentally generated tyre curves from the previous chapter.

The second case study looks at how β-angle control may be implemented using the β-angle sensor as a potential vehicle control input. The corner exit problem is used as a key example in which a driver has allowed the vehicle to maintain a high β-angle out of the corner and now needs to reduce this angle to maximise straight line acceleration. As with the previous case study, the transmission configuration and control is investigated for a vehicle fitted with electro-hydraulic actuated differentials. This is finally extended to demonstrate the potential to induce and control vehicle β-angles at magnitudes to correspond with maximum performance demonstrated in the first case study.

The third case study presents a further example where β-angle control of variable torque splitting transmissions is presented. Although these type of transmissions are only just becoming commercially available it will be shown that such flexibility can result in improving vehicle feel and performance. One attribute of a nimble car is the ability to accelerate through a double lane change manoeuvre without excessive β-angle or oscillations in β-angle (so-called *fish-tailing*. Three examples are shown representing a small executive class passenger car with varying degrees of torque vectoring capability. Each increase in complexity is shown to produce a significant reduction in the magnitude of β-angle witnessed during the manoeuvre. As torque vectoring can also be employed to enhance yaw dynamics, the simulations were performed in such a manner as to produce nearly identical paths between the three models; this allowed the direct affect on β-angle to be understood without the added complexity of considering active yaw control influences.

This case study is based on the research presented at the IAVSD conference in Milan 2005[84].

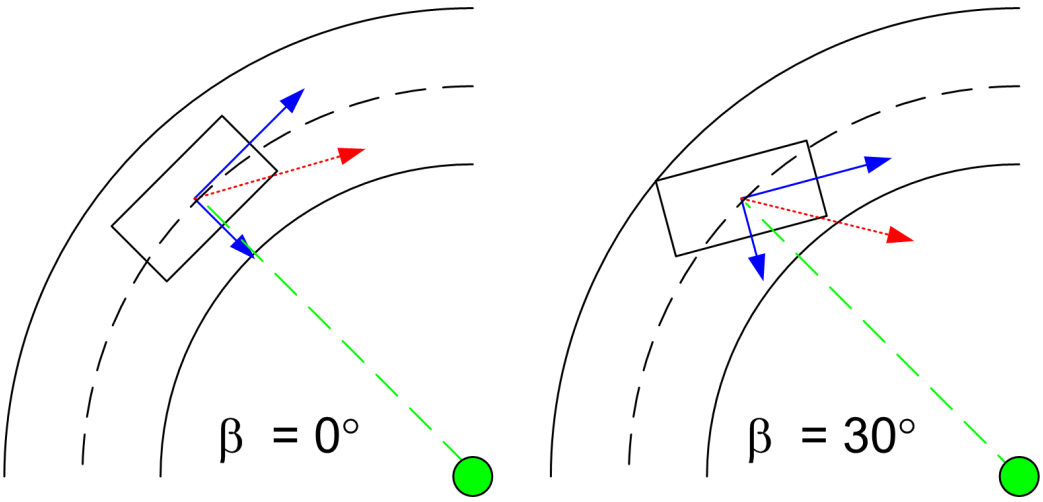

Figure 5.1: Force Vectors During Cornering Under Power - with 0° and 30° of β-angle

5.1 Cornering with high β-angles

There are two primary reasons that explain why rally drivers achieve higher performance with high β-angles. The first relates to the way the driver looks to power through the corner under the higher rolling resistance of loose gravel surfaces compared with tarmac roads[83]. This results in combined slip in each tyre of the 4WD rally car generating both lateral and longitudinal force. These two forces are slightly contradictory in that the lateral component aids cornering whereas the longitudinal component will be a hinderance. By using a high β-angle, the combined force vector of the two components will also be rotated such that it points more toward the centre of the corner and maximising the centripetal force. This is shown in Figure 5.1 where the red arrow, denoting the net force on the vehicle during cornering, pointing more towards the centre of the corner (shown as a green dot) for the vehicle with 30° of β-angle.

This has been seen in other research, for example, Nozaki[15] presents a similar case when investigating the notion of 'drifting' around a corner. He comments that tyres can attain a high cornering force at large β-angles during experiments to accelerate around a fixed radius circular course.

The second reason for high β-angle cornering is described well by Casanova[62] when discussing the comparisons between rally and formula one cars.

> "On a low-friction surface the vehicle yaw mode becomes under-damped and oscillatory. Professional rally drivers take advantage of the vehicle natural dynamics by sliding the car in order to enhance the vehicle yaw rate when turning, ultimately achieving greater cornering speeds. It is typical for a rally driver approaching a sharp turn after a straight to apply an oscillatory steer control input much in advance from the corner, with the purpose of exciting the vehicle yaw mode. When the vehicle finally enters the turn with greater yaw rate and speed, the driver must apply a steer control input with a different phase in order to damp the oscillation. A similar strategy applies when changing direction from one turn to the next. With the car already proceeding with large side slip angles, for example on a right hand turn approaching a left hand one, the driver would quickly apply a sharp steer input to the right, which upsets the delicate car equilibrium, and then quickly steer to the left. The car responds with a rapid variation in yaw rate and changes direction very quickly. The driver must subsequently control these induced oscillations by applying opposite lock."

Here Casanova is describing a manoeuvre that is also known as the "Scandinavian Flick" and is used to induce the required high β-angles before a driver reaches the corner.

The next section will demonstrate this technique using simulation before continuing to investigate how effective the resultant β-angle is in influencing cornering performance.

All subsequent simulations are performed using the validated 4WD 7DOF rally car model presented in chapter 4. It was configured with three open differential models unless otherwise stated.

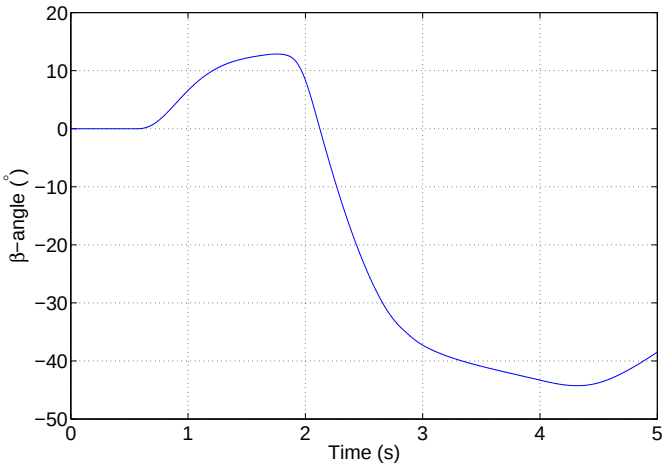

Figure 5.2: Simulated 'Scandinavian Flick' - β-angle

5.1.1 Corner Entry β Induction

Although each simulated manoeuvre begins with the vehicle model initiated with a β-angle of between 0 and -70^o (the angles being negative in order for the model to correspond to the SAE conventions), in reality the driver has to attempt to induce this angle in their approach to a corner.

This technique, as previously described, consists of flicking the steering in the opposite direction to the corner being approached before applying a high steer angle in the direction of the corner. During this flick the driver switches rapidly between the brakes and the throttle. This control input combines to induce a high β-angle on corner entry and is known to increase vehicle performance through the corner.

As the exact control inputs required are usually determined by the drivers feel of the car and the road surface, a trial-and-error technique is employed here to discover the exact control input to produce the required β-angle. Using this technique it is possible to produce control histories that generate all the initial β-angles used in simulations. Figure 5.2 shows the β-angle induced during this manoeuvre in degrees. It can also be seen that this angle is relatively stable and not a transient.

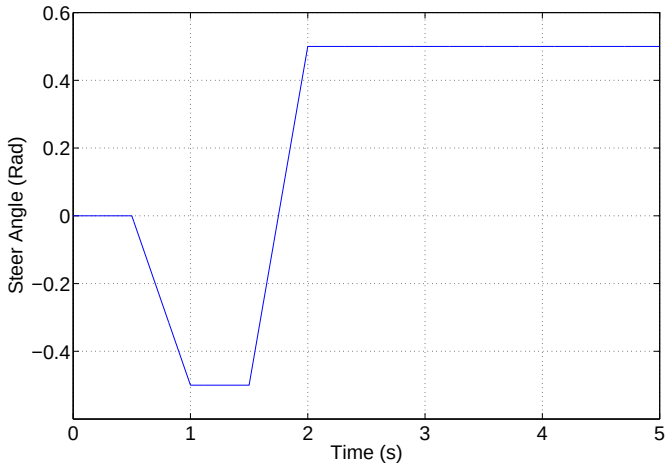

Figure 5.3: Simulated 'Scandinavian Flick' - Steer input to achieve 45°β with 25ms^{-1} initial velocity

Figures 5.3 and 5.4 show the time-history for both throttle/brake control and steer angle input that generate a 45^o β-angle for the 7DOF model equipped with three open differentials. With careful timing, the required angle could be induced to correspond with the corner entry.

For this simulation, the vehicle was travelling in a straight line at 25ms^{-1} before attempting the manoeuvre. The steer angle is shown in radians, the throttle/brake position ranges from +1 for full throttle to −1 for maximum braking torque.

As the driver approaches a right turn driving in a straight line with full throttle, they briefly steer left causing the rear of the vehicle to swing out to the right. Then quickly steering right and briefly applying the brakes. The rear of the car now swings back out to the left. By returning to full throttle and adjusting the steering, a high β-angle is maintained.

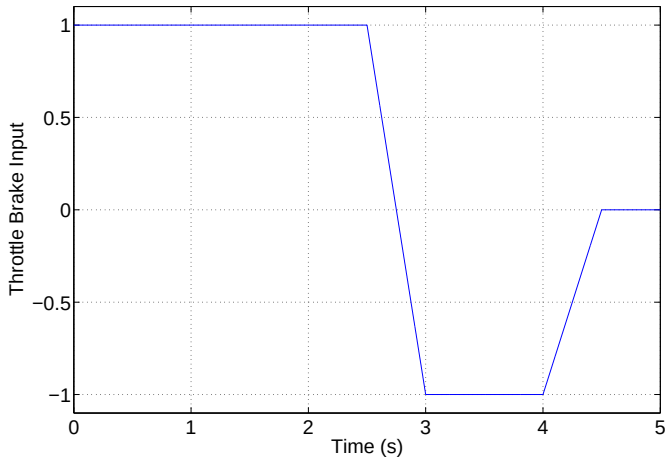

Figure 5.4: Simulated 'Scandinavian Flick' - Throttle/Brake input to achieve $45°\beta$ with 25ms^{-1} initial velocity

5.1.2 The Cornering Manoeuvre on a Loose Gravel Surface

For the simulations it was decided that to reduce the influence of driver input on the results, each run would see the same control inputs being applied to the vehicle. This meant that the path taken would vary and the radius of curvature obtained with each initial β-angle could be compared. The choice of steer and throttle settings were based on a simplified logic of how a real driver attempts such manoeuvres and were set to produce the required performance from the vehicle. It was not the intention of this case study to produce an optimum control history or to stay on a fixed width road, more to investigate the direct influence of β-angle on a standard manoeuvre.

The vehicle model used for this simulation was the WRC model as described in Chapter 4. Vehicle parameters and futher information can be found in Appendix C.

The simulated manoeuvre is a 90° right hand corner, its completion being the point at which the velocity vector of the vehicle rotates to match the desired exit trajectory vector from the corner. The velocity vector direction can be determined with reference to the fixed coordinate system by subtracting

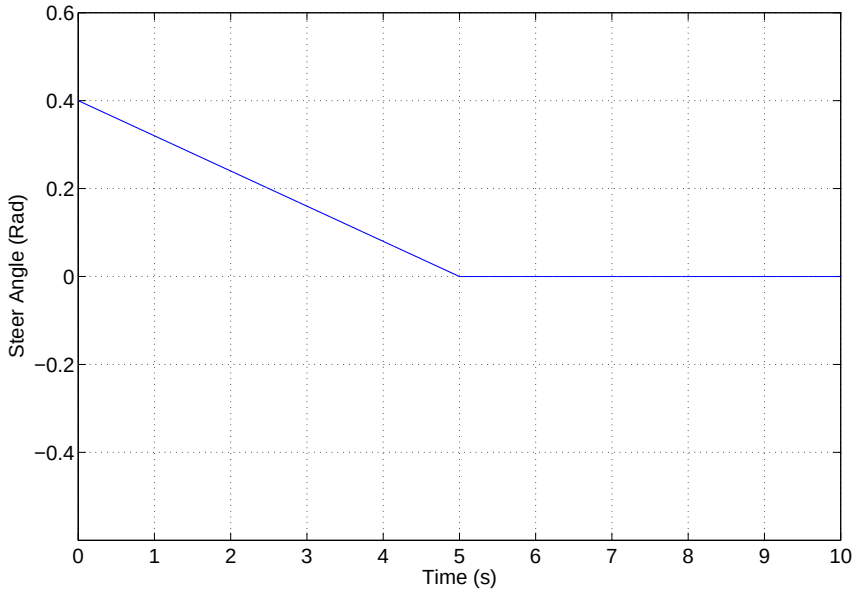

Figure 5.5: High β-angle cornering - Steer Time History Input

the attitude of the vehicle from its orientation.

Throughout the initial stage, the steer angle is progressively reduced from 0.4 radians to 0 (straight ahead). The throttle input is gradually increased from zero to half throttle over the first second of cornering. This represents the driver applying throttle after braking in the approach to the corner. The vehicle begins each manouevre with an initial velocity of 15 ms^{-1}. Time histories for both throttle and steer input are shown in Figures 5.5 and 5.6. The simulated manoeuvre was repeated with different initial β-angles between 0 and -70°.

5.1.3 Initial Results

Figure 5.7 plots the time taken for the vehicle to rotate its velocity vector through 90° against the initial β-angle with which the manoeuvre was started. It can clearly be seen that the cornering performance can be influenced and improved through entering the manoeuvre with a moderate attitude.

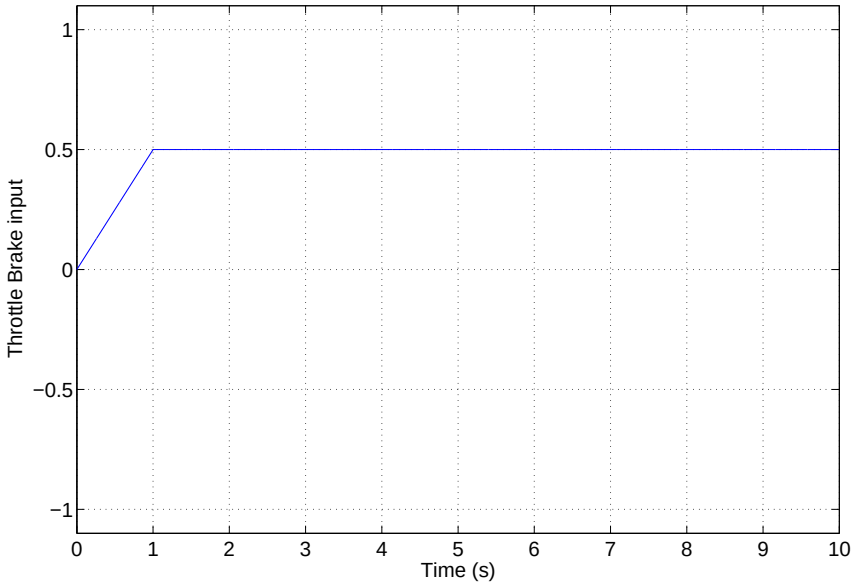

Figure 5.6: High β-angle cornering - Throttle Time History Input

In Figure 5.7, it appears that for an initial β-angle of -55°, the manoeuvre time for a 90° corner can be reduced from the 4.32 seconds, obtained with no initial β-angle, to 3.99, an improvement of around 8%.

If such high β-angles were recreated on tarmac, the lateral forces acting on the tyres rubber carcass may be significant enough to remove the tyre from the rim. Modern tyres are stiff enough to reduce the likelihood of this occuring and instead begin to scrub sideways generating reduced lateral force and very high tyre temperatures. At this point the tyre dynamics become more complicated as the rubber at the contact patch begins to melt.

On gravel though, the lateral forces and surface μ are much lower and this becomes less of an issue.

Figure 5.8 shows the path taken for each simulated manoeuvre. This reinforces the completion time results as it demonstrates that the higher initial β-angles produce a tighter radius of curvature and shorter path length. It is interesting to note though that even though the completion time begins to increase again after -55°, higher angles seem to produce an even tighter

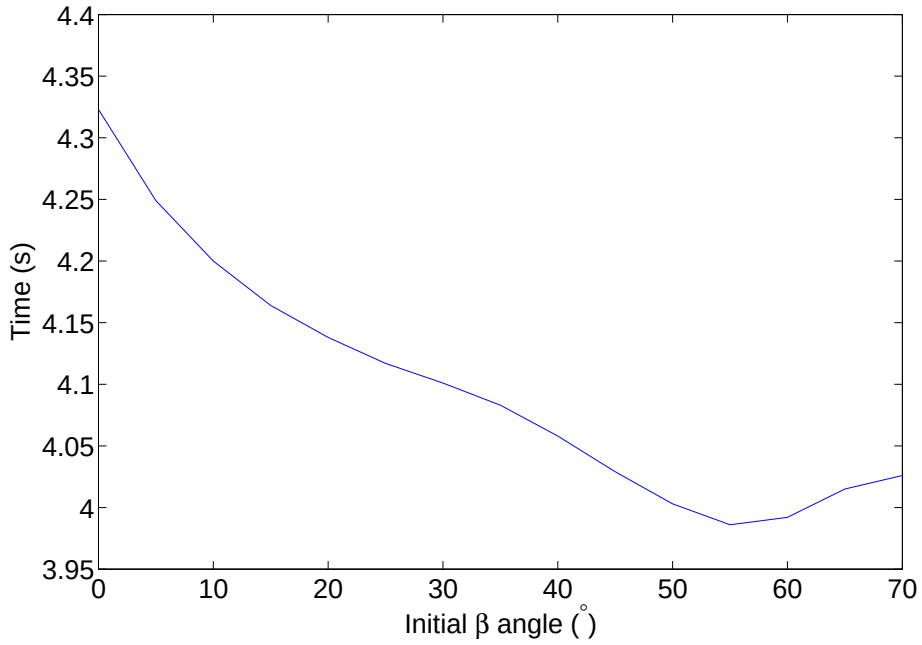

Figure 5.7: Time Taken to Complete Manoeuvre against Initial β-angle

corner. This can be explained if the first section of the corner is examined where it would appear the higher angles take longer to begin to rotate and hence have a slower overall manoeuvre time.

Figure 5.9 plots the time-histories of β-angle for all simulated manoeuvres and shows how high β-angles are quickly dampened to much smaller and stable values. If the manoeuvre with the quickest completion time is considered, the vehicle model completes the desired manoeuvre with only -1.7° of β - given that the driver will then be looking to accelerate at full throttle out of the corner, a small value is very beneficial.

5.1.4 The Yawing Moment

The β-angle method, described in Chapter 2, showed that at higher angles the yaw moment generated would reduce to a relatively low self-restoring moment. This implies that the vehicles will not be able to generate high yaw angle accelerations at such angles. It is at this point that it becomes important to stress two points.

Firstly, β-angle and yaw angle are linked but are not dependent on each other. It is technically possible for a vehicle to experience a change in β-angle without any change in yaw. This requires a change in either longitudinal or lateral velocity to occur.

Secondly, the notion of high β-angle cornering implies that the vehicle is already pointing towards the exit of the corner on entry. Therefore a quantity of the required change in yaw angle has already occured and instead of the vehicle needing to yaw around the 90° of the corner, the required amount of yaw is much less.

This means that although the yaw moment capabilities are reduced at higher β-angles, it does not mean that the vehicle must be slower in completing the specified cornering manoeuvre.

To verify this the yaw rate produced for the simulation with an initial β-angle of 70° with the base tyre set and three open differentials was used to determine the yaw moment. Plotting this against β-angle gives something that can be compared with the β-angle method. Figure 5.10 shows this

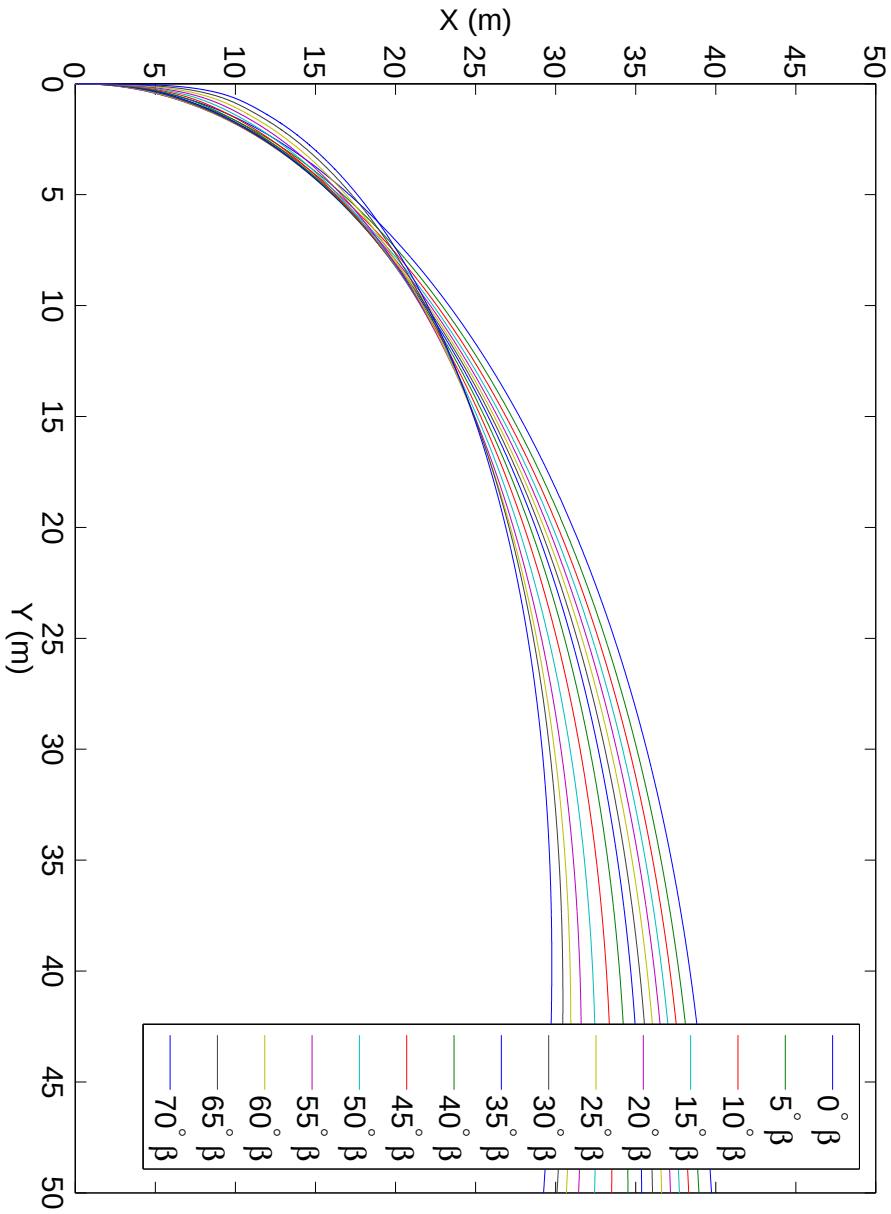

Figure 5.8: Paths Taken by each Simulated Manoeuvre

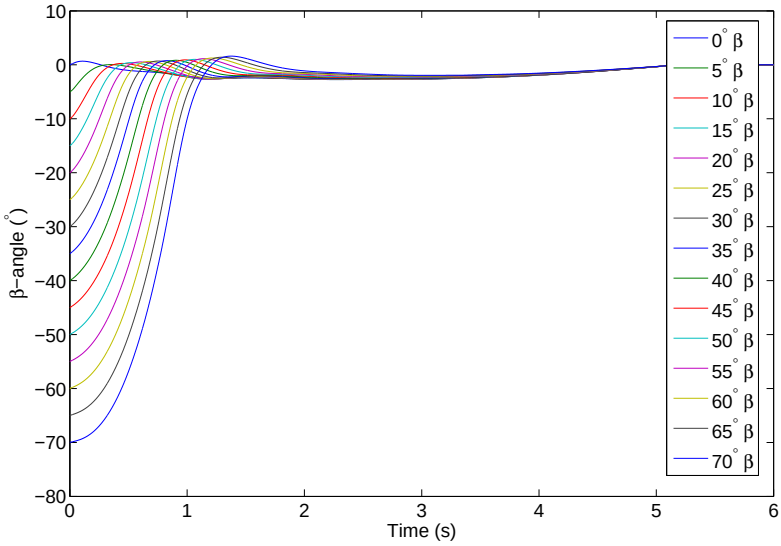

Figure 5.9: β-angle - Three Open Differential Simulations

plot. It is worth noting at this point that even with extremely high initial β-angle, this simulation completed the manoeuvre significantly quicker than the simulation with zero initial β, as can be seen in Figure 5.7.

Figure 5.10 confirms that the vehicle is conforming to the outcomes of the β-angle method by only generating high yaw moments at low β-angles. At the higher angles the smaller moment is also negative, in this case making it contrary to the direction of the corner and against the β-angle. That is to say that the yaw moment is trying to yaw the vehicle in a manner to reduce the β-angle.

During this attempt to yaw the vehicle into a state of reduced β-angle, the vehicle is also experiencing a centripetal acceleration and as such the velocity vector is rotating into the corner. As this vector rotates, it also causes the vehicles β-angle to deminish.

These two factors combine to influence the vehicles β-angle but as the first is independent of the direction of the velocity vector and the second is independent of the vehicles yaw rate, it is very difficult to equate the two.

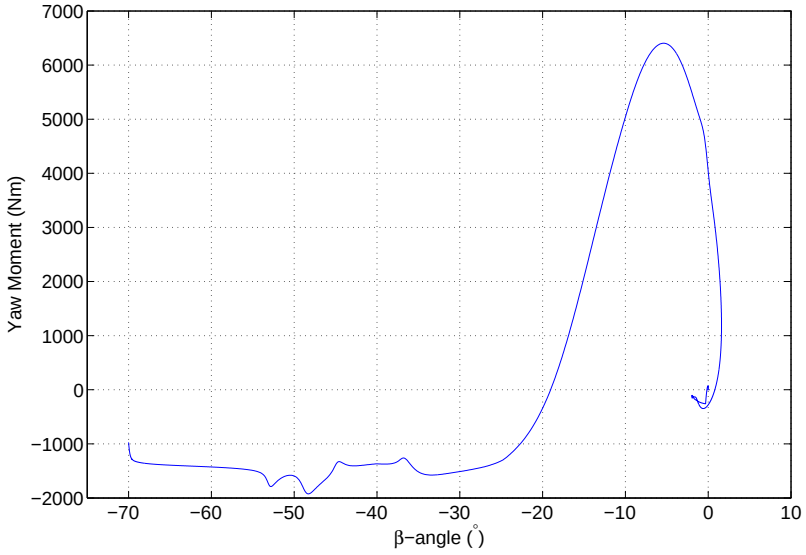

Figure 5.10: Yaw Moment against β-angle

5.1.5 The Influence of Differentials

Open Differentials

The first set of simulations used a model configured with three open differentials. This permitted large wheel speed differences between all four wheels as can be seen in Figure 5.11. Figure 5.11 is taken from the simulation with an initial β-angle of -55°.

In the first few seconds, it can be seen that the front wheels, in particular the left front wheel, begin to rotate significantly faster than the rear wheels. This occurs as the throttle is being increased and the vehicle attempts to accelerate forward with its high β-angle. As the vehicles attitude angle reduces to a lower level, the wheel speed can be seen to converge back to those expected from a steady state cornering manoeuvre.

Limited Slip Differentials

In circuit racing, the use of limited slip differentials has been employed to assist in reducing potential losses in tractive forces that may occur when

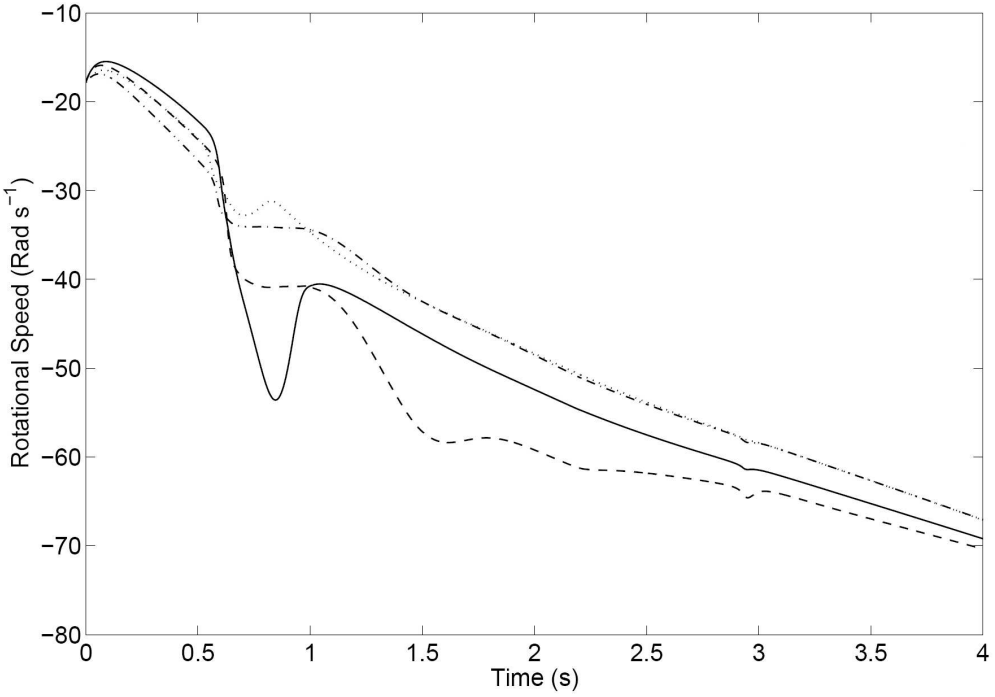

Figure 5.11: Individual Wheel Speeds - Three Open Diffs, initial $\beta = 55°$ (—— LF, – – – RF, - - - LR, — - — RR)

cornering or driving on an uneven, split-μ or loose surface.

This raises the question of whether such differentials may assist in someway with the the higher β-angle cornering of this case study. To discover this, the model was reconfigured with three limited slip differentials which acted to reduce any large differences in wheel speed.

Figure 5.12 depicts the same manoeuvre as Figure 5.11 with initial β-angle set to 55°. However, this model is configured with three limited slip differentials. Now when the front left wheel begins to speed up about half a second into the manoeuvre in the same way as seen in Figure 5.11, the differentials apply a resistive torque according to the wheel speed difference and the other three wheels are now forced to speed up as well.

Torque is transferred from the faster wheel to the slower wheel as a result.

As the vehicle continues through the corner, the wheel speeds can be then seen to diverge again at around 2 seconds. This coincides with dramatic increase in β-angle caused by the oscillation that occurs in this manoeuvre. The implication is that the locking action applied due to the wheel speed differences at half a second induces the oscillation and the secondary β-angle peak, in which the individual wheel speeds diverge again before returning to more consistent values as the vehicles steer angle is reduced and it exits the corner.

With the limited slip model, the quickest manoeuvre time dropped significantly to around 3.127 seconds with an optimum β-angle of -35°. However, if the vehicle at completion is compared, the three limited slip model finishes with over -40° of β-angle remaining. This high angle is far from conducive to accelerating out of a corner and hints at a more fundamental problem.

Figure 5.13 shows the β-angle time-histories for each manoeuvre. Unlike the three open differential model (Figure 5.9) the vehicle swings dramatically back and forth demonstrating considerable instability in cornering even without high initial angles. This instability may be countered with a more realistic human driver but it is clear that such extra effort is not required with the three open model.

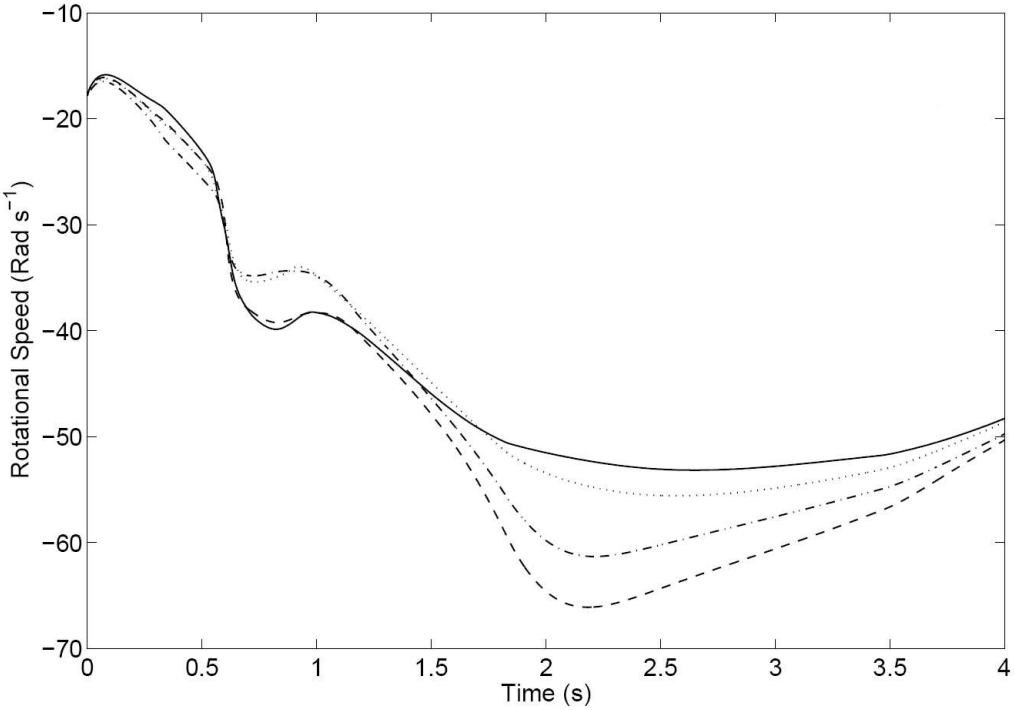

Figure 5.12: Individual Wheel Speeds - Three LS Differentials, initial $\beta = 55°$ (—— LF, – – – RF, - - - LR, — - — RR)

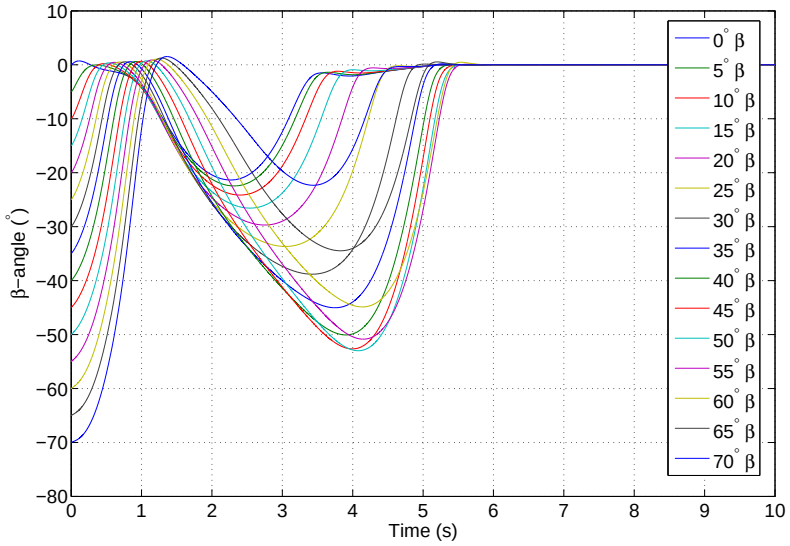

Figure 5.13: β-angle - Three LS Differential Simulations

Other Configurations

Three other configurations of transmission where simulated in addition to the three open and three limited slip differentials. The configurations were an open centre with front and rear LSDs, an open front with centre and rear LSDs and an open rear with centre and front LSDs. To summarise the effect on performance, Table 5.1 shows the quickest time that the specified manoeuvre was completed in and what the initial βangle was that generated the result. It also shows the β-angle which remains at the end of the manoeuvre for the fastest run.

Table 5.1: Summary of Simulation Results

Configuration	Time (s)	Initial β	Exit β
3xLSD	3.127	-35°	-41.3°
Open Centre	3.225	-50°	-3.8°
Open Rear	3.307	-55°	-2.6°
Open Front	3.464	-50°	-2.5°
3xOpen	3.985	-55°	-1.7°

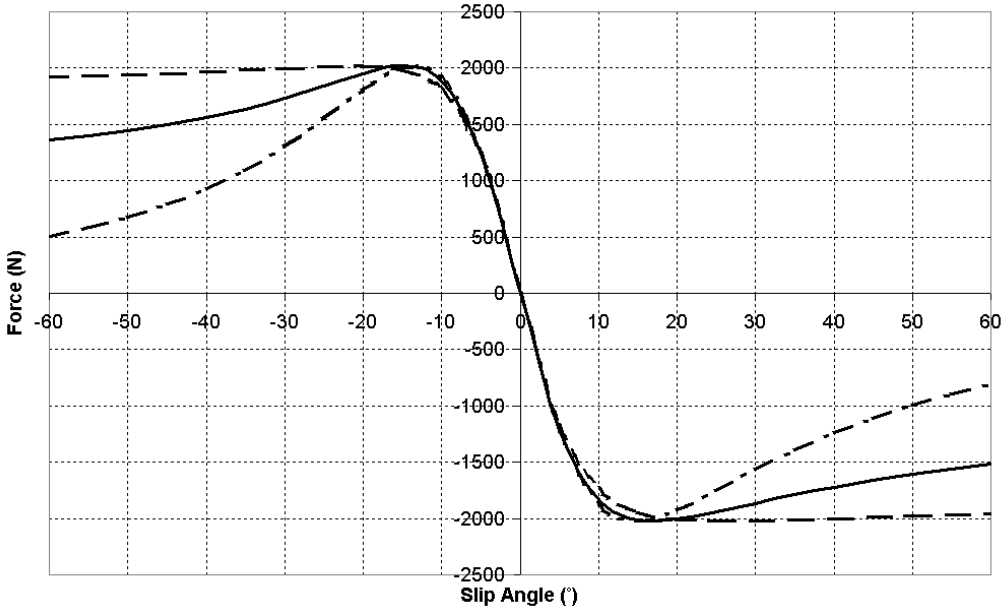

Figure 5.14: Lateral Tyre Force Curves for Sensitivity Analysis ($F_z \approx 3000N, \mu = 0.6$) (– – – Tyre A, —— Tyre B, — - — Tyre C)

5.1.6 The Influence of Tyres

Although initial results show peak performance occurring at around 50° to 55° of β-angle on corner entry and on loose gravel, these simulation results are heavily dependent on the particular tyre model used. The base set of Pacejka parameters adopted for the tyre, those for a high performance example, show next to no decline in lateral force potential even at extreme slip angles (Figure 5.14, Tyre A). This is not entirely realistic and as such the simulations were repeated with the tyre parameters altered to create a tyre that gently diminishes with slip angle and a tyre that dramatically diminishes with slip angle. The lateral force curves for these tyres on a surface with a μ of 0.6 to represent the gravel surface, are shown in Figure 5.14

5.1.7 Results

Figure 5.15 shows that as the tyre's lateral capabilities are reduced (see Tyre B in Figure 5.14) the optimum corner entry β-angle also drops. This is

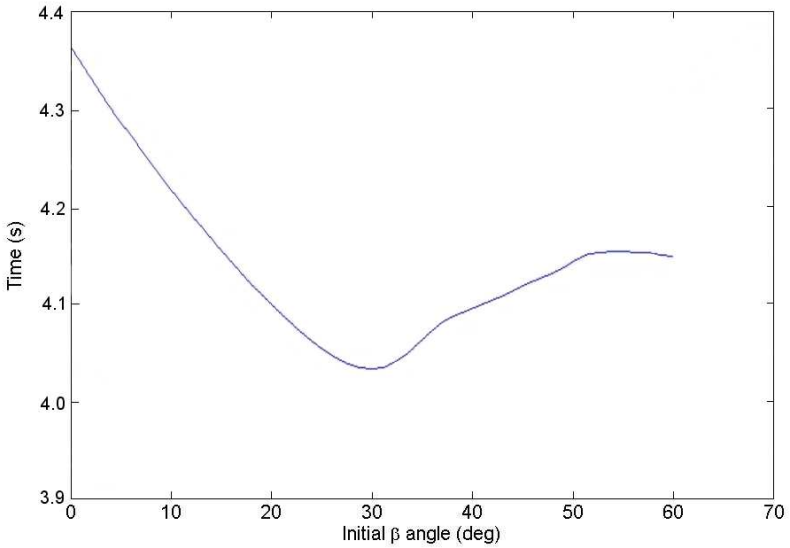

Figure 5.15: Time Taken to Complete Manoeuvre against Initial β-angle - Tyre B

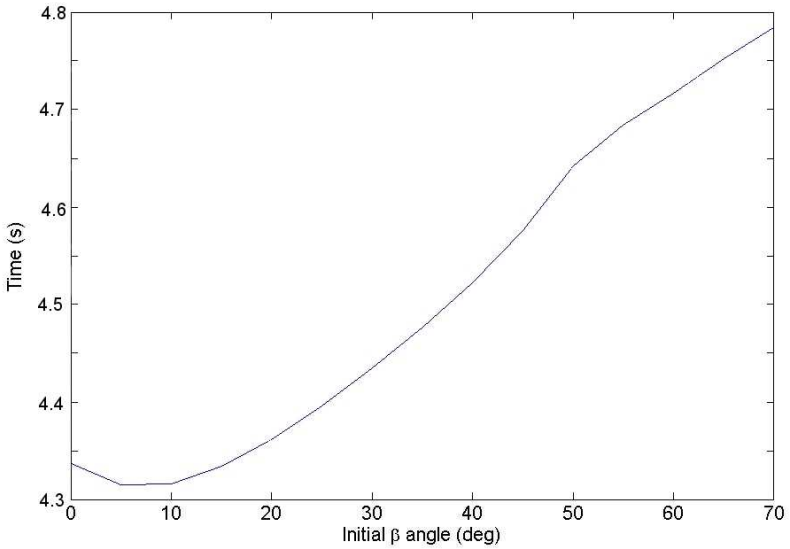

Figure 5.16: Time Taken to Complete Manoeuvre against Initial β-angle - Tyre C

expected as now the tyre model cannot generate the same high forces at higher slip angles. Despite this the optimum entry angle is still around 30° although it is now slightly slower than the fastest time obtained for Tyre A at around 4.03 seconds.

Figure 5.16 continues this trend. Now the tyre model is configured to diminish severely as slip angle increases and the tyres can only perform effectively around their saturation point, at somewhere between 5° and 10°. Any increase in corner entry β-angle now has a dramatic effect in reducing the cornering performance.

From this it is clear that an optimum corner entry strategy is heavily dependent upon the tyre model. Interestingly, if the experimentally derived tyre curves obtained in Chapter 4 are considered, tyre B represents a close match to the data from the real tyres.

Furthermore this would suggest optimum corner entry angles of around 30°, which is also the range of β-angles seen from the telemetry data. This would suggest that the drivers feel for their vehicles does seem to have a sound vehicle dynamic basis. Further investigation could confirm this by considering more closely matched manoeuvres and telemetry.

5.1.8 Case Study Conclusions

The instability seen with the three limited slip differential configuration is only apparent for this model. All other models demonstrated similar β-angle time-histories to the three open case.

This instability in the cornering would therefore make it a drastic choice despite it generating the fastest cornering time. If the centre differential is opened up though, the fastest corner manoeuvre time only increases marginally, see Table 5.1, but the vehicle now exits the manoeuvre with a much more modest β-angle that will have only a negligible detriment in terms of the ensuing attempt to accelerate out of the corner. Operating rally cars with an open centre differential and limited slip front and rear differentials is, therefore, a rational choice.

Furthermore, higher β-angles of around 50° to 55° can produce noticeably

increased performance. This should be taken into account in development of any control systems that may look to prevent such angles.

5.1.9 Potential for β-angle control

From the results seen, it is in theory possible to calculate an optimum corner entry β-angle that will minimise the time required for that corner. If it were possible to control the transmission in such a manner as to assist in the generation of that β-angle, the effort in predicting how the car will behave can be offloaded from the human driver onto the chassis controller.

Although current WRC cars utilise only actively locking differentials, recent developments have seen the potential for a torque distributing unit that can adjust and control the ratio with which the input torque is split between the two output shafts. One of the earliest differentials with this potential is the Mitsubishi AYC unit as described in Chapter 2.

With this in mind, a simulation model was created in which a differential model was implemented as the centre differential to allow the torque split between the front and the rear wheels to be adjusted.

The common understanding is that a rear wheel drive vehicle will tend to increase its β-angle if given enough throttle, usually referred to as oversteering, whereas front wheel drive cars tend to reduce their β-angle, or understeer. This logic relates to the relative saturation points between the front and rear tyres, with rear wheel drive vehicles saturating their rear tyres sooner when throttle is applied. The converse holds for front wheel drive vehicles.

Therefore if the vehicle has too high a β-angle, by pushing the drive torque forward, a reduction should be seen. Similarly if too low a β-angle for the optimum corner entry, torque pushed to the rear should correct this. It is worth noting though that as there is no left-to-right torque distribution differentials on the front and rear axle, the driver would be required to induce some angle through a flick of the steering wheel. Without this the centre differential cannot generate the yawing moment required to create a β-angle.

To demonstrate this, a vehicle was initiated to a 45° β-angle and driven

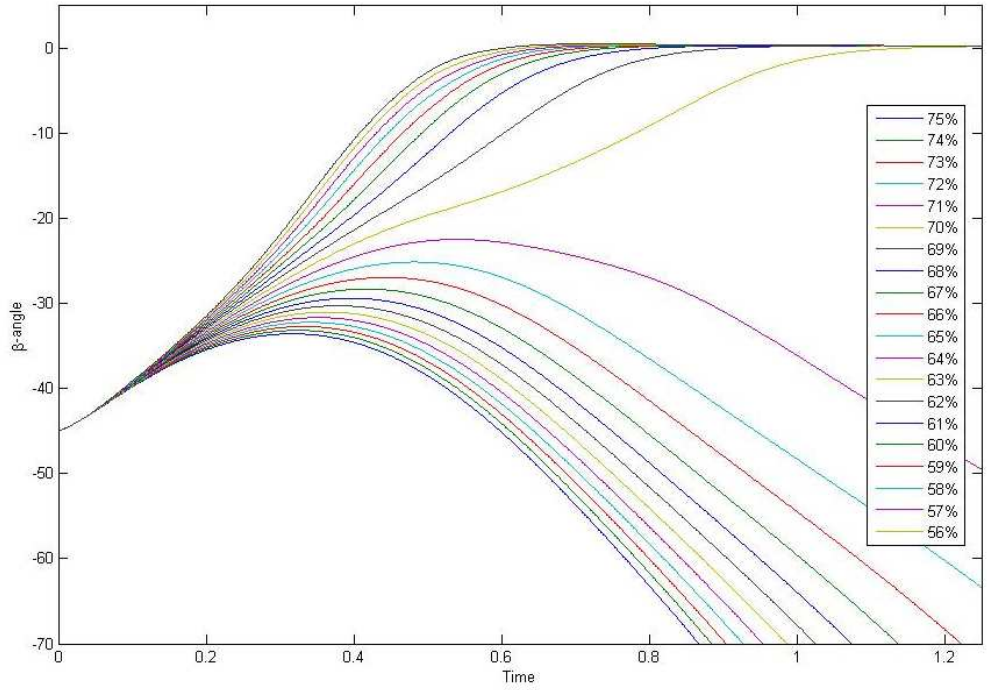

Figure 5.17: Influence on β-angle for varying front-rear torque splits

under full throttle with varying front-to-rear torque splits on a surface with a μ of 0.6, representative of a loose gravel. Figure 5.17 shows the resultant β-angle time histories.

Figure 5.17 clearly shows that this philosophy is essentially correct and that a torque split of somewhere between 63% and 64% rear should produce a stable angle. It is unlikely an exact figure could be determined given the nature of the unknowns, but using the β-angle sensor and a suitable control algorithm that adjusts torque as required, the task is possible.

It should be noted though that these results are specific for the vehicle model and that changes in factors such as weight distribution would probably move the stable point.

5.2 Corner Exit Strategy

In order to maximise performance the driver will look to apply full throttle as soon as possible on exiting the manoeuvre. However, if a residual β-angle remains when the driver attempts to apply full throttle, controlling the vehicle becomes problematic with the driver having to make drastic steer inputs or reduce throttle to bring the vehicle back under control before accelerating out of the corner once more. This instability in the car can be influenced by the transmission configuration and may be able to assist the driver in achieving the desired results without excessive effort to keep the vehicle on the path intended.

During pure longitudinal acceleration, the accepted philosophy is that the transmission should be locked. This results in maximum tractive effort and, in circumstances where the road surface is slippery or loose, reduces any unwanted wheel speed on an individual tyre.

This section examines the end of the corner where an excess of β-angle is most undesirable. The driver needs to reduce the vehicles β-angle as quickly as possible as they attempt to maximise their lateral acceleration into the next straight. Different configurations of differential demonstrate this.

5.2.1 Simulated Corner Exit

To simulate a corner exit manoeuvre, the steering is centred and full throttle applied.

This represents the easiest option available to the driver and is intended to demonstrate the effect that residual β-angle may have. In reality the driver may use high frequency counter steer inputs and ease off the throttle in order to reduce β-angle and achieve straight line acceleration but this would not represent maximum performance.

To that end, two simulations are presented. The first, Figure 5.18 demonstrating the path taken when a vehicle model with three limited slip differentials attempted to accelerate out of a corner with varying degrees of residual β-angle. The second, Figure 5.19 presents the same scenario but with three open differentials. The surface μ was again set to 0.6 to represent a loose

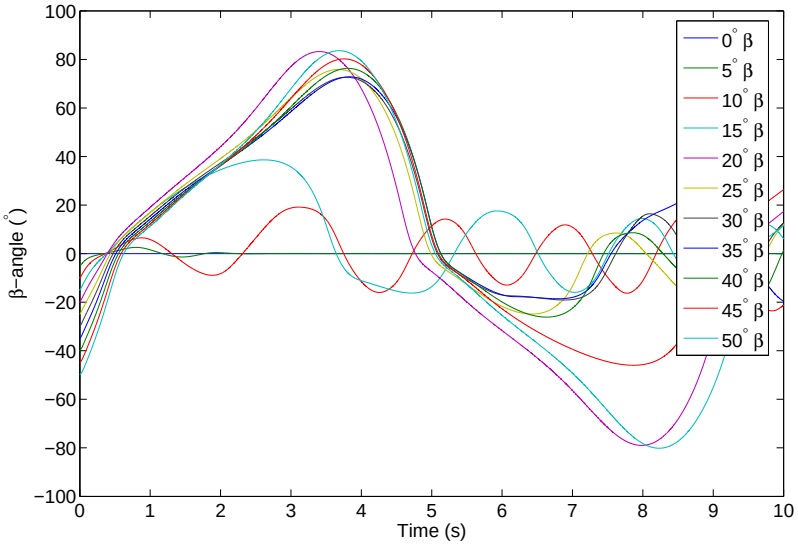

Figure 5.18: Corner Exit β-angles - Three Limited Slip Differentials

gravel surface as in the first case study.

From Figure 5.18 it is clear that even with low initial β-angles, the vehicle becomes oscillatory and fish-tails down the straight. With higher initial angles, the vehicle begins to swing dramatically back and forth in a manner that, without driver input to dampened the action, would probably lead to an accident.

Figure 5.19 however shows a different picture. With all three differentials open, the differing wheel speeds are not restricted and the vehicle quickly returned to a steady zero β-angle state while accelerating away from the corner. This occurred at all angles simulated and would require the least driver input of the two.

5.2.2 Optimum Strategy

Despite the clear benefits in terms of rapidly reducing β-angle, leaving the differentials open for hard acceleration is not the optimum solution for loose surface driving. Any difference in the level of grip between the four wheels

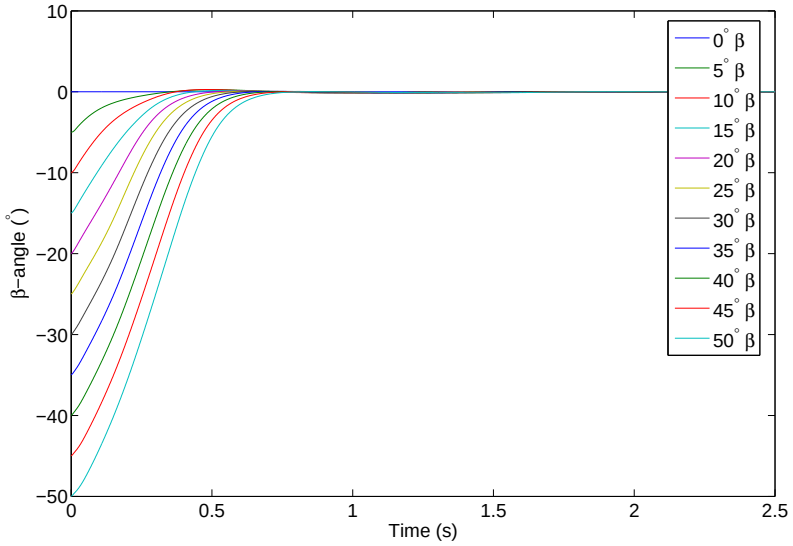

Figure 5.19: Corner Exit β-angles - Three Open Differentials

would result in a loss of traction and effectively would slow down the rate of acceleration.

Fortunately, WRC cars employ active differentials and can be controlled to increase or reduce their locking action based on a suitable control algorithm. This would allow for an algorithm that would detect the corner exit, say from the driver straightening the steering and applying full throttle, detect the residual β-angle using the β-angle sensor and open up the differentials long enough to allow the angle to be reduced before reapplying the differential locking for maximum traction.

Such a control strategy though would have to conform to the rules and regulations of WRC but the results of the simulation show that with the aid of the β-angle sensor, some of the control elements currently under the influence of the human driver, could be replaced with a suitable control system that would maximise performance potential.

5.2.3 Case Study Conclusions

Through simulation it has been shown that entering a corner on a loose surface with a high β-angle can reduce the time required to complete the manoeuvre. It has also been shown that the transmission configuration and tyre properties have significant effects on both performance and stability, measured in terms of β-angle, throughout the cornering and beyond.

A philosophy towards high performance cornering is beginning to emerge.

For a given corner, it is now possible to obtain an approximate value for optimum entry β-angle. The exact value is more difficult to obtain due to the unknowns such as road conditions and tyre properties. Tyre properties are coming to light through the application of the β-angle sensor and this should help to reduce uncertainty.

Furthermore, the transmission results demonstrate that a centre limited slip unit can help cornering by reducing front-rear axle speed differences without the detrimental effects on stability that appear to occur when front and rear limited slip differential units are employed. In corner entry, it has been seen that any excess β-angle is disadvantageous and by opening all three differentials, even under full power, the vehicle will quickly scrub the excess and allow the transmission to be locked up for maximum traction without unwanted instability.

It has also been put forward that the potential now exists, enabled by the β-angle sensor, to develop a car and control system that can aid the driver in inducing and reducing β-angle as appropriate for maximum performance. Although only initial studies have been put forward, the results suggest that such a system could have dramatic effects for vehicle control on loose surfaces.

Future work in developing this system though is dependent on advances in differential technology to allow rapid changes in torque distribution and the rules and regulations of WRC.

5.3 Torque Vectoring using β-angle Control

This case study is based on three scenarios where the complexity of the AWD transmission increases. The first with three open differentials, the second with a 70/30-30/70 switchable centre differential with open front and rear, and third, a fully left-to-right vectoring front and rear differential capable of any ratio of torque distribution (centre differential being left open).

The results show some of the benefits of adding a smarter centre differential to a standard open differential AWD system, and then the effect of adopting full torque vectoring whereby the torque transferred to each road wheel is controlled independently.

The benefits are described in terms of effective vehicle β-angle and its rate of change under acceleration through an ISO double lane change manoeuvre[11] shown in Figure 5.20. A reduction in the magnitude of the angles observed being indicative of a more nimble and agile vehicle.

The double lane change change manoeuvre is negotiated using the path-following optical lever directional controller and configured to accelerating briskly at 2.5 ms^{-2}. The model begins the manoeuvre at an initial starting speed ranging from 10ms^{-1} to 30ms^{-1}.

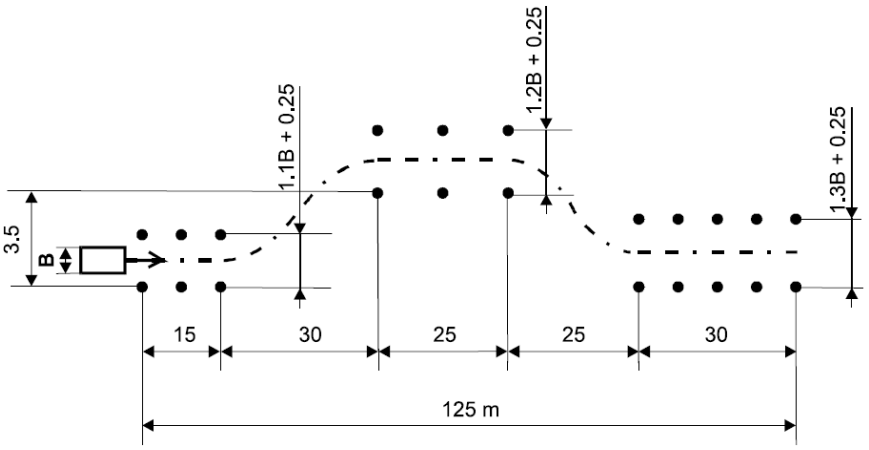

Figure 5.20: ISO Double Lane Change Manoeuvre[11]

5.3.1 Three Open Differentials

The results for the first case study (with three open differentials) are shown in Figure 5.21, 5.22 and 5.23. Figure 5.21 shows the path taken by the vehicle at ground speeds in the range 10 ms^{-1} to 30 ms^{-1} The steer controller is less successful in finding a smooth path through the ISO double lane change manoeuvre as the speed increases. Figure 5.22 shows the β-angle time history at 30ms^{-1} which is significant and changing rapidly. Figure 5.23 shows the steering time history.

This case study represents the baseline performance against which the torque vectoring studies are compared.

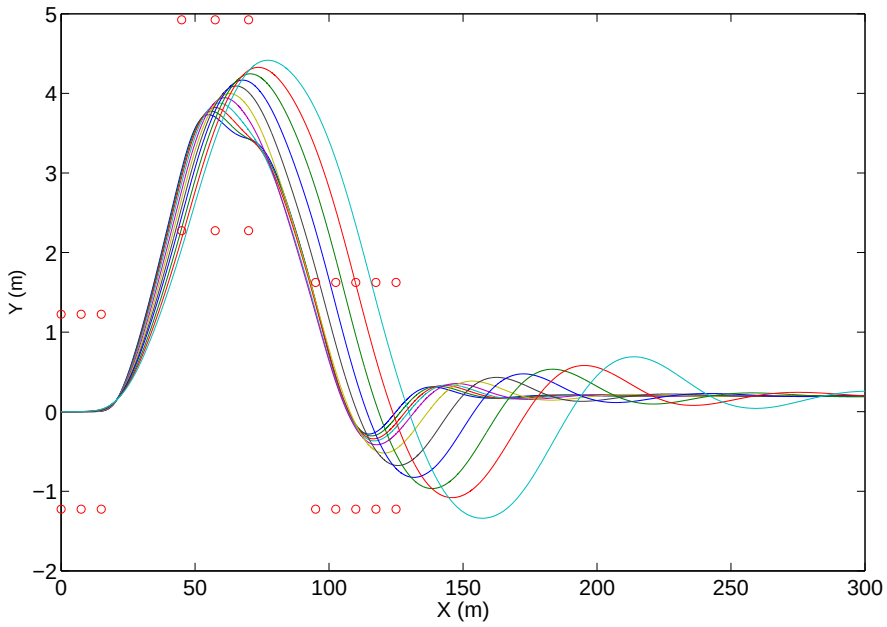

Figure 5.21: Three Open Differentials - Paths Taken

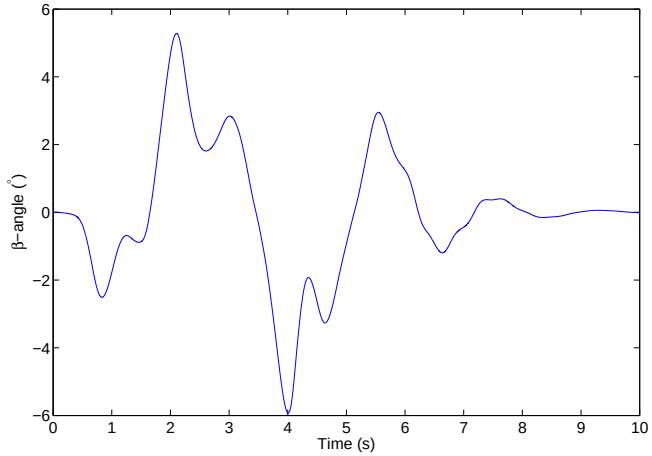

Figure 5.22: β-angle for 30ms^{-1} Simulation

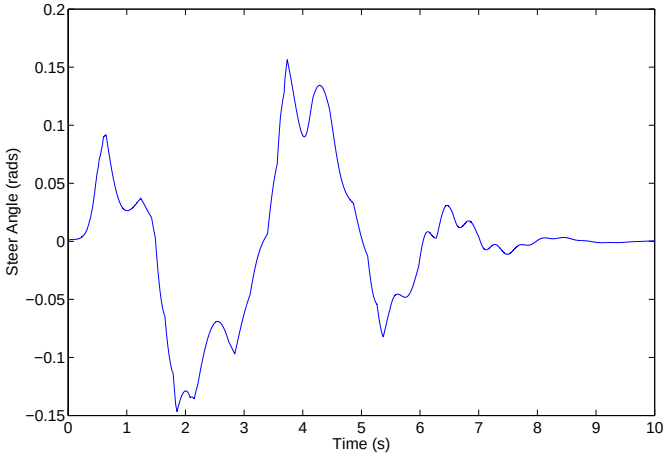

Figure 5.23: Steer Angle Input for 30ms^{-1} Simulation

5.3.2 70/30-30/70 Switchable Centre Differentials

In the second example the vehicle model undergoes the same manoeuvre but with a switchable centre-differential (the so-called 70/30 differential). This device switches between two modes using a system of clutches. In one mode it transfers 70% of the available torque to the front differential and 30% to the rear. In the other mode, the torque distribution is reversed. Because of this switching of modes, the control strategy for this device has earned the label bang-bang control. When the β-angle exceeds 1.5°, the centre-differential switches between modes in order to minimise the β-angle.

Comparing the baseline results of the three open differential case to those in Figure 5.24, 5.25 and 5.26, which relate to the 70/30 differential, it is clear that with a switchable centre differential, the vehicle is prone to a strong oscillation in β-angle. The impact on the path followed is remarkably slight because the preview steer controller has been successful in countering the path effects of vehicle attitude using counter-steering. Notwithstanding the unwanted oscillations the bang-bang differential control did successfully reduce β-angle before the oscillations arose.

The oscillations can be seen to grow rapidly and dramatically as the path following steering controller is operating to maintain vehicle path. Between 5 and 10 seconds the controller is applying large high frequency steer inputs as the vehicle fish-tails (oscillates in β) in an attempt to maintain the desired acceleration. A sympathetic steer and throttle control provided by a live driver would act to suppress the oscillation either through easing off on the throttle or the steer input until the oscillation is suitably damped. Another possible method for suppressing the fish-tailing would be to adjust the differential controller in such a way to avoid changing the front-to-rear torque distribution ratio until the β-angle rate has diminished.

In the initial sections of the manoeuvre, peak β-angle and rate can be seen to be reduced compared with the baseline results. For short duration manoeuvres, the bang-bang strategy would give the vehicle an improved sense of nimbleness.

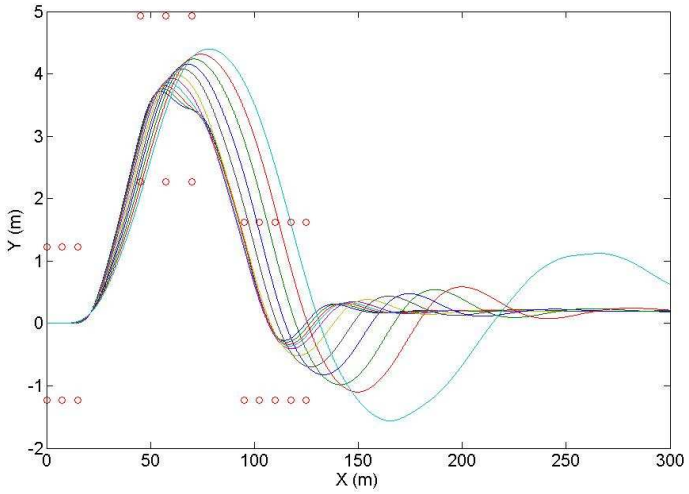

Figure 5.24: 70/30-30/70 Centre Differential - Paths Taken

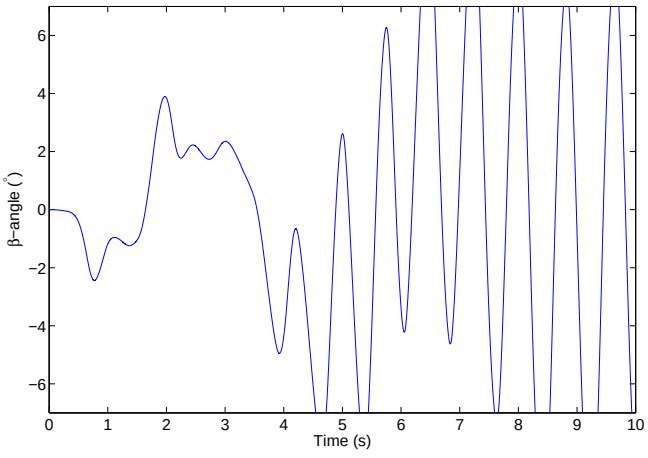

Figure 5.25: β-angle for 30ms^{-1} Simulation

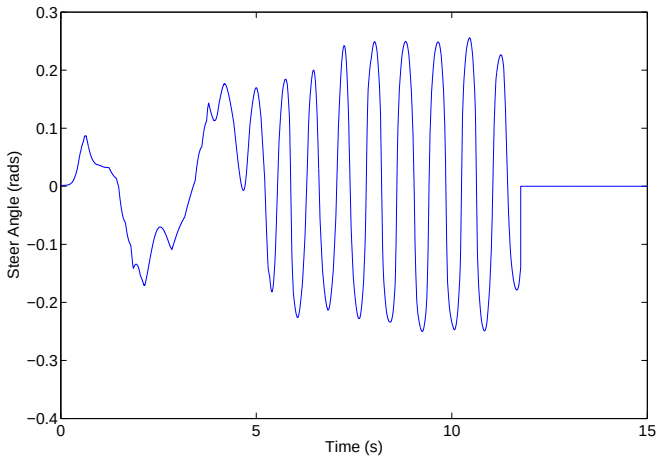

Figure 5.26: Steer Angle Input for 30ms^{-1} Simulation

5.3.3 Left-Right Torque Vectoring

In the third example, the vehicle is configured with torque vectoring differentials at the front and at the rear where the torque delivered to each wheel is independently controlled. The centre differential is of the open design. A PI controller is applied to both front and rear differentials in order to minimise β-angle. In order to produce similar path following abilities as the first and second case studies, the individual gains used in the PI controller were adjusted using a trial and error approach until a good approximation was achieved.

Figure 5.27, 5.28 and 5.29 show the comparative results for the vehicle fitted with torque-vectoring differentials front and rear and an open centre differential. This time β-angle is reduced even further with no oscillations.

The gains employed in the β-angle PI controller have been chosen to deliberately reduce the deviation in path followed (compared with the other two case studies) in order that a like-for-like comparison can be made. However, a more liberal choice of gains would reveal a more significant control of β-angle, but with the unwanted side-effect of worsening path following qualities.

The benefits of adopting this sophisticated AWD system, although modest when compared with the cost and weight penalties imposed, are clear even for the short duration manoeuvre found in the ISO double lane change. For the case of accelerating through a small radius curve, the positive impact of the torque vectoring system would be more marked.

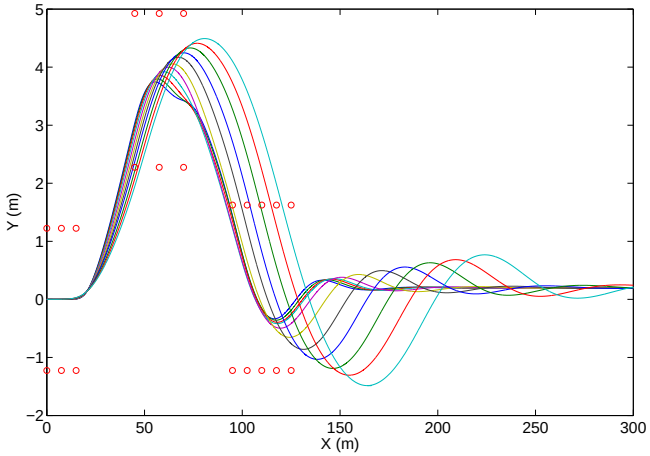

Figure 5.27: Left-Right Torque Vectoring Differentials - Paths Taken

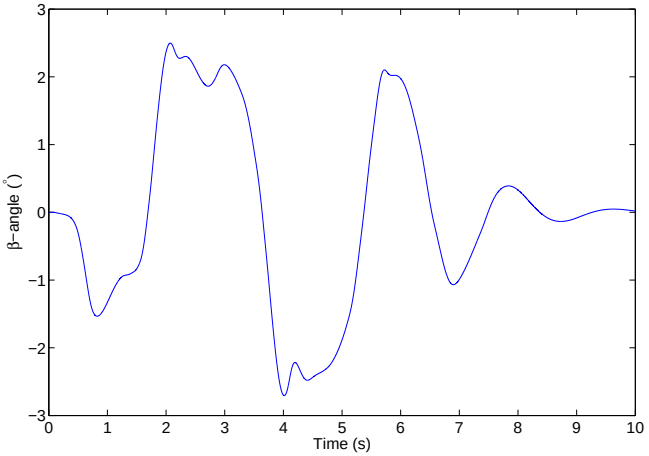

Figure 5.28: β-angle for 30ms^{-1} Simulation

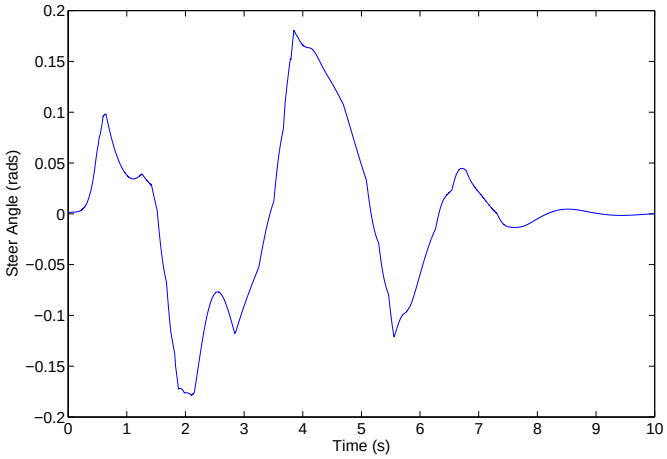

Figure 5.29: Steer Angle Input for 30ms^{-1} Simulation

5.3.4 Case Study Conclusions

The results have shown that the more complex torque vectoring differentials can produce a significant improvement in perceived vehicle agility and nimbleness. Peak β-angles were reduced to around 40% of the base case simulations and fewer high frequency steer inputs were required to maintain the desired path.

The addition of an active centre differential showed marked improvement over the base case, although it did tend to create a slightly unstable vehicle under heavy acceleration, this being characterised by the fish tailing effect seen on exiting the double lane change manoeuvre. A live driver would obviously be able to rapidly suppress this although a more intricate control strategy may reduce the need for this intervention

An even more significant improvement was also noted with the introduction of left-to-right torque vectoring ability without the instability seen in the active centre case.

This model, however, maintained an open centre differential to avoid any potential for conflicting control strategies. Further studies could investigate whether an active centre differential and sophisticated controller could be

added to this model to produce a more agile vehicle.

In summary, this case study shows a method of applying β-angle control to the small executive passenger car to provide the driver with a more enjoyable ride and feel to the vehicle. It has also been shown that by adjusting the control of the transmission, the vehicle dynamics can be altered and therefore could be tuned to the drivers style or mood in real-time.

Chapter 6

Conclusions

This research began by identifying a gap in the vehicle dynamics field relating to the specific case of rally driving, particularly on loose surfaces.

Through various processes, this work looked to begin to fill this gap and in doing so has laid a foundation but also has opened up various other possibilities and applications.

6.1 β-angle Sensor

This work has presented a novel method for the direct measurement of β-angle and has shown the development of an appropriate sensor to implement the method.

The sensor was taken from a conceptual stage, through initial testing, calibration, refinement and validation processes to result in a practical, reliable and robust device that could be used for vehicle dynamic study and investigation.

One major advantage of this sensor has been its robust nature that allowed it to be used in the investigation of β-angle dynamics in WRC cars on loose gravel surfaces. Through testing with WRC vehicles on loose gravel conditions at full racing speeds, an extreme case was taken and confirmed the sensor's durable nature by surviving these environments without failure or incident. New insight has been obtained through its use as well as potential

to develop analytical techniques to examine driver style, dynamics on loose surfaces and tyre properties in real time.

Unfortunately due to recent changes in the rules and regulations of WRC, the use of GPS technology has been banned during rallies. This reduces the potential applications of the sensor although it is still an important tool that could be developed into an essential part of the testing and vehicle development process.

Furthermore with the increased adoption of 4WD and active transmissions in road cars, and given that the implementation of the β-angle sensor is relatively cheap, there may be a future use in traction control or tuneable dynamic behaviour systems for the more pro-active drivers and car owners.

To continue the development of the β-angle sensor, more validation which compares the performance of the sensor with significantly more expensive and complex dual-antennae GPS systems that are only just becoming commercially available, would confirm the available accuracy and resolution.

There is also scope for an extended calibration method of the magnetometers that results in an more sophisticated method of removing pitch and roll inaccuracies. The lead for this may be taken from the likes of the stability control systems, such as the Bosch ESP[16] system, which infers such values from an array of additional sensors.

In addition, there still exists a geographical element to the calibration of the magnetometer corrections. This was overlooked in this study as testing occurred within a small enough area in which the Earth's magnetic field could be considered to be constant. If the sensor was to be developed for practical commercial use in a non-competitive road car application, this would need to be overcome.

In summary, the β-angle sensor has been developed to a state where it can be used as a useful tool in potential research or control applications where other alternative methods are either too expensive or rendered ineffectual due to the need to operate in a harsh environment.

6.2 Tyre Curve Inference

Tyre forces are one of the fundamental factors in the performance of a vehicle and one which is difficult to quantify due to the number of unknowns that can affect them.

The use of test rigs can provide some element of understanding but these do not always reflect true performance when fitted to a vehicle. Through the application of the β-angle sensor, a suitable vehicle dynamic model and various other sensor data, a method of inferring the performance of the tyres in real time has been presented.

Even though it was not possible to perform the steady state manoeuvres recommended to generate clear tyre curves from the WRC test car on gravel and tarmac, it was possible to see the tyre data extracted directly from the telemetry of full-speed test runs. This data shows many transient properties and noise but does clearly represent a structure that conforms with the accepted Pacejka[53] model theory. In addition, the data from the gravel telemetry gives valuable insight into tyre performance on that surface. The limited lateral capabilities of the tyre and its rate of drop off with increased slip angle proving of great interest in order to help improve the accuracy of simulations relevant to this field.

The ability to produce this tyre data could be refined and improved to allow quantitative analysis of different tyre compounds or tread patterns as well the potential to monitor the degradation of tyres in real time. Although the process presented here is relatively new, it can be seen as a proof of concept that should now be taken forward to develop sophisticated tyre measurement capabilities.

6.3 β-angle in Vehicle Dynamics

In order to try and quantify the importance of β-angle in vehicle dynamic theory, particularly for the realms of WRC, a 7-DOF model has been created and used in appropriate case studies.

This model benefited from validation against a set of real world telemetry

data from a fully instrumented WRC test car, particularly in relation to β-angle as originally measured using a Correvit[12]. Furthermore, the lessons learnt from tyre curve research and β-angle sensor measurement have allowed this simulation to be applied to loose gravel surface analysis with a high degree of confidence that its accuracy has been preserved.

Through this process, the application of vehicle dynamic simulation to WRC style problems has become a real possibility in a field that is traditionally seen as being unsuited to such an approach. Despite this, there is still significant scope for future development work.

Three case studies were subsequently presented. The first demonstrating that high β-angle has a place in loose surface racing for maximising tyre performance and cornering speeds albeit at the expense of the ability to command full control of the vehicle. The second showing how differentials can be used to influence the β-angle behaviour and vehicle stability with the emphasis on performance related issues. Finally the third demonstrating the potential for β-angle control on sophisticated torque vectoring differentials as a means of providing a more exciting and potentially tuneable driving experience for small-executive class passenger cars.

Again these three case studies represent initial starting points that build on the concept of having a cheap, robust and reliable β-angle sensor. Future work is virtually limitless in its scope and prospective application and not restricted to any particular field, although WRC does represent a likely target through the predominance of high β-angle driving styles.

6.4 Future Work

To summarise, this research has formed a solid basis and starting point for the development of β-angle related work. Below are a few recommendations that flow from this work.

- Continued development of the β-angle sensor towards a cheap, reliable and robust commercially viable product for vehicle dynamics analysis.

- Continued development of the potential for tyre curve inference through the use of the β-angle sensor or similar.
- An investigation into the potential for real-time tyre performance monitoring applications.
- Research into the effectiveness of β-angle control systems, in particular tuneable drivability for future cars with sophisticated torque vectoring transmissions.

References

[1] W. Milliken and D. Milliken. *Race car vehicle dynamics.* Society of Automotive Engineers, 1995.

[2] C. Cohen B. Parkinson and B. McNally. Flight tests of attitude determination using gps compared against an inertial navigation unit. In *Journal of the Institute of Navigation*, volume 41, 1994.

[3] J. How N. Pohlman and C. Park. Gps estimation algorithms for precise velocity, slip and race-track position measurement. Technical report, SAE (02MSEC-93), 2002.

[4] M. Caruso and L. Withanawasam. Vehicle detection and compass applications using amr magnetic sensors. Technical report, Honeywell, 1999.

[5] P. Haney. *The Racing & High-Performance Tire.* SAE, 2003.

[6] W. Rowley. *An Introduction to Race Car Engineering.* Rowley Race Dynamics, 3rd edition, 2006.

[7] Honeywell. Hmc2003 three axis magnetic sensor hybrid datasheet. http://www.ssec.honeywell.com/.

[8] M. Caruso. Applications of magnetic sensors for low cost compass systems. Honeywell SSEC, www.ssec.honeywell.com.

[9] D. Brayshaw. *The use of numerical optimisation to determine on-limit handling behaviour of race cars.* PhD thesis, Cranfield University, 2004.

[10] A. Soliman K. Abd El-Gawwad D. Crolla and F. El-Sayed. Off-road tyre modelling iii: effect of angled lugs on tyre performance. *Journal of Terramechanics*, 36:63–75, 1999.

[11] ISO/TR 3888:1975. Road vehicles - test procedure for a severe lane-change manoeuvre. Technical report, International Organisation for Standardisation (ISO), Geneva, Switzerland, 1975.

[12] Corrsys-Datron. Correvit lf datasheet. www.corrsys-datron.com, 2003.

[13] W. Milliken F. Dell'Amico and R. Rice. The static directional stability and control of the automobile. Technical report, SAE (760712), 1976.

[14] Y. Shibahata K. Shimada and T. Tomari. Improvement of vehicle manoeuvrability by direct yaw moment control. *Vehicle System Dynamics*, 22(5-6):465–481, 1993.

[15] H. Nozaki. Compromise between sensing of critical cornering and drift control. Technical report, SAE (2005-01-3538), 2005.

[16] A. van Zanten. Bosch esp systems: 5 years of experience. Technical report, SAE (2000-01-1633), 2000.

[17] Mitsubishi Corporation. Active yaw control. *http://www.mitsubishi-cars.co.uk/features/ayc.asp*, 1998.

[18] M. Hancock R. Williams T. Gordon and M. Best. A comparison of braking and differential control of road vehicle yaw-sideslip dynamics. Jaguar Research/Loughborough University.

[19] K. Sawase and Y. Sano. Application of active yaw control to vehicle dynamics by utilizing driving/breaking force. *JSAE Review*, 20:289–295, 1999.

[20] Y. Ikushima and K. Sawase. A study on the effects of the active yaw moment control. Technical report, SAE (950303), 1995.

[21] K. Koibuchi M. Yamamoto Y. Fukada and S. Inagaki. Vehicle stability control in limit cornering by active brake. Technical report, SAE (960487), 1996.

[22] H.Tseng B.Ashrafi D.Madau T. Allen Brown and D. Recker. The development of vehicle stability control at ford. *IEEE/ASME Transactions on Mechatronics*, 4 No 3:223–234, 1999.

[23] R. Haas and R. Manwaring. Development of a limited slip differential. Technical report, SAE (710610), 1971.

[24] S. Chocholek. The development of a differential for the improvement of traction control. Technical report, SAE (884368), 1988.

[25] C. Liu V. Monkaba J. Tan C. McKenzie H. Lee and S. Suo. Driveline torque-bias-management modeling for vehicle stability control. Technical report, SAE (2002-01-1584), 2002.

[26] Peter Wright. *Formula 1 Technology*. SAE, 2001.

[27] A. van Zanten R. Erhardt and G. Pfaff. *Electronic Braking, Traction and Stability Controls*, volume PT-76 in Automotive electronics series, pages 395–412. Society of Automotive Engineers, 1999.

[28] H. Sasaki and T. Nishimaki. A side-slip angle estimation using neutral network for a wheeled vehicle. Technical report, SAE (2000-01-0695), 2000.

[29] D. Barber and M. Atkinson. Method of measuring displacement using optical gratings. *Journal of Scientific Instruments*, 36:501–504, December 1959.

[30] K. Imou M. Ishida T. Okamoto Y.Kaizu A. Sawamura and N. Sumida. Ultasonic doppler sensor for measuring vehicle speed in forward and reverse motions including low speed motions. *Agricultural Engineering International*, 3, 1994.

[31] H. Laqua. Dynamic microwave speckles and their application to contactless velocimetry of vehicles. *Measurement Science and Technology*, 6:4–10, 1995.

[32] B. Hofmann-Wellenhof H. Lichtenegger and J. Collins. *GPS, Theory and Practise*. Springer Wien New York, 2001.

[33] J. Farrell and M. Barth. *The Global Positioning System and Inertial Navigation*. McGraw-Hill, 1998.

[34] G. Xu. *GPS, Theory, Algorithms and Applications*. Springer, 2003.

[35] Racelogic. Vbox professional gps data acquisition datasheet. www.racelogic.co.uk.

[36] Thales Navigation. Dg16 and dg14 gps oem board receiver datasheet. www.thalesgroup.com/navigation.

[37] Racelogic Ltd. www.racelogic.co.uk.

[38] Racelogic. Comparison of non-contact speed sensors. www.racelogic.co.uk.

[39] R. Kornfield R. Hansman and J. Deyst. Single-antenna gps-based aircraft attitude determination. *Journal of the Institute of Navigation*, 45, 1998.

[40] J. Ryu J. Rossetter and J.Christian Gerdes. Vehicle sideslip and roll parameter estimation using gps. In *proceedings of AVEC 2002 6th (Internation Symposium of Advanced Vehicle Control)*, 2002.

[41] A. Hac and M.D. Simpson. Estimation of vehicle side slip angle and yaw rate. Technical report, SAE (2000-01-0696), 2000.

[42] D. Bevly et al. The use of gps based velocity measurement for improved vehicle state estimation. In *proceedings of the American Control Conference*, pages 2538–2542, 2000.

[43] J. Hahn R. Rajamani and L. Alexander. Gps-based real-time identification of tire-road friction coefficient. In *IEEE Transactions on Control Systems Technology*, volume 10, pages 331–343, May 2002.

[44] H. Bae J. Ryu and J. Christian Gerdes. Road grade and vehicle parameter estimation for longitudinal control using gps. In *IEEE Conference on Intelligent Transportation Systems Proceedings*, pages 166–171, 2001.

[45] J. Crassidis and E. Lightsey. Attitude determination using combined gps and three-axis mangetometer data. *Space Technology*, 22 No 4:147–156, 2001.

[46] Q. Ladetto J. van Seeters S. Sokolowski Z. Sagan and B. Merminod. Digital magnetic compass and gyroscope for dismounted soldier position and navigation. NATO Research and Technology Agency, Sensors and Electronic Technology Panel.

[47] Q. Ladetto V. Gabaglio and B. Merminod. Combining gyroscopes, magnetic compass and gps for pedestrian navigation. In *Symposium on Kinematic Systems in Geodesy, Geomatics and Navigation (KIS 2001)*, 2001.

[48] J. Kinkel and M. Thomas. Estimation of vehicle dynamic and static parameters from magnetometer data. In *Journal of Guidance, Control and Dynamics*, number 20 in 1, pages 111–116, Jan-Feb 1997 1997.

[49] M. Psiaki F. Martel and P. Pal. Three-axis attitude determination via kalman filtering of magnetometer data. *Journal of Guidance, Contol and Dynamics*, 13 (3):506–514, 1989.

[50] M. Caruso. Applications of magnetoresistive sensors in navigation systems. Honeywell Inc.

[51] Racelogic. Driftbox datasheet. www.driftbox.com.

[52] B. Siegler Deakin and D. Crolla. Lap time simulation: Comparison of steady state, quasi-static and transient racing car cornering strategies. Technical report, SAE (2000-01-3563), 2000.

[53] H. Pacejka and J. Besselink. Magic formula tyre model with transient properties. *Vehicle system dynamics*, 27:234–249, 1997.

[54] J. Dixon. *Tires, suspension and handling, 2nd Edition.* Society of Automotive Engineers, 1996.

[55] M. Blundell and D. Harty. *The Multibody Systems Approach to Vehicle Dynamics.* Elsevier, 2004.

[56] R. Sharp. The application of multi-body computer codes to road vehicle dynamics modelling problems. In *Proceedings of the Institute of Mechnanical Engineers*, number 208 in 1, pages 55–61, 1994.

[57] M. Arnold A. Carrarini A. Heckmann and G. Hippmann. Simulation techniques for multidisciplinary problems in vehicle system dynamics. *Vehicle System Dynamics Supplement*, 40:17–36, 2003.

[58] M. Sayers. Introductory guide to autosim version 2.0. The Regents of the University of Michigan.

[59] Msc adams. www.mscsoftware.com.

[60] Simpack. www.simpack.de.

[61] D. Crolla. *An Introduction to Vehicle Dynamics.* Vehicle Dynamics Group, Department of Mechanical Engineer, University of Leeds, UK., 1991.

[62] D. Casanova. *On minimum time vehicle manoeuvring: The theoretical optimal lap.* PhD thesis, Cranfield University, 2000.

[63] G. Prokop. Modeling human vehicle driving by model predictive online optimization. In *Vehicle System Dynamics*, volume 35, pages 19–53, 2001.

[64] K. Guo and H. Guan. Modelling of driver/vehicle directional control system. In *Vehicle System Dynamics*, volume 22 (3-4), pages 141–184, 1993.

[65] D. Brayshaw and M. Harrison. The driver's control of high performance vehicles on the limit, the influence of vehicle setup and the effects of active chassis systems. In *Proceedings of the Total Vehicle Technology Conference (University of Sussex, Brighton, UK)*, pages 3–13, 2004.

[66] Introduction to the new off-road dynamics facility. www.silsoe.cranfield.ac.uk/caee.

[67] R. Bergh H. Lefevre and H. Shaw. An overview of fiber-optic gyroscopes. In *Journal of Lightwave Technology*, volume 2, pages 91–107, 1984.

[68] Crossbow Technology inc. Cxm113 3-axis fluxgate magnetometer datasheet.

[69] Honeywell. Hmr3000 digital compass module datasheet. http://www.ssec.honeywell.com/.

[70] Iec 60529 (standard) degrees of protection provided by enclosures (ip code). www.iec.ch.

[71] Honeywell. Set/reset function for magnetic sensors (application note an213).

[72] Pi Research Ltd. www.piresearch.com.

[73] Crossbow Technology Inc. Measurement of a vehicle's dynamic motion, imu application note.

[74] Anon. *Pi Toolbox Manual*. Pi Research Ltd.

[75] Anon. *Year Book Automobile Sport 2005*. Fédération Internationale de l'Automobile, Geneva, 2005.

[76] B. Siegler and D. Crolla. Lap time simulation for racing car design. In *Computer simulation for automotive applications, SP-1663 proceedings of the SAE World Congress*, 2002.

[77] R. Sharp D. Casanova and P. Symonds. A mathematical model for driver steering control, with design, tuning and performance results. *Vehicle System Dynamics*, 33:289–326, 2000.

[78] D. Eckman. *Automatic Process Control*. John Wiley and Sons, Inc, 1958.

[79] Entran Sensors and Electronics. Acceleration vibration and shock catalogue, April 2002.

[80] W. Garrott M. Monk and J. Chrstos. Vehicle inertial parameters-measured values and approximations. Technical report, SAE (881767), 1988.

[81] Bixel Heydinger Durisek Guenther and Novak. Developments in vehicle center of gavity and inertial parameter estimation and measurement. Technical report, SAE (950356), 1995.

[82] H. Pacejka. *Tyre and Vehicle Dynamics*. Butterworth Heinemann, 2002.

[83] J.Y. Wong. *Theory of ground vehicles*. Wiley, 3rd edition, 2001.

[84] M. Croft-White and M. Harrison. Study of torque vectoring for all-wheel-drive vehicles. *Vehicle System Dynamics*, 44, 2006.

Appendix A

Set/Reset Pulse Generator Circuit Diagram

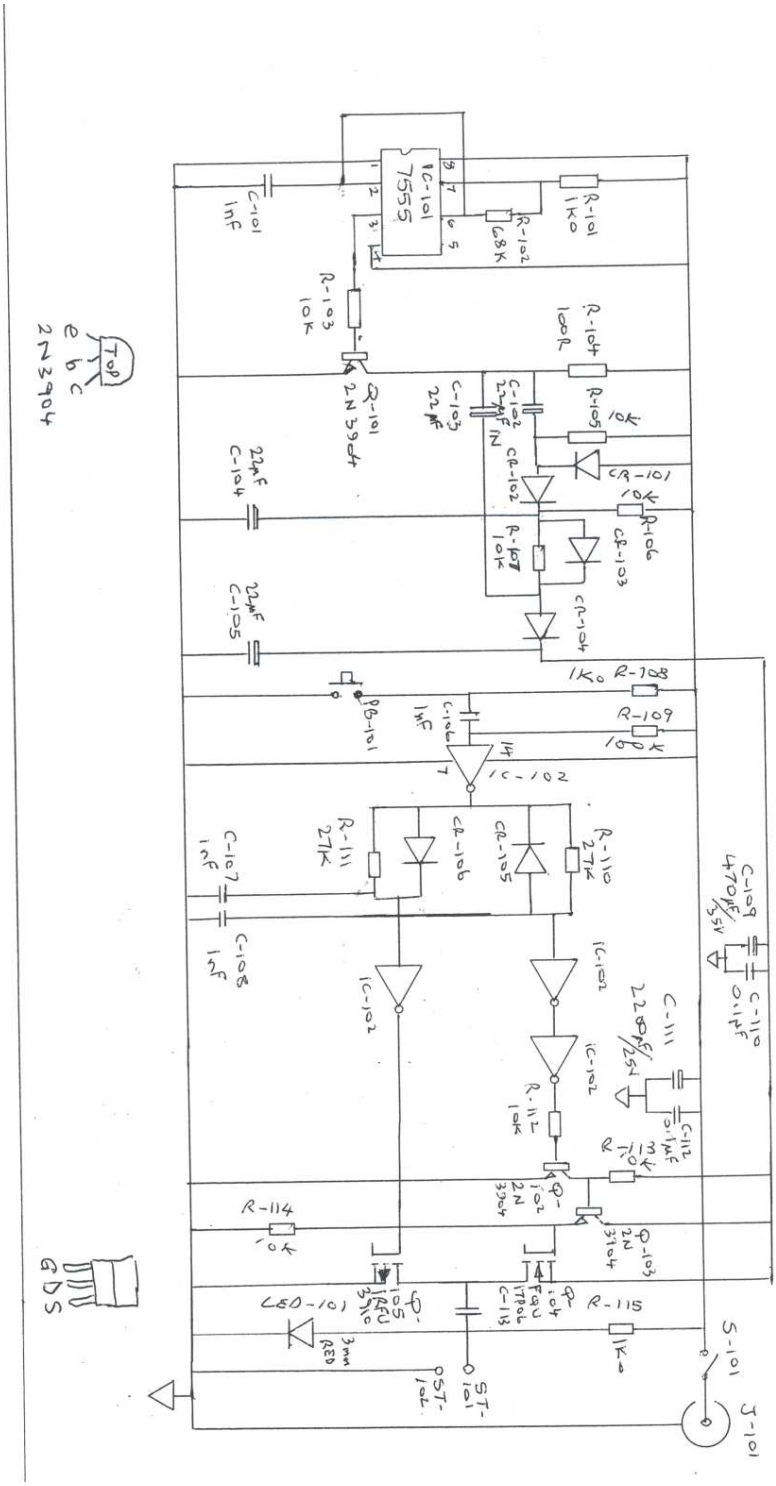

GILDEN RESEARCH LTD. HONEYWELL HMC2003 SET-RESET UNIT SCHEMATIC TRIM 2nd FEBRUARY 2005

Appendix B

Model Comparison

B.1 Straight Line Acceleration

The pitch and roll angles are simulated values based on a constant spring rate derived from experimental data obtained from a WRC vehicle in tarmac specification being analysed on a Kinematics and Compliance test rig.

B.2 Straight Line Deceleration

At 0ms^{-2} the small pitch angle is due to downforce distribution. The front lifts slightly more than the rear at speed.

Note: Due to the non-constant rate of deceleration, the pitch angles are an average value over the main braking region of the simulated manoeuvre.

Table B.1: Pitch and Roll under Straight Line Acceleration

Acceleration Target (ms^{-2})	Pitch (deg)	Roll (deg)
2	-0.15	0.00
4	-0.29	0.00
6	-0.44	0.00
8	-0.60	0.00
10	-0.73	0.00

Table B.2: Pitch and Roll under Straight Line Deceleration

Deceleration Target (ms^{-2})	Pitch (deg)	Roll (deg)
0	-0.02	0.00
2	0.14	0.00
4	0.28	0.00
6	0.45	0.00
8	0.61	0.00
10	0.74	0.00

B.3 Constant Radius and Speed Cornering

In these comparisons the model was configured to follow a 12 metre radius circular path with a zero longitudinal acceleration target (PI throttle, Optical level steer). Table B.3 compares the values of lateral acceleration, yaw rate and percentage lateral load transfer expectations as calculated using the equations of Milliken[1] (shown in brackets) and the values from the simulated model.

Table B.3: Comparison of Simulated and Calculated Values

Speed (ms^{-2})	Lat Acc (ms^{-2})	Yaw rate ($rads^{-1}$)	% Lat Load Transfer
2	0.34 (0.33)	0.167 (0.166)	0.9 (0.9)
4	1.34 (1.34)	0.334 (0.333)	3.4 (3.5)
6	3.00 (3.00)	0.500 (0.500)	7.9 (7.9)
8	5.32 (5.33)	0.664 (0.666)	14.0 (14.0)
10	8.28 (8.33)	0.830 (0.833)	22.0 (21.9)

Appendix C

Model Parameters

C.1 Chassis Data

Table C.1 contains the parameters used in the seven degree of freedom model.

Table C.1: Chassis Parameters

Parameter	Value	Unit
Height of CofG	0.4	m
Height of Roll Centre	0	m
Position of Roll Centre from Front	0	m
Position of Roll Centre from Rear	0	m
Yaw Moment of Inertia	2700	kgm^{-2}
Front Axis Polar Moment of Inertia	0.7	kgm^{-2}
Engine Moment of Inertia	0.017	kgm^{-2}
Rear Axis Polar Moment of Inertia	0.7	kgm^{-2}
Distance of CofG from Front Axle	1.1	m
Distance of CofG from Rear Axle	1.5	m
Mass	1230	kg
Front Wheel Radius	0.33	m
Rear Wheel Radius	0.33	m
Front Roll Stiffness	58	%
Rear Roll Stiffness	42	%
Front Track	1.55	m
Rear Track	1.55	m
Wheelbase	2.6	m

C.2 Aerodynamic Data

Table C.2 details the front-rear downforce distribution as well as the necessary coefficients to calculate both drag and lift. The frontal surface area is also listed.

Table C.2: Aerodynamic Parameters

Parameter	Value	Unit
C_x	0.3	-
C_z	-0.005	-
Downforce Distribution Front	70	%
Downforce Distribution Rear	30	%
Frontal Surface Area	1.88	m^2

C.3 Powertrain Data

C.3.1 Gears

The model has a six speed gear box. The gear ratio is changed when the models longitudinal speed with rises above or falls below the specified velocities shown in Table C.3.

Table C.3: Powertrain Parameters - Gearbox

Gear	Ratio	Velocity for Gear Change (ms^{-1})
1	12.56	18.16
2	9.13	24.96
3	6.23	36.62
4	5.1	44.75
5	4.4	51.82
6	3.8	70.13

C.3.2 Differentials

The model contains three active differentials - front, centre and rear. The hydraulic pressure is limited to a range of between 5 Bar minimum and 200 Bar maximum.

Table C.4: Powertrain Parameters - Differentials

Parameter	Front	Centre	Rear	Unit
Number of Plates	3	3	3	-
Inner Plate Radius	0.025	0.025	0.025	m
Outer Plate Radius	0.03	0.03	0.03	m
Thrust Bearing Area	0.0008	0.0008	0.0008	m^2
Frictional Coeff (m_0)	0.05	0.05	0.05	-
Frictional Coeff (m)	0.0001	0.0001	0.0001	-
Torque (interal friction)	20	20	20	Nm

C.4 Engine Data

The engine produces a maximum torque of 400Nm and has a maximum rotational speed of 7000 rpm.

Table C.5: Engine Parameters - Torque Curve

RPM	Overdrive (%)	Torque (%)
0	0	0.0
2500	-10.1	52.3
3000	-10.1	46.5
3500	-10.1	69.7
4000	-10.1	92.8
4500	-10.1	93.0
5000	-10.1	94.0
5500	-11.3	96.0
6000	-12.5	96.0
6500	-12.8	94.0
7000	-13.0	82.0

C.5 Brake Data

The Brakes can exert a maximum torque of 5500 Nm distributed 65% to the front brakes and 35% to the rear brakes.

Appendix D

Base Tyre Parameters for Simulation

Table D.1 presents the coefficients for the Pacejka '97 variant Magic Tyre Formula that were used as the base set for the simulations in this research. Camber was set at zero degrees for all four tyres. The coefficients are representative of a performance road tyre.

Table D.1: Pacejka Tyre Coefficients

Coeff.	Front Tyres	Rear Tyres		Coeff.	Front Tyres	Rear Tyres
pCx1	1.65	1.65		qEz3	0	0
pDx1	1.713	1.7325		qEz4	0.11464	0.12472
pDx2	-0.07738	0.026135		qEz5	10.876	9.1471
pEx1	0.40839	0.70969		qHz1	0.007124	0.00698
pEx2	0.23267	-0.28966		qHz2	-0.00573	-0.00434
pEx3	-0.58098	-0.27092		qHz3	-0.21898	-0.3037
pEx4	0	-0.20289		qHz4	0.17854	0.22493
pKx1	60.039	67.029		rBx1	19.038	17.411
pKx2	52.873	55.354		rBx2	21.592	19.23
pKx3	-0.77268	-0.8776		rCx1	1.1219	1.1211
pHx1	0	0		rHx1	0	0
pHx2	0	0		rBy1	17.812	18.191
pVx1	0	0		rBy2	19.528	15.143
pVx2	0	0		rBy3	-0.01097	-0.00196
pCy1	1.75	1.75		rCy1	1.0244	0.98793
pDy1	-1.5033	-1.5158		rHy1	0	0
pDy2	0.3201	0.30257		rVy1	0	0
pDy3	0.46794	6.571		rVy2	0	0
pEy1	-0.14418	-0.03076		rVy3	0	0
pEy2	-0.10511	-0.02086		rVy4	0	0
pEy3	2.8169	9.6751		rVy5	0	0
pEy4	23.797	106.44		rVy6	0	0
pKy1	-37.281	-41.954		ssz1	-0.00841	0.015828
pKy2	1.0987	0.93374		ssz2	0.005695	0.010874
pKy3	0.03559	-0.71886		ssz3	-1.17177	-0.84611
pHy1	0	0		ssz4	0.848501	-0.00793
pHy2	0	0		Fz0	4000	4000
pHy3	0	0		R0	0.32725	0.3263
pVy1	0	0		lFz0	1.01	1.02
pVy2	0	0		lmx	1	1
pVy3	0	0		lmy	1.015	1.035
pVy4	0	0		lKx	1	1
qBz1	19.603	19.127		lKy	0.88	0.88
qBz2	-2.1057	-2.0276		lCx	1	1
qBz3	1.1019	1.3341		lCy	1	1

Table D.2: Pacejka Tyre Coefficients Cont.

qBz4	-0.11937	0.045639		lEx	1	1
qBz5	-0.11937	0.045639		lEy	1	1
qBz9	29.924	29.753		lHx	1	1
qCz1	1.1348	1.1348		lHy	1	1
qDz1	0.10849	0.12287		lVx	1	1
qDz2	0.059517	0.05851		lVy	1	1
qDz3	0.17618	0.40916		lgy	1	1
qDz4	-25.824	-64.204		lgz	1	1
qDz6	-0.00188	0.002461		lt	1.023	1.023
qDz7	-0.0178	-0.01905		lMr	1	1
qDz8	1.5478	2.0554		lxa	1	1
qDz9	0.72528	0.48231		lyk	1	1
qEz1	-0.65433	-0.67073		lVyk	1	1
qEz2	0.61078	0.56648		ls	1	1